ON THE CONFORMATION OF DNA CONFINED IN A NANOCHANNEL OR ABSORBED AT THE INTERFACE

ZHANG CE

NATIONAL UNIVERSITY OF SINGAPORE

2008

Acknowledgements

First of all, I would like to express my cordial gratitude to my supervisor, Professor Johan R C van der Maarel, for guiding me into the interesting field of statistics of polymers. His deep understanding of the structure and dynamics of biopolymers subjected to various forms of confinement have not only been of great help to me, but also provided the world with a nice book, which by the way also helps me a lot. The many long discussions with him have shown me a direction in the ocean crowded by a tremendous amount of scientific interests. And the freedom of research that he tolerates has greatly increased both my level of confidence and my enthusiasm in science. I have learnt invaluable knowledge from him on how to do research work and how to enjoy doing research.

Special thanks go to Professor Jeroen van kan Anton for providing stamps, without which nothing can be done and Ms. Zhang Fang, for helping me with the nano-fabrication work at the early stage. I also thank Mr. Teo and Mr. Michael of biophysics teaching lab for their help in running Fluorescence Microscopy. I am especially grateful to some names I can not remember right now, for their help or their existence.

Finally, I would like to thank my wife and my huge family for their love, help and support.

Summary

The major focus of work in this thesis concerns the relationship between molecular behavior of DNA and a range of processing conditions including ionic strength, multi-valent ions, solvent, molecular weight etc. A variety of techniques including atomic force microscopy (AFM), fluorescence microscopy (FM) and nano-fluidics were utilized in order to uncover the role that these experimental conditions play in the formation of many 2D surface-directed and 1D channel-directed DNA structures. In previous years, attention was directed towards understanding the physical and chemical phenomena that are important in the condensation of DNA. In this thesis, we seek to uncover the behavior of single stranded and double stranded DNA molecules, and explore the mechanism behind the compaction into 1 and 2 dimensional structures.

For surface-directed condensation, the conformation of DNA under various experimental conditions was studied by atomic force microscopy (AFM). Different surface structures were observed on a mica surface for single-stranded and double-stranded DNA molecules. If ultra-pure water was used as the dilution solution, double-stranded DNA molecules tended to denature due to the repulsion force between the two strands. Flat-lying networks of hybridized single-stranded DNA were obtained. If buffered conditions were maintained during the whole of the preparation procedure, double-stranded DNA molecules were adsorbed on mica surface. The adsorbed double-stranded DNA molecules subsequently could be condensed in situ on

the surface by a brief rinse with anhydrous ethanol in the presence of divalent magnesium cations. The majority of these surface-directed and ethanol-induced condensed structures were toroids, but a small fraction of rods have also been observed. Analysis of the height and lateral dimensions shows that the toroids are single-molecular and disk-like with a height of one to two DNA diameters. We discovered that the thin toroid morphology is a general phenomenon of surface-directed condensation, irrespective the nature of the condensing ligands and the specific surface interaction.

Another important part of this thesis is the study of single T4-DNA molecules confined in rectangular-shaped nano-channels. Micro- and nano-channels located in different layers were fabricated by Proton Beam Writing (PBW) and UV lithography technologies respectively. The micro-channel size is about $5\times5\mu m$. The sizes of the nano-channels in lateral and vertical directions ranged from 150 nm to 500 nm. This novel double layer technique reduces fabrication and packaging complexity, and allows for reusability of the device. In micro-channels, the electro-kinetics of lambda-phage and T4 DNA were investigated by monitoring the transportation velocities under various experimental conditions. Statistical studies showed that the electroosmosis and electrophresis motion of polyelectrolytes could be optimized by modifying channel wall surface properties (glass cover slides and PDMS) and the buffer conditions.

In nano-channels, the extensions of the DNA molecules were measured with

fluorescence microscopy as a function of the ionic strength and composition of the buffer as well as the intercalation level by the YOYO-1 dye. The data was interpreted with scaling theory for a wormlike polymer, including the effects of confinement, charge, and self-avoidance. It was found that the elongation of the DNA molecules with decreasing ionic strength can be interpreted in terms of an increase of the persistence length. Self-avoidance effects are moderate due to the small correlation length imposed by the channel cross-sectional diameter. Intercalation of the dye results in an increase of the DNA contour length and a partial neutralization of the DNA charge, but it has no significant effect on the bare persistence length. In the presence of divalent cations, the DNA molecules were observed to contract below the Gaussian chain limit, but they do not collapse into a condensed structure. It is proposed that this contraction results from a divalent counterion mediated attractive force between the DNA segments.

Table of contents

List of Publications

1. J.A. van Kan, F. Zhang, C. Zhang, A.A. Bettiol and F. Watt (2007). "Exposure parameters in Proton Beam Writing for Hydrogen SilsesQuioxane." Nuclear Inst. and Methods in Physics Research, B. (Accepted).

2. C. Zhang and J. R.C. van der Maarel, "Surface-Directed and Ethanol-Induced DNA Condensation on Mica" The Journal of Physical Chemistry B, March (2008), Vol. 112 (issue 11), 3552.

3. C. Zhang, F. Zhang, J. A. van Kan and J. R.C. van der Maarel, "Effects of electrostatic screening on the conformation of single DNA molecules confined in a nanochannel", The Journal of Chemical Physics, June (2008), Vol. 128, Issue 22.

Chapter 1
Introduction

One important aspect of this thesis is the condensation of DNA induced by various condensing agents (multivalent ions and nanoparticles). As a highly condensed form is essential for the reproduction of life, DNA condensation has become a active area of research. In biochemistry, biophysics, and molecular biology it represents a process by which the genetic information is packaged and protected. In polymer physics and condensed matter physics, it presents intriguing problems in the area of phase transitions, liquid crystal behavior, and polyelectrolytes. And in biotechnology and medicine, it provides a promising means for transferring DNA into cells (gene therapy). However, due to technique limitations, little research has been done to investigate the topological response of biopolymer chains during the condensation process.

Top-down approaches to create 'nano-objects' have the potential to revolutionize biology. Chip-based devices for single biopolymer studies are important examples. A number of devices have been proposed. These devices have in common the confinement of DNA to nanometer scales, which is typically in the range of 5–200 nm. Confinement alters the statistical mechanical properties and Brownian dynamics of biopolymer molecules. In 1999, J. Han et al. studied DNA molecules, which were driven through a 90 nm wide nanochannel by a electric field. DNA molecules were trapped inside the confinement and escaped with a characteristic lifetime. Counter intuitively, longer DNA molecules were found to escape these entropic traps faster than the shorter ones. DNA molecules overcome the entropic barrier by stretching their segments into the constriction. As a result, DNA escape is independent of the

chain length.

In recent years, micro- and nano-fluidic devices have been developed and utilized for analyzing the properties of long biopolymer chains such as DNA. Different architectures have been designed, including entropic trap arrays, micro and nano-pillar arrays, nano-pores and nanochannels [1,2,3,4]. The nano-fluidic devices are complementary to other single molecule manipulation techniques such as those based on optical tweezers [5,6,7]. In the case of confinement in a long and straight nano-channel, a long biomolecule elongates because of the restriction in configurational degrees of freedom imposed by the channel walls. This effect is similar to the situation in a single molecule stretching experiment, in which the biomolecule is subjected to a tensional force. The role of the strength of the stretching force is the same as the value of the cross-sectional diameter of the nano-channel, in the sense that both a stronger force and a decrease in diameter result in a more extended conformation. Besides the similarities of these single-molecule manipulation techniques, there are also some important differences. For instance, in the confinement experiment there is no need for chemical modification to attach the biomolecule to molecular pincers.

The statistics of a DNA molecule confined in a nano-channel depends on the ratio of the cross-sectional channel diameter and the DNA persistence length [9]. In a narrow channel, with a cross-sectional dimension less than the persistence length, the molecule will undulate inside the channel and will only bend when it bounces off the wall [10]. In this thesis, the channel diameters exceed the persistence length, but they

are smaller than the radius of gyration of the unconstrained, free DNA coil. In the latter situation, the DNA molecule inside the channel remains coiled at all length scales, albeit it will be elongated in the longitudinal direction [11]. The advantage of such configuration is that the data can be interpreted using well established polymer theory, including the effects of the local bending rigidity (persistence length) and interaction of spatially close segments which are separated over a long distance along the contour (excluded volume). The scaling relations for the extension of DNA molecules confined in nano-channels of various diameters have been verified by Reisner et al. [12]./The effects of electrostatic screening on the conformation of DNA molecules inside nano-slits and nano-channels of various dimensions also have been reported before [13,14]. In general the DNA molecule has been observed to stretch out with decreased screening of Coulomb interaction, which was interpreted in terms of a variation in the persistence length. Contradictive results were reported however for the relative importance of excluded volume effects. Accordingly, we thought it is of interest to reinvestigate the effects of electrostatic screening and, in particular, to gauge the relative importance of self-avoidance with respect to the variation in persistence length.

In order to understand the conformation of biopolymer molecules during various biological processes, excluded volume effects have to be taken into account. Excluded volume interactions between segments separated over a large distance along the contour length are important to understand the behavior of both relaxed and condensed systems. An example of excluded volume effect is the molecular basis of

the polymer induced protein-precipitation. Although excluded volume interactions have been recognized as being an important factor, they have attracted little attention. The reason may be that the excluded volume interactions are expected to induce a minor alteration in the free-solution polymer conformation, which is hard to observe due to the technological limitations.

Thus, there is a need for a device that allows analysis of these single DNA molecules under certain buffer conditions. In 2005, Reisner et al. presented measurements of DNA confined in nano-channels. Below a critical width, which is roughly twice the persistence length, they showed that there is a crossover in the polymer statistics [25]. In 2007, the same group showed that the ionic environment plays a critical role in determining the configurational properties of DNA confined in the nano-channels [26]. The extension of DNA, increases as the ionic strength is reduced, almost tripling over two decades in ionic strength for channels with a cross-sectional diameter of around 100 nm. The effect is mainly due to increasing bending rigidity of the DNA chain created by the reduced screening of electrostatic interactions at lower ionic strength.

Single biopolymer investigations have been conducted for many years. All the employed techniques, including optical tweezers, magnetic tweezers and nano-fluidic devices, have in common that they require some chemical modifications for the purpose of observation. Examples are chemical alteration of bears attached to the DNA molecules for the tweezer experiments and the intercalating of dye molecules for the fluorescence imaging of .DNA. These factors should be duly taken into

account in the interpretation of the data.

Research Objectives

The main aim of this thesis is to investigate the conformational response of DNA to various experimental conditions. In particular, we have investigated surface-directed DNA condensation induced by a range of processing conditions. I have also investigated the extension of single DNA molecules in nano-channels mediated by a change in screening buffer conditions (such as ethanol, Tris-borate/EDTA (TBE) and Tris/HCl) and depletion interactions induced by dextran nanoparticles.

This study sheds light on the behavior of DNA under various conditions. One of the most promising applications is the investigation of the effects of binding and non-binding proteins on the properties of confined DNA. The results are expected to be of importance from a biophysical point of view (the behavior of the genome in congested and confined states). Moreover, there are also implications for biotechnological lab-on-a-chip applications. Based on these reasons, numerous researches have been conducted on biopolymer condensation. In Chapter 2, a review of the relevant literatures will be presented.

In chapter 3, the adsorption of λ-phage DNA onto mica was investigated with atomic force microscopy. We found that the morphologies depend on the solvent conditions in the sample preparation procedure. Flat-lying networks of hybridized single-stranded DNA are obtained if ultra-pure water is used. If buffered conditions are maintained during the whole of the preparation procedure, single double-stranded

DNA molecules are adsorbed. The adsorbed double-stranded DNA molecules subsequently can be condensed in situ on the surface by a brief rinse with anhydrous ethanol in the presence of divalent magnesium cations. The majority of these surface-directed and ethanol-induced condensed structures are toroids, but a small fraction of rods has also been observed. Analysis of the height and lateral dimensions shows that the toroids are single-molecular and disk-like with a height of one to two DNA diameters. The thin toroid morphology appears to be a general phenomenon of surface-directed condensation, irrespective the nature of the condensing ligands and the specific surface interaction.

Chapter 4 reports the design, fabrication, and testing of a multilayer polydimethylsiloxane (PDMS) based nanofluidic chip for the investigation of biopolymer behavior in a confined and congested state. The chip contains a set of parallel nanochannels, which are connected through sets of microchannels to two reservoirs. The micro- and nanochannels are located within different layers of the chip and are fabricated with the help of UV and Proton Beam Writing (PBW) lithography technologies, respectively. As determined by the thickness of the SU-8 photoresist layer, the microchannels have a square cross-section of $5 \times 5\ \mu m^2$. The nanochannels have a width in the range of 150 to 500 nm and a depth of 300 nm. Compared to more traditional protocols, our method is relatively easy to implement and allows the fabrication of cheap and reusable polymer-based biochips. The integrated chip was tested by injecting of λ- or T4 bacteriophage DNA molecules into the reservoirs. The DNA molecules were subsequently driven through the nanochannels with the help of

an electric field and visualized through the fluorescence of the YOYO-1 staining dye.

In chapter 5, single T4-DNA molecules were confined in rectangular-shaped channels with a depth of 300 nm and a width in the range 150-300 nm casted in a poly(dimethylsiloxane) nanofluidic chip. The extensions of the DNA molecules were measured with fluorescence microscopy as a function of the ionic strength and composition of the buffer as well as the DNA intercalation level by the YOYO-1 dye. The data were interpreted with scaling theory for a wormlike polymer, including the effects of confinement, charge, and self-avoidance. It was found that the elongation of the DNA molecules with decreasing ionic strength can be interpreted in terms of an increase of the persistence length. Self-avoidance effects are moderate due to the small correlation length imposed by the channel cross-sectional diameter. Intercalation of the dye results in an increase of the DNA contour length and a partial neutralization of the DNA charge, but besides effects of electrostatic origin it has no significant effect on the bare bending rigidity. In the presence of divalent cations, the DNA molecules were observed to contract, but they do not collapse into a condensed structure. It is proposed that this contraction results from a divalent counterion mediated attractive force between the segments of the DNA molecule.

In Chapter 6, structural changes in T4 DNA induced by the addition of a neutral dextran nanoparticles were examined by the method of single-molecule observation in nanochannels. We present a new experimental strategy for the study of the depletion effect on large DNA chains exerted by nanoparticles. A clear phase diagram is observed as a function of the nanoparticle concentration. In nanochannels DNA

molecules exhibit a more extended conformation with the addition of nanoparticles at relatively low concentration, irrespective of the ionic strength of the medium. Under concentrated nanoparticle conditions, individual DNA molecules assume a highly compacted state. Surprisingly, the nanoparticle molecular weight has no obvious effect on the phase diagram.

Chapter 2
Literature Review

2.1. Material for Biological Research

For the investigation of the conformation of DNA, a range of materials are used. These materials include mica and polydimethylsiloxane (PDMS). PDMS is widely used in micro- and nanofluidics in the area of lab-on-chip applications. These devices comprised of PDMS and glass are also used in large amounts to transport and separate biopolymer molecules.[33] Chemically processed mica can be employed as a substate for various biological studies.[32] Both PDMS- and mica-involved experimental strategies allow the investigation of the conformations and real-time responses of DNA.

2.1.1.General Features of Mica

Mica is a non-swelling clay mineral. It has a laminar crystalline structure and the negative charge density due to positive ions of the impurities contained in the crystalline structure is very high. To neutralize this negative charge, inter-laminar positive ions are adsorbed. These positive ions are most often potassium ions. The crystal surface of clay has oxygen atoms arranged on it. These oxygen atoms have a structure composed of rings known as six-member rings, which have cavities at their centers. The inter-laminar positive ions adsorbed in mica are accommodated in the holes produced by the six-member rings of two crystals that are adjacent in the vertical direction. As a result, it is very difficult for bulk mica structure to exchange the inter-laminar positive ions with other positive ions in a solution. But for a fleshly cleaved mica layer, positive ions are removed from the negative charge rings. The

removal of positive counter-ions makes the surface negatively charged. By sharing positively charged ions as bridges, negatively charged biopolymers can be bonded to a mica surface.

2.1.2.General Features of Polydimethylsiloxane (PDMS)

Polydimethylsiloxane (PDMS) is the most widely used silicon-based organic polymer, and is particularly known for its unusual rheological (or flow) properties. Its applications range from contact lenses and medical devices to elastomers, in shampoos as Dimethicone makes hair shiny and slippery, lubricating oils and heat resistant tiles. After polymerization and cross-linking, solid PDMS samples will present an external hydrophobic surface.[35] This surface chemistry makes it difficult for polar solvents (such as water) to wet the PDMS surface, and may lead to adsorption of hydrophobic contaminants. Plasma oxidation adds silanol (SiOH) groups to the surface and is commonly used to alter the surface chemistry. This treatment renders the PDMS surface hydrophilic and allows water to wet (this is frequently required for, e.g. water-based microfluidics).

Oxidized surfaces are stable for approximately 30 minutes irrespective of the surrounding medium.[36] After 30 minutes, the PDMS surface recovers its hydrophobicity. Most organic solvents will diffuse into the material and cause it to swell.[35] Accordingly, the solvents are incompatible with PDMS devices. Alcohols and polar solvents such as methanol, glycerol and water do not swell the material appreciably. Accordingly, they can be used in micro- and nanofluidics made out of

PDMS without restriction.[37]

2.2. PDMS-based Micro- and Nano-fluidic Device

Over the decades of its existence, polydimethylsiloxane (PDMS) micro-fluidics has progressed from the plain micro-channel through pneumatic valves and pumps to an impressive set of specialized components organized by the thousands in multilayer large-scale-integration chips.[38,39,40,41] These devices have become the hydraulic elastomeric embodiment of Richard Feynman's dreams of samll machines.[42,43] The now established technology has found successful applications in protein crystallization, DNA sequencing, nanoliter PCR, cell sorting and cytometry, nucleic acids extraction and purification, immunoassays, cell studies, and chemical synthesis, while also serving as the fluid-handling component in emerging integrated microelectromechanical devices (MEMS).[44,45,46,47,48,49]

In 2006, Emil P. Kartalov et al. reported on a fundamental technological advance that allows a large increase in the architectural complexity of micro-fluidic devices.[50] In their research, the previously undescribed device ‘‘via’’ was compared to its analog in modern semiconductor electronics. Vias are vertical micro-passages that connect channels fabricated in different layers of the same PDMS multilayer chip. As the field moves to functionally complex heterogeneous devices integrated on the same chip, laying out the respective circuitry would inevitably necessitate convenient, simple, and reliable vertical connectivity just as it did in the semiconductor industry. Micro-fluidic vias provide that 3D connectivity and contribute morphological and

functional capabilities.

The pursuit of 3D fluidic devices is not new. Whitesides and colleagues at Harvard University developed an ingenious scheme wherein a complex system of multilayer photoresist molds, photoresist pre-masters, and PDMS masters were fabricated and then used in an involved many-step process to produce a 70 μm-thick PDMS layer housing 100 μm-wide vertical cylinders connecting 70 μm-tall channels fabricated in thick PDMS slabs.[51] The resulting 3D technique was successfully used in protein and cell patterning.[52] Jo et al. demonstrate a similar method involving physical clamping to control layer thickness.[53] Whitesides and colleagues also developed a technique to produce 3D channels by mechanical deformation of straight channels.[54] However, the challenging and labor-intensive fabrication of the above devices has largely dissuaded researchers from further work with these methods.

2.3. Introduction to Biopolymer

2.3.1. General features of single-stranded (ssDNA) and double-stranded DNA (dsDNA)

For DNA molecule, the chain stiffness is characterized by the persistence length, Lp. dsDNA is very stiff with Lp in the range of 50–100 nm [55,56]. ssDNA is much more flexible with Lp estimated around 2 nm [57,58,59]. Chain sections shorter than Lp have a one dimensional character, like stiff rods, while at scales larger than Lp the chain is easily deformed and assumes a swollen-coil conformation.

For the studies on the behavior of surface-tethered single- and double-stranded

DNA at the polarized solid/liquid interface, the differences in flexibility are more pronounced [60]. First, the equilibrium conformations as well as the dynamic transitions are predominantly governed by interactions of the short-ranged electric field with a few DNA segments which are closest to the surface. Second, for that reason, the stiffness of the polyelectrolyte largely determines its behavior on the surface. For instance, rigid dsDNA can be aligned more efficiently by repulsive electrode potentials than flexible ssDNA. Finally, the dissimilar dynamic behavior which is observed for ss- and dsDNA can be related to the distinct flexibilities of the molecules. One particular important issue in this area is the distinct response of ss- and dsDNA to various biological conditions.

2.3.2. Shape Transition of Double-stranded DNA

Chain-like macromolecules in solution, whether biological or synthetic, transform from a spatially extended conformation to a compact one upon change of temperature or solvent qualities. This sharp transition plays a key role in various phenomena, including DNA condensation, protein folding, and the behavior of polymer solutions.[79,80,81,82] In biological processes such as DNA condensation the collapse is sensitively induced by a small amount of added molecules. If the persistence length, the characteristic distance along which the chain retains its direction, is smaller than the range of attractive correlations induced by the agent (typically up to several nanometers), the chain contracts gradually. Stiffer chains undergo sharp collapse. When material scientists wish to change the conformation of

dissolved polymers, thereby controlling the phase and flow behavior of the solution [54], they tune overall parameters such as temperature, pH or salinity. In biological systems a similar goal is achieved by introducing a small quantity of condensing agents, such as short polyamines (spermine and spermidine) in the case of DNA condensation [79,83,84]. Studies have shown that DNA collapse can be induced by other, non-specific agents, e.g. inorganic multivalent ions and ionic surfactants [85,86,87]. Apart from the basic interest in DNA condensation, such mixtures are important for potential gene delivery applications, where the DNA is shielded by oppositely charged molecules to help it penetrate the nuclears [79,87].

Theoretical studies have been focused on the complex electrostatics among chain groups and the surrounding ions [78], While electrostatics evidently plays a central role (all known condensing agents are charged) there are other factors to consider. For example, monovalent ionic surfactants can condense DNA [86,87], whereas simpler ions must be multivalent. Beyond mere charge, the key feature of a successful agent seems to be its ability to co-operatively associate with the chain, thereby inducing strong attractive correlations. Indeed, all of the aforementioned agents can be viewed as molecular clips —having associated with a monomer, they attract other monomers and agent molecules to the same region.

2.4. Electroosmosis & Electrophoresis

2.4.1. Electroosmosis of DNA molecules in microchannels

Electroosmosis is a basic phenomenon experienced in all electrophoretic separation

processes. It is the flow generated by the action of an electric field on a fluid with a net charge, which is created by the zeta potential and confined in the Debye layer. This basic phenomenon in the electrokinetic transport is applied in the design of many microfluidic devices / systems being used today [89,90]. Applications where such phenomena play an important role are in the cooling of microelectronics, lap-on-a-chip diagnostic devices, and in vivo drug delivery systems. In fact, electrically neutral liquids have a distribution of electrical charges near a surface because of a charged surface. This region is known as the electrical double layer (EDL) which induced the electro-kinetic flow.

In addition, hydrophobic materials (such as untreated PDMS) have become increasingly attractive for use in micro-fluidic devices. Contrary to hydrodynamic flows, where one finds a parabolic distribution of the flow velocities with the maximum velocity at the center of the channel and zero velocity at walls, electro-osmotic flow (EOF) is generated close to the wall and therefore produces a nearly uniform (i.e., plug-like profile) velocity distribution across the entire cross section of the channel. In most cases, the Debye length of typical electrolytes used in micro-channels is much smaller than the hydraulic diameter of the channels. Typical ratios of channel diameter to Debye length are larger than 10^4. The liquid flow rates induced by electro-osmotic potentials are typically small with average velocities of the order of a few millimeters per second.

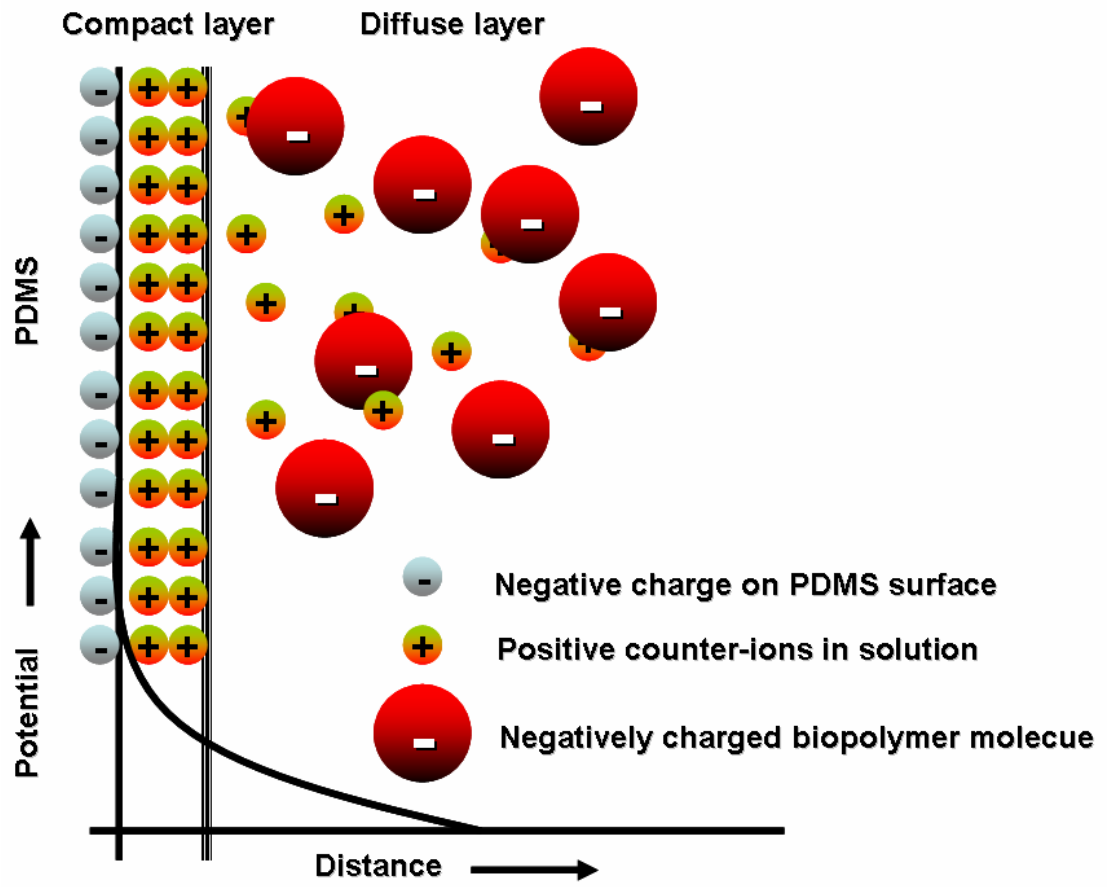

FIG. 1. The Electrical double layer near the surface of PDMS. According to the pH and buffer solution this surface can be protonated or deprotonated. As PDMS is negatively charged at PH = 8.6, a negative surface potential will be provided.

2.4.2. Electrophoresis of DNA molecules in microchannels

DNA electrophoresis is an analytical technique that is used to separate DNA fragments according to their size. ‘Electro’ refers to the energy of the electricity, whilst ‘phoresis’ comes from the Greek verb phoros, which means 'to carry across'. During DNA electrophoresis, the DNA molecules migrate from negative to positive potential driven by an electric field. This effect is closely related to electroosmosis, and the analysis of particle moving in fluids necessarily includes some drag models to account for the effect of fluid on the particle. As the micro-channel dimension in our research (5 micrometer) is far larger than the double layer thickness, the electric double layer (EDL) dynamics are approximately reduced to the flat plane discussed in the case of electroosmosis.

2.5. Possible mechanism for various DNA behaviors

2.5.1. Adsorption on Mica

The adsorption of DNA molecules onto a flat mica surface is one necessary step to perform atomic force microscopy (AFM) studies of DNA conformation and observe DNA-protein interactions in physiological environment. This is a crucial issue because the DNA / surface interactions could affect the DNA biological functions. Models that can explain the mechanism of the DNA adsorption onto mica have been proposed. In 2003, David Pastré suggested that DNA attraction is due to the sharing of the DNA and mica counterions.[91] The correlations between divalent counterions on both the negatively charged DNA and the mica surface can generate a net attraction

force whereas the correlations between monovalent counterions are ineffective in the DNA attraction. DNA binding is then dependent on the fractional surface densities of the divalent and monovalent cations, which can compete for the mica surface and DNA neutralizations. In addition, the attraction can be enhanced when the mica has been pretreated by transition metal cations (Ni^{2+}, Zn^{2+}). Mica pretreatment simultaneously enhances the DNA attraction and reduces the repulsive contribution due to the electrical double-layer force. Determined by end-to-end distance measurement of DNA chains, the DNA binding strength appears to be constant for a fixed fractional surface density of the divalent cations at low ionic strength ($I < 0.1$ M) as predicted by the model. However, at higher ionic strength, the binding is weakened by the screening effect of the ions. The electrostatic attraction due to the sharing of counterions is particularly effective if the polyelectrolyte and the surface have nearly the same surface charge density.

2.5.2. Electrostatic Blobs

Polyelectrolyte solutions exhibit a significantly more varied and complex behavior than solutions of uncharged polymers because their properties depend on a number of additional parameters. For instance, apart from the number of monomers in a chain, the persistence length, and the solvent quality for the polymer backbone, which are the parameters that determine the static behavior of linear homopolymers, extra factors such as the fraction of disassociated ionic groups, the charge valency of these groups, the dielectric constant of the solution, and the concentration of counterions

and salt ions in the solution, play an important role in governing the rich behavior observed in polyelectrolyte solutions.[93,94] Consequently, the success of scaling theories built on the electrostatic blob model of de Gennes et al. in achieving a coherent representation of experimental and simulation data of dilute polyelectrolyte solutions at equilibrium, in terms of a vastly reduced number of scaling variables, is remarkable.[95,96,97] In 2008, S. K. Pattanayek examined whether the equilibrium blob model of de Gennes et al. is useful as a framework to obtain a parameter free representation of Brownian dynamics simulation data for the properties of dilute polyelectrolyte solutions, in a far from equilibrium situation such as shear flow.[99]

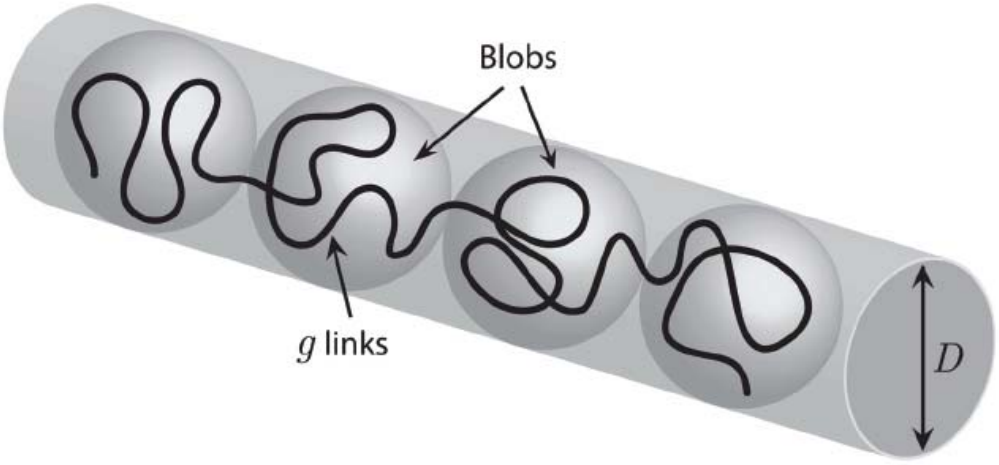

FIG. 2. A confined polymer in the de Gennes regime: D $\gg$ P. The molecule can be subdivided equally into a series of blobs with contour length L_b; the stretch arises from the mutual repulsion of the blobs.

2.5.3. DNA Deflection

As the channel width drops below the persistence length, the physics is dominated not by excluded volume but by the interplay of confinement and intrinsic DNA elasticity. In the strong confinement limit, which is much smaller than the persistence length, back-folding is energetically unfavorable and contour length is stored exclusively in deflections made by the polymer with the walls. These deflections occur on average over the Odijk scale. [100,101] As presented by Odijk in 1983, a new length scale λ is defined as $\lambda^3 \simeq D^2 P$. P is the contour length at which the pore boundary starts influencing the wormlike chain statistics markedly. This implies that the behavior of a large wormlike chain is very similar to a completely stiff rod of the same length. By analyzing all the accessible configurations, the increase in free energy due to confinement can be readily derived. Knowing the fact that the coil is extremely stiff on a length scale λ , it is easy to understand that the large biopolymer chain is deflected back and forth by the cylinder boundary. The characteristic contour length between deflections is of the order of λ on the average (see Figure 3).

In the Odijk regime, D can not be rigorously replaced by average of two confinement dimensions D_{av} if the channel aspect ratio is not unity. In the case that D1 and D2 are close then the substitution is a reasonable approximation. The nature of the crossover behavior between the de Gennes and Odijk regimes, D ~ P, is currently not understood. The crossover regime is important as it is likely to occur within the range of scales used in devices [102].

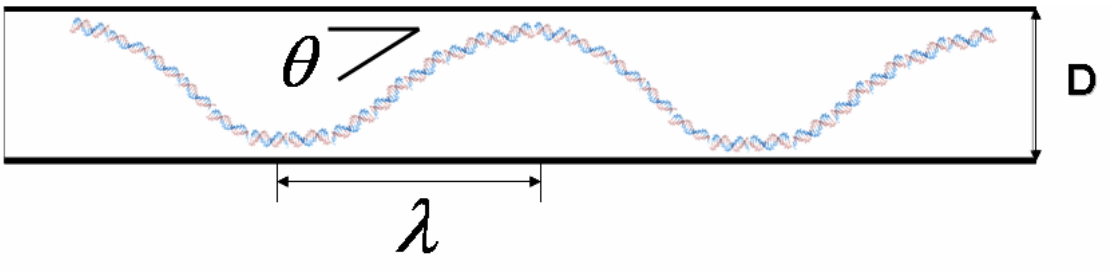

FIG. 3. A confined polymer in the Odijk regime: D ≪ P.

2.6. Experimental Techniques

2.6.1.Single Molecule Experimental Techniques

During the last decade, the field of single molecule studies on biological systems has strongly grown in importance. A very rapidly developing part of these activities concerns force measurements on DNA molecules. In 1997, Bockelmann et al. reported experiments where single DNA molecules are unzipped with a soft glass micro-needle. Force signals had been recorded that reflect the proportion of G/C compared to A/T basepairs on an average scale of ~100 base-pairs. A typical force versus displacement curve consists of a series of sawtooth-shaped features. This characteristic shape is explained theoretically in the frame of equilibrium statistical mechanics. The calculated physical effect, called molecular stick-slip motion, is a reversible molecular process caused by an interplay of the energy landscape given by the genomic sequence, the elasticities of molecule and measurement device, and the Brownian motion. Theoretical papers that directly relate to this experimental configuration have been published (Cocco et al., 2001; Lubensky and Nelson, 2000; Nelson, 1999; Thompson and Siggia, 1995; Viovy et al., 1994). Different groups have reported on AFM measurements of the force to separate the two strands of the DNA double helix (Colton et al., 1994; Rief et al., 1999).

2.6.2.Atomic Force Microscopy

Atomic force microscopy (AFM) is a powerful technique for imaging DNA and DNA-protein complexes on ultra-flat surfaces [106,107,108,109]. This microscope

generates a three-dimensional (3D) image by probing the sample surface with a sharp tip attached to the end of a flexible cantilever. One of the most attractive features of AFM is that it can operate in liquid, making it possible to image DNA under biological conditions. The key element is to preserve the activity and integrity of the specimen. This requirement is not easy to reach because it implies that DNA molecules should be loosely attached to move freely above the surface. The most popular substrate in this respect is muscovite mica, a highly negatively charged surface. Those crystals exhibit a large degree of basal cleavage, allowing them to be split into atomically flat sheets. Weak electrostatic attachment of the DNA to the surface is obtained by using divalent cations (Mg^{2+}, Ni^{2+}, Ca^{2+}…) in the buffer and either with a pretreated mica or not [109,110,111,112,113,114]. Mg^{2+} ions are generally preferred, for binding DNA to mica, to the transition metal cations that coordinate strongly to the DNA bases [115,116,117].

2.6.3.Nano-fluidic Experiment in combination with Fluorescence Microscope

The demand for increased analytical ability in the biological sciences has spurred the development of micrometer and nanometer scale structures for single molecule analysis. These structures facilitate the manipulation and analysis of biological molecules with higher speed and precision than is possible with conventional technology. Such capabilities promise to be useful in applications ranging from genomic sequencing to pathogen detection, and in fundamental research in fields such

as molecular biology and biophysics.

Sub-micrometer and nanometer scale fluidic channels used in conjunction with fluorescence spectroscopy have shown significant potential for the manipulation and analysis of single DNA molecules. Much of this work has focused on the implementation of rapid and sensitive analytical techniques such as fragment sizing [118,119], correlation spectroscopy [120], binding assays [121], identification of nucleic acid engineered labels [122], mobility measurements [123] and PCR analysis [124]. The physical behavior and genetic analysis of single DNA molecules in nanochannels are subjects of particular interest as well [125,126].

DNA has been hydrodynamically linearized in sub-micrometer fluidic devices, which can be used for genomic sequencing when combined with repeated fluorescence detection [127,128,129,130,131]. DNA molecules have been shown to become elongated to an extended equilibrium length when introduced into a nano-channel, which has been utilized for restriction mapping.[132] Further work has investigated other aspects of the physics of elongated DNA strands in nano-channels, including entropically driven dynamics and compression against nano-scale constrictions.

Recently, Christian H. Reccius et al. presented a method, which is described to quickly and precisely measure the conformation, length, speed and fluorescence intensity of single DNA molecules constrained by a nano-channel. DNA molecules were driven electrophoretically from a nano-slit into a nano-channel. The biopolymer molecules were confined and dynamically elongated beyond their equilibrium length

in nano-channels. The use of a nano-channel reduced fluorescent background noise, increased excitation uniformity, and allowed single molecule detection at higher concentrations when compared to measurements made in larger fluidic channels or free solution. For each DNA molecule detected, photon bursts from the two fluorescent signals were matched and subsequently fit to analytical models describing the conformation, length, speed and intensity of the DNA strands. The analysis in this journal paper made possible a direct determination of molecular length and conformation with spatial resolution beyond the optical diffraction limit, established in the presented work at 114 nm, with an analysis time of 20 ms per molecule.

Chapter 3

Surface-directed and ethanol-induced DNA condensation on mica

Abstract

The adsorption of λ-phage DNA onto mica was investigated with atomic force microscopy. We found that the morphologies depend on the solvent conditions in the sample preparation procedure. Flat-lying networks of hybridized single-stranded DNA are obtained if ultra-pure water is used. If buffered conditions are maintained during the whole of the preparation procedure, single double-stranded DNA molecules are adsorbed. The adsorbed double-stranded DNA molecules subsequently can be condensed in situ on the surface by a brief rinse with anhydrous ethanol in the presence of divalent magnesium cations. The majority of these surface-directed and ethanol-induced condensed structures are toroids, but a small fraction of rods has also been observed. Analysis of the height and lateral dimensions shows that the toroids are single-molecular and disk-like with a height of one to two DNA diameters. The thin toroid morphology appears to be a general phenomenon of surface-directed condensation, irrespective the nature of the condensing ligands and the specific surface interaction.

3.1.Introduction

In biological systems such as cells and viruses, DNA is found in tightly packaged states. The structural organization within these states is largely unknown, but bears some resemblance to condensed DNA phases observed in vitro. The term condensed refers to situations in which the DNA assembly has an orderly morphology, in contrast to precipitates or aggregates with a disordered molecular arrangement. Model systems that can produce condensed DNA phases are hence of great interest for understanding the mechanisms involved in vivo. DNA condensation can be induced by the addition of condensing agents and/or ligands, e.g. multivalent cations of valence three or greater, cationic polypeptides such as polylysine, basic proteins, alcohols, and neutral crowding polymers.[151] When condensation is induced by the addition of a condensing agent to very dilute DNA solutions at low ionic strength toroids and rods are observed.[152]

At higher DNA concentration liquid-crystals are formed.[153,154] DNA condensation can also be assisted and directed by a surface. Surface-directed condensation is particularly relevant from a biophysical point of view, because the interface can be considered a model system for the scaffolding inside the cell. In surface-directed condensation, DNA is first adsorbed onto a surface, after which it is condensed with a condensing agent. Examples which have been reported in the literature are the condensation of single DNA molecules with basic protein nucleoprotamine and silanes.[155,156] In the former case, DNA was first loosely bound to a mica surface with the help of $MgCl_2$, after which well defined toroidal structures were formed by the subsequent addition of the nucleoprotamine. Silanes are functionalized cationic polyamines which loosely bind to a silicon surface. The surface adsorbed silanes are

hence mobile and were observed to bind and condense DNA in rods and toroids. As in the solution studies, DNA is condensed by cationic agents, but the surface-directed toroidal structures are rather spread out and thin with an height on the order of one to two DNA diameters (2-4 nm).

Condensed DNA structures adsorbed onto a surface can also be obtained by dropping a droplet of a highly diluted DNA solution onto a mica surface, transferring the specimen to ultra-pure water for development, followed by a rinse with anhydrous ethanol.[157,158] This procedure results in flat-lying and densely packed DNA network structures. During the development process, these structures are supposedly produced by contacting, crossing and overlapping of DNA chains, as well as by hybridizing complementary bases of sticky ends created by sample handling (see Ref. [158] and references therein). The final rinse with anhydrous ethanol stops the development process and enhances the stabilization of the DNA film. Since ethanol is also known to condense highly diluted DNA into single-molecular rod and toroidal structures,[159,160] the formation of the flat-lying DNA networks seems to be at odds with the above mentioned surface-assisted condensation experiments.[155,156]

In the present contribution we will systematically explore the conditions under which single-molecular or extended network structures of bacteria λ-phage DNA (48,502 base pairs, contour length in the B-form 16.5 μm) on mica can be obtained. We will show that the morphologies critically depend on the solvent and buffer conditions in the preparation procedure. We will also show that single λ-phage DNA molecules can be condensed by a rinse of the specimen with anhydrous ethanol after the molecules have been adsorbed onto the mica with divalent magnesium cations. Finally, the condensed

nanostructures resulting from this surface-directed and ethanol-induced condensation process will be analyzed and characterized with atomic force microscopy.

3.2.Experimental Section

Bacteria λ-phage DNA was purchased from New England Biolabs, Ipswich, MA and used without further purification. As received from the manufacturer the λ-phage DNA stock solution has a concentration of 0.5 g of DNA/L. The solvent is TE buffer, which is composed of 10 mM Tris-HCl, pH 8.0, and 1 mM EDTA. Anhydrous ethanol was purchased from SINO, Singapore. Water was deionized and purified by a Millipore system and has a conductivity less than $1 \times 10\text{-}6\ \Omega^{-1}cm^{-1}$. Muscovite mica was purchased from Structure Probe, West Chester, PA and cut into about 1 cm^2 square pieces. Both sides of the mica surface were always freshly cleaved before use.

For adsorption studies, the stock solution was diluted 1,000 times to a final λ-phage DNA concentration of 5 mg/L. For this initial dilution step we have used TE buffer (method A) or ultra-pure water (method B). The 1,000 fold diluted stock was then mixed with a 2 mM $MgCl_2$ solution in 1:1 volume ratio and incubated at 38 °C for one hour. A 20 micro-liter droplet (2.5 mg/L DNA, 1 mM $MgCl_2$) was spotted onto a fleshly cleaved mica surface. After 8 minutes to allow for DNA adsorption onto the mica surface, the specimens were developed by immersing them in TE buffer (method A) or ultra-pure water (method B) for 30 minutes. Following development, most specimens were rinsed with anhydrous ethanol for approximately three seconds and subsequently dried under ambient conditions.

All imaging experiments were carried out at room temperature in air with a Dimension 3000 atomic force microscope, Veeco, Woodbury, NY. Images were acquired in the tapping mode with silicon (Si) cantilevers (spring constant 20-100 N/m) and operated below their resonance frequency (typically 230 – 410 kHz). The images were flattened

and the contrast and brightness were adjusted for optimum viewing conditions. Inner diameter, outer diameter, and height of the toroidal structures were always measured in nine different directions away from the center of the toroid with an angular 5 increment of 40 degrees with the NanoScope software. The estimated experimental resolution in height is 0.2 nm, but in the lateral direction the 5 nm resolution is worse due to the finite sharpness of the AFM tip.

3.3.Results and Discussion

3.3.1.Effect of dilution conditions.

DNA is often dispersed in a buffer medium such as TE with an ionic strength in the milli-molar range. In AFM adsorption studies it is necessary to spot a highly diluted solution with a concentration in the range 1-10 mg of DNA per liter on a flat surface such as mica. Since DNA is usually available at much higher concentration, spotting solutions need to be prepared by dilution with the appropriate medium. In recent works, the stock solution was diluted 1,000 fold with ultra-pure water, then mixed and incubated with a magnesium salt solution, subsequently spotted onto a surface for adsorption, followed by development in pure water for various times.[157,158] This procedure results in flat-lying and densely packed DNA network structures. Since the double-helical structure of DNA is known to be unstable without supportive electrolyte, we suspect that the surface-directed DNA network morphologies are related to the 1,000 fold dilution in ultra-pure water and concomitant (partial) melting of the double-helix.

In order to verify the effect of the dilution conditions on the surface morphologies, we have prepared specimens by dilution and development with TE buffer (method A) as well as with ultra-pure water (method B). After the initial dilution step, the DNA solutions were mixed and incubated with $MgCl_2$ solution at a slightly elevated temperature for one hour. Solution droplets (2.5 mg/L DNA, 1 mM $MgCl_2$) were then spotted on freshly cleaved mica and developed in TE buffer (method A) or ultra-pure water (method B) for 30 minutes. Since mica carries a negative surface charge, the Mg^{2+} ions serve as a bridge and allow DNA molecules to adsorb. During development excess $MgCl_2$ is diluted away from the interface and the DNA molecules rearrange themselves and form a specific

surface-directed morphology depending on the preparation procedure (i.e., method A vs. B). The specimens were air-dried, but not rinsed with anhydrous ethanol. Representative tapping mode AFM images are displayed in Fig. 1. If method A is followed, individual λ-phage DNA molecules are clearly discernible. Owing to the high magnification of the atomic force microscopy, only sections of the molecule are visible. The DNA molecules are extended and stretched out on the surface, probably related to surface tension effects during the air-drying process. The measured height of these adsorbed DNA molecules is 1.5±0.3 nm. In the case of dilution and development in ultra-pure water (method B), the AFM images are fundamentally different. In the latter case, DNA networks are observed. The height of the connecting DNA sections of these networks is only 0.3±0.1 nm.

Double-stranded DNA is known to be unstable in the absence of supporting electrolyte due to the unscreened electrostatic repulsion of the phosphate moieties of the opposing strands in the double helix. Accordingly, we suspect that the double helix (partially) melts in the 1,000 fold dilution step with ultra-pure water (method B) before it is mixed and incubated with the $MgCl_2$ solution. At the mica surface, the single-stranded DNA segments can then hybridize with other segments and thus form a densely-packed and flat-lying network. This also explains the relatively small value of the height of the segments of this network, which is the same as the value reported for single-stranded DNA adsorbed on 3-aminopropyl triethoxysilane (APTES) modified mica (0.3±0.1 nm).[161] If the ionic strength is maintained at a sufficiently high level in order to stabilize the double-helical structure during the whole of the preparation procedure (TE buffer conditions), the images clearly show sections of individual λ-phage DNA molecules with a height 1.5±0.3 nm. Due to compression effects by the AFM tip and/or

the fact that the specimens are air-dried, the measured height is somewhat smaller than the outer diameter of the duplex in the B-form (2 nm).[162,163,164]

3.3.2.Ethanol induced condensation

Under TE buffer conditions, λ-phage DNA molecules can be adsorbed onto mica with the help of divalent magnesium ions (method A). The tapping mode AFM images revealed extended molecules with a height measured from the surface in agreement with the value expected for the Watson-Crick double-helix in the B-form. We will show that these adsorbed molecules can be condensed in situ on the mica surface by a brief wash of the specimens in anhydrous ethanol. As displayed in Fig. 2, the condensed structures take the form of toroids, rods, and partially condensed toroids with a single protruding linear segment. Furthermore, DNA aggregation and/or network formation was not observed, although some of the toroids may contain multiple λ-phage DNA molecules (see below).

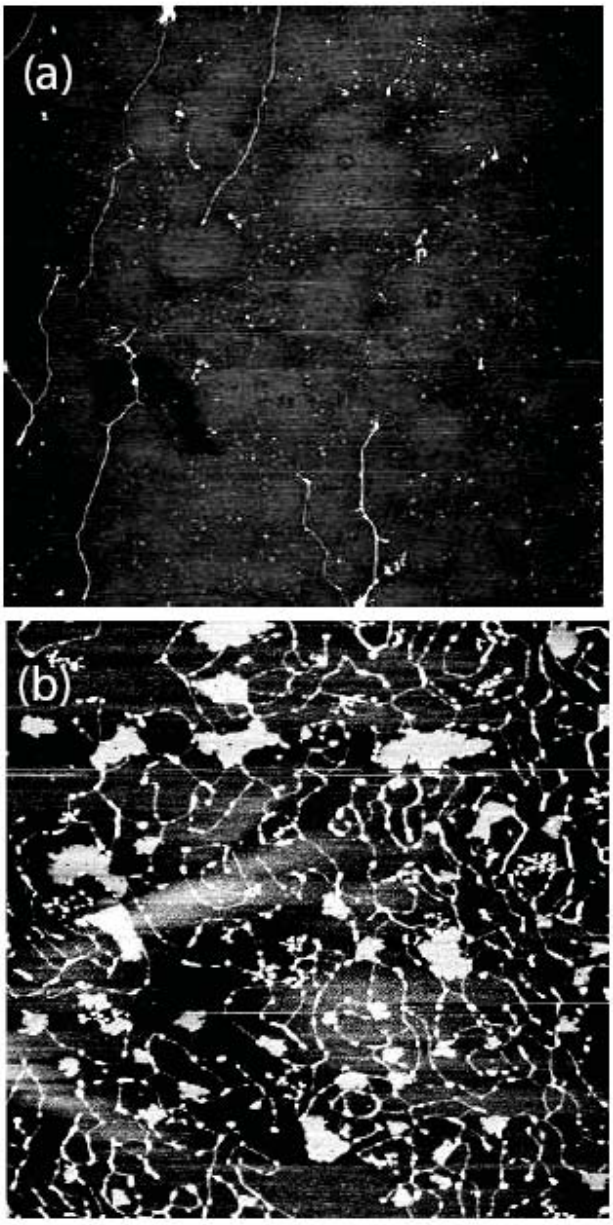

Figure 1. Typical tapping mode AFM images of λ − phage DNA (2.5 mg/L DNA, 1 mM MgCl2) on mica. The images represent a 3.3 ×3.3 μm2 area. For initial dilution and sample development, TE buffer (method A, panel a) or ultra-pure water (method B, panel b) was used. The specimens were air dried but not washed with ethanol.

Our procedure differs from previously reported work on ethanol-induced DNA condensation. The common procedure is to incubate a DNA solution with ethanol in the presence of soluble multivalent cations of valence three or greater such as spermidine or cobalt hexamine prior to the adsorption on a surface.[151,159] Fang et al. have shown that ethanol can induce DNA condensation in the presence of divalent magnesium only, but, again, a DNA solution was incubated with ethanol and the condensed structures were formed in the bulk phase and not surface-directed.[159] We obtained the condensed structures by a scaffolding-assisted and ethanol-induced condensation of single DNA molecules adsorbed onto the mica surface with magnesium cations. Note that the magnesium cations serve to attach the DNA molecules to the surface and that they also can induce condensation provided the dielectric constant of the medium is reduced by the addition of alcohol.[151,165]

An important feature of ethanol is that it also can induce a transition in secondary structure of double-stranded DNA from the B to the A-form. The double-stranded duplex in the A-form is thick with a diameter 2.6 nm and compressed in the longitudinal direction with a 3.2 nm pitch per turn of the helix. We were unable to determine the contour length of the condensed λ-phage DNA molecules after the rinse with ethanol. In order to obtain information about the DNA's secondary structure, we measured the height of the protruding sections of the partially condensed toroidal structures (see Fig. 2d). The average height of these sections is 1.6 ± 0.4 nm, which is, within experimental error, the same as the height of the individual DNA molecules as measured in the preparation procedure without rinsing with ethanol. We consider the

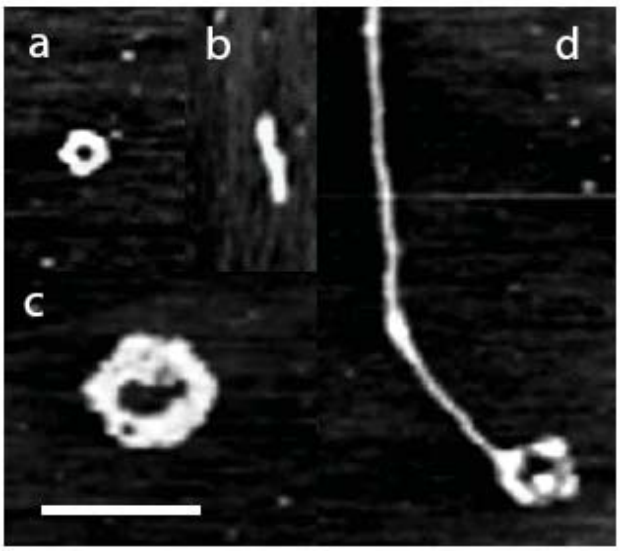

Figure 2. Composition tapping mode AFM images of condensed lambda phage DNA structures. A 2.5 mg/L DNA, 1 mM MgCl2 solution was prepared according to method A, spotted onto a freshly cleaved mica surface and developed for 30 minutes in TE buffer followed by a rinse with anhydrous ethanol. Toroidal structures are displayed in (a) and (c), whereas (b) represents a typical rod structure. A partially condensed toroidal structure is displayed in (d). The scale bar represents 0.5 μm.

similarity in the measured heights of the molecules as strong support that the brief rinsing with ethanol has not resulted in a change in secondary structure of the duplex.

3.3.3.Condensation morphologies

We have further investigated the morphologies of the condensed DNA structures by analysis of the tapping mode AFM images. A close image of a typical toroid is displayed in Fig. 3. The cross-section displayed in Fig. 3b shows a void at the center of the condensed structure. This observation agrees with a toroid made of circumferentially wound DNA rather than a globular structure. The structure of the toroid is typically quite irregular; there are often protrusions or even gaps and there is a strong variation in lateral thickness and height along the contour of the toroid in the azimuthal direction. The distribution in azimuthally averaged inner diameter Di , outer diameter Do , and height H in a population of 16 toroidal structures is shown in Fig. 4. We obtained a rather broad distribution in these parameters. The inner diameter ranges from around 40 to 150 nm with a strong bias towards the smaller values. The toroids are fairly big with outer diameters in the range 100-450 nm. As is often observed in surface-directed condensation, the toroids are disk-like with moderate heights as measured from the mica surface in the range 2.2-3.4 nm with a prevailing value 2.8 nm.[155,156] In view of the fact that the duplex has an outer diameter of 2 nm, the toroids should hence be composed of one or two layers of DNA.

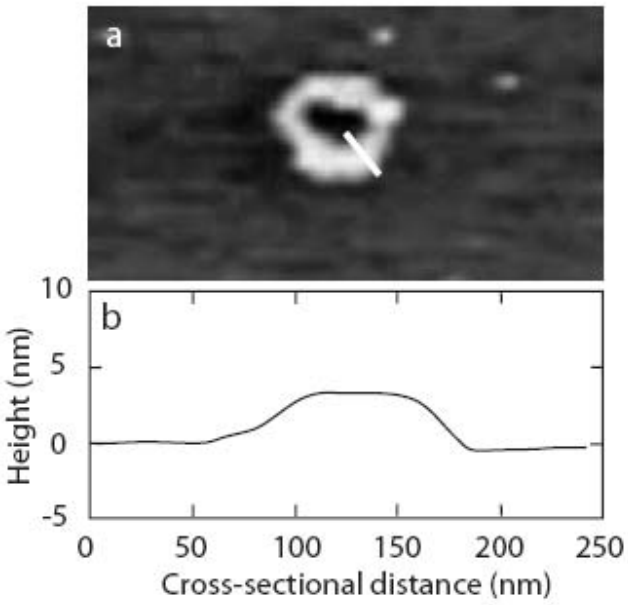

Figure 3. (a) Tapping mode AFM image of surface-directed and ethanol-induced toroid of λ − phage DNA. (b) Height profile of the cross-section of the toroid at the position indicated by the bar in panel (a). Notice that the toroid has a rather irregular structure with cross-sectional diameter on the order of 75 nm and a height around 3 nm.

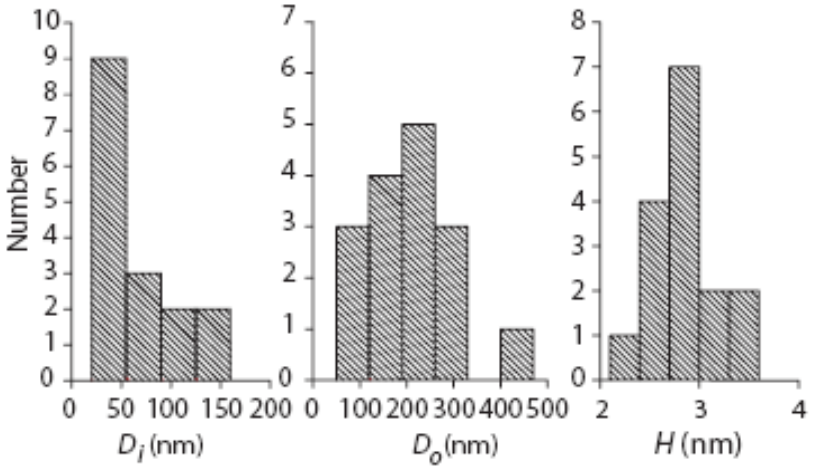

Figure 4. Distribution in inner diameter Di, outer diameter Do, and height H in a population of 16 toroids.

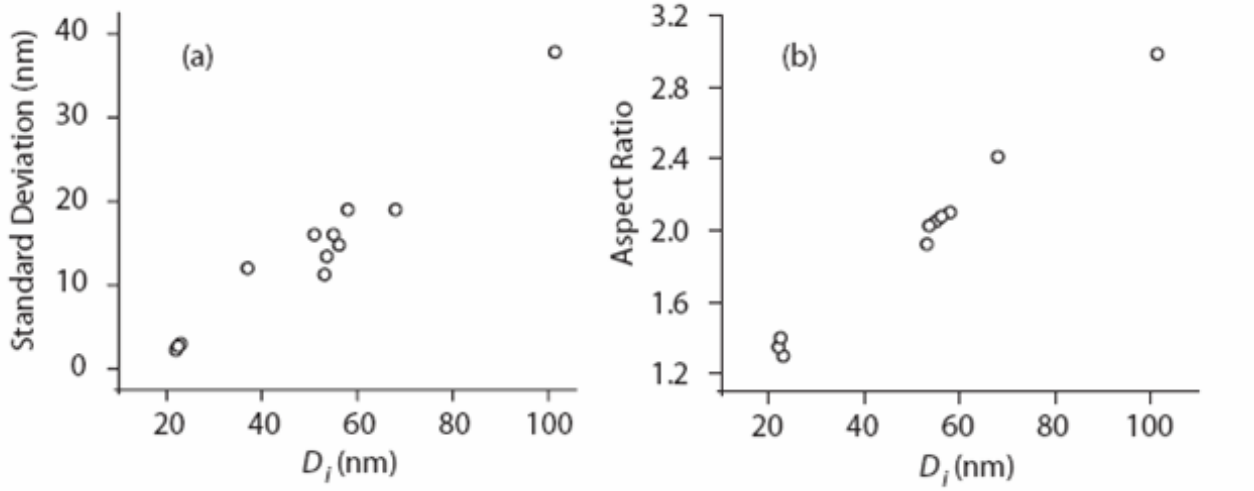

Figure 5. (a) Standard deviation in inner diameter versus the mean inner diameter measured in nine radial directions away from the center of the toroid with an increment in angle of 40 degrees. (b) Ratio of the maximum and minimum inner diameter (aspect ratio) versus the mean inner diameter. Note that each data point refers to an individual toroidal structure.

Individual toroids show an irregularity in both height and lateral dimensions in the azimuthal direction along the circular contour. For instance, the height of the toroid in Fig. 3 ranges from 1.8 to 3.0 nm. Another illustrative example is the partially condensed toroid shown in Fig. 2d. The extended part has a height 1.6 ± 0.4 nm, whereas the condensed part has a height in the range 2 to 3 nm. For a subset of nine toroidal structures, we have listed the corresponding structural parameters in Table 1. Note that the standard deviations refer to the azimuthal variation along the contour of individual toroids rather than the statistics of the whole population of toroids. The variation in height is typically on the order of a nanometer. Similar to the variation in height, there is also a strong variation in inner and outer diameter. As shown in Fig. 5a, the standard deviation in inner diameter increases with increasing mean inner diameter and becomes on the order of 30% for the largest structures. The deviation from circular symmetry of a particular toroid can also be expressed as the ratio of the maximum and minimum value of the inner diameter. This aspect ratio versus the mean inner diameter is displayed in Fig. 5b. From the results it is clear that the smaller toroids with inner diameters in the range 20 to 40 nm are fairly circular. With increasing size however the inner voids of the toroids become increasingly asymmetric with aspect ratios on the order of three.

An important issue is whether the condensed structures are uni- or multi-molecular, i.e. do they contain a single or multiple λ-phage DNA molecules? This question can be answered from an analysis of the inner and outer diameters. Let us consider a DNA molecule with contour length L (16.5 μm for λ-DNA in the B-form) circumferentially

Table 1 Inner diameter Di, outer diameter Do, and height H of some toroidal structures. The standard deviations refer to the statistical average of measurements of a single toroidal structure in nine different directions away from the center of the toroid with an angular increment of 40 degrees. The inter-axial spacing divided by the number of layers R n is calculated according to Eq. (1) with a contour length L = 16.5 μm pertaining to λ-phage DNA in the B-form.

Toroid number	1	2	3	4	5	6	7
D_i (nm)	42±4	36±12	56±16	52±16	58±20	68±18	95±37
D_o (nm)	162±14	170±16	214±18	224±6	246±14	246±26	404±19
H (nm)	2.7±0.7	2.5±0.6	3.1±0.4	2.3±0.5	3.4±0.6	2.9±0.4	3.5±0.3
R/n	1.2	1.3	2.0	2.3	2.7	2.7	7.3

wrapped in a toroidal structure with inter-helix spacing R and with inner and outer diameter Di and o Do , respectively. If the number of stacked layers is n (as judged from the height n should be between one and two), the inter-axial spacing follows from the total contour length stored in the toroid

$$\frac{R}{n} = \frac{\pi}{4L}\left(D_o^2 - D_i^2\right) \qquad (1)$$

For the subset of nine toroids the results are listed in Table 1. The inter-axial spacing of bulk-phase condensed DNA structures is around 2.8 nm.[152,166] As judged from the entries in Table 1, the dimensions of toroid number 5 and 6 comply with one layer with an inter-axial spacing acing 2.7 nm (n =1). Toroid number 1 and 2 are composed of two layers (n = 2), whereas toroid number 3 and 4 are intermediate consisting of partially one and partially two layers. The inner and outer diameters comply hence with a single λ-phage DNA molecule circumferentially condensed in a toroidal structure of one to two molecular layers height.

In Table 1, toroid number 7 is exceptional in the sense that it has a very large inner and outer diameter and a large R / n value. The latter value implies that the average spacing between the strands exceeds 7.3 nm (the minimum value of n is obviously one). Another possibility is that the toroid accommodates multiple λ-phage DNA molecules. For instance, in the presence of two DNA molecules, the stored contour length doubles and the minimum average inter-axial spacing is reduced by a factor of two and takes the value 3.6 nm. Close scrutiny of the corresponding AFM image in Fig. 2c reveals that the toroid is however not closely packed and even exhibits some gaps in its structure. Accordingly, the large size and R / n value do not necessarily imply that the toroid includes multiple λ-phage DNA molecules. The dimensions of exceptionally large toroids such as number 7

can also be rationalized in terms of condensation of a single molecule, but not closely packed with a relatively open morphology. The R / n values in Table 1 have been calculated with a contour length L = 16.5 μm pertaining to λ-phage DNA in the B-form. If the DNA molecules have undergone a transition from the B to the A-form during the rinse with ethanol, their contour length decreased by 6% due to the concomitant change in helical pitch from 3.4 to 3.2 nm per turn of the helix. In this case, the values for R n in Table 1 are underestimated by 6%, but this has no effect on our conclusion regarding the single-molecular composition of the toroids.

Besides toroids, we have also observed rod-like condensed structures. The rod-like structures constitute no more than 10% of the total number of condensed structures and are therefore far less abundant. The lengths are in the range 220-300 nm, widths in the range 80-110 nm, and heights around 4 nm. The measured heights indicate that the rod-like structures contain two to three stacked DNA layers. Based on a single circumferentially wrapped DNA molecule, just as a toroidal structure with a collapsed void, the dimensions agree with an inter-axial spacing in the range 2.5 to 3 nm.

The variation in dimensions and the irregularity in condensed morphologies can be understood in terms of the pathway controlled ethanol-induced condensation process. During the rinse with ethanol, which is a poor solvent for DNA, the adsorbed DNA molecules minimize their interaction with the organic solvent by forming a nucleation loop followed by wrapping of the duplex around the nucleation loop in a circumferential manner. A similar mechanism has been proposed for condensation in the bulk phase, but, here, the process is surface-directed because the DNA molecules remain adsorbed at the mica surface.[152] For toroids, the size of the inner diameter is on the order of the

bending persistence length 50 nm, which complies with the bending energy of the nucleation loop on the order of the thermal energy kT. The competition between the unfavorable DNA-solvent interaction and the magnesium ion facilitated DNA-surface interaction eventually results in an overall thin disk-like structure. The toroidal structure is however not perfect; there is a strong variation in height and spread of the adsorbed DNA molecules due to the competing interactions.

The rod-like condensed structures may be formed by a similar mechanism. The condensation process is nucleated by the formation of a nucleation loop, but now the radius of curvature exceeds the bending persistence length and is on the order of 100 to 200 nm. As shown by the aspect ratios in Fig. 5b, the inner voids of larger toroids are increasingly asymmetric and opposing segments of the toroid may not be too far separated across the void. In order to reduce unfavorable DNA-ethanol interaction, but at the cost of extra bending energy at the end-points of the condensate, the larger nucleation loops and/or toroids are likely to collapse in a side-by-side manner and thereby forming rod-like structures. Whether this happens at the nucleation stage or after the toroids have already been formed can unfortunately not be deduced from these imaging experiments.

3.4.Conclusions

It is often, if not always, necessary to spot a highly diluted DNA solution on a surface in order to investigate the properties of single molecules in DNA adsorption studies. We have shown that the resulting DNA morphologies depend on the way the solutions are prepared. If the stock solution is diluted and if the specimens are developed in ultra-pure, deionized water, flat-lying densely packed DNA networks are observed in agreement with earlier observations.[157,158] The height of the segments of the network, as measured with tapping mode atomic force microscopy indicates that the DNA is single-stranded. Since the Watson-Crick double-helical structure of DNA is known to be unstable at minimal ionic strength under salt-free conditions, we suspect that the DNA double helix is (partially) melted in the sample preparation procedure. At the surface, the single DNA strands can hybridize with other strands pertaining to the same or other DNA molecules and thus form a network. This conjecture is supported by the fact that double-stranded, non cross-linked or hybridized DNA molecules are observed if the dilution and development procedures are carried out under TE buffer conditions so that the stability of the double helix is ensured.

The adsorbed single DNA molecules can subsequently be condensed in situ by a brief rinse of the specimens with anhydrous ethanol. It should be noted that the condensation occurs after adsorption of DNA onto the mica and that the process is assisted and directed by the surface. Furthermore, we obtained the condensed structures by a change in solvent quality in the presence of divalent magnesium (magnesium also serves to attach the DNA molecules to the surface). The predominant morphology is a toroid, but a small fraction of rod-like structures was also observed. Analysis of the height and lateral dimensions

shows that the toroids are single-molecular and disk-like with a height of one to two DNA diameters. Similarly thin toroidal structures have previously been observed in nucleoprotamine or cationic silane-induced DNA condensation studies on mica and silicon surfaces, respectively.[155,156] Accordingly, the thin toroid morphology appears to be a general phenomenon of surface-directed condensation, irrespective the nature of the condensing ligands and the specific surface interaction. The rod-like structures may be formed by a side-by-side collapse of the inner (nucleation) loop of the larger toroidal structures. The condensed morphologies are not perfect. There is a strong variation in shape, height, and spread of the adsorbed DNA molecule, which can be attributed to the competing DNA-surface and solvent interactions in the pathway controlled condensation process.

Chapter 4

Fabrication of Poly(dimethylsiloxane) based Biochips for High-Performance Nanofluidics

Abstract

This chapter reports the design, fabrication, and testing of a multilayer polydimethylsiloxane (PDMS) based nanofluidic chip for the investigation of biopolymer behavior in a confined and congested state. The chip contains a set of parallel nanochannels, which are connected through sets of microchannels to two reservoirs. The micro- and nanochannels are located within different layers of the chip and are fabricated with the help of UV and Proton Beam Writing (PBW) lithography technologies, respectively. As determined by the thickness of the SU-8 photoresist layer, the microchannels have a square cross-section of $5 \times 5\ \mu m^2$. The nanochannels have a width in the range of 150 to 500 nm and a depth of 300 nm. Compared to more traditional protocols, our method is relatively easy to implement and allows the fabrication of cheap and reusable polymer-based biochips. The integrated chip was tested by injecting of λ- or T4 bacteriophage DNA molecules into the reservoirs. The DNA molecules were subsequently driven through the nanochannels with the help of an electric field and visualized through the fluorescence of the YOYO-1 staining dye.

4.1. Introduction

Over the decades of its existence, poly(dimethylsiloxane) (PDMS) micro-fluidic devices have progressed from plain microchannels through pneumatic valves and pumps to an impressive set of specialized components organized by the thousands in a large-scale multilayer integrated biochip [167, 168, 171, 172]. The by now well established technology has found successful applications in, among others, protein crystallization, DNA sequencing, nanoliter Polymerase Chain Reaction (PCR), cell sorting and cytometry, nucleic acids extraction and purification, immunoassays, cell studies, and chemical synthesis [173, 174, 175, 176, 186]. A successful performance of such on-chip (bio)chemical analysis depends on the mechanisms of mass transfer: capillary action, electro-kinetics, and molecular diffusion. Despite the numerous applications, our understanding of biomolecular structure and transport at the nanometer sized level is incomplete and deserves further investigation. Furthermore, the confinement of biomolecules in nanochannels adds to the body of experimental techniques for the investigation of single molecules; a field which has proven to be extremely successful in molecular biophysics.

For an investigation of the conformation of DNA molecules confined in nanochannels, we have fabricated PDMS-based biochips, which carry nano- and microfluidic structures. This chapter consists of two parts: (i) the employed technologies for the fabrication of the micro- and nanochannels and (ii) some nanofluidic applications. The first part aims to help the reader to navigate through the large number of technologies which have been utilized in this thesis. The applications

highlighted in the second part illustrate how the nanofluidic devices can be used to study the structure and dynamics of biopolymers.

4.2. Fabrication Technologies

4.2.1. HSQ and SU-8 stamp

The stamp for the nano/micro fluidic device was made in a two-step lithography process. In the first step, a nano-patterned structure was fabricated on Hydrogen Silsequioxane (HSQ) (Dow Coming Co.) photo-resist using proton beam writing (PBW) [168]. In the second step, a microstructure is superposed on this nanostructure utilizing SU-8 (MicroChem) photo-resist and UV lithography. We will describe both steps subsequently.

As illustrated in Fig. 1, the preparation of the HSQ nano-patterned stamp involves the following steps:

- The fabrication process begins with the deposition of a 200 nm thick gold (Au) thin film on a silicon wafer.
- A solution of HSQ in 4-methyl-2-pentanone is wet-spun onto the Silicon/Au wafer in order to form a film with a thickness of 300 nm. The wafer is subsequently baked at 120 ℃ in an oven.
- Patterning of the resist layer by PBW. HSQ is a negative photo-resist, which means that areas of the resist exposed to a beam of protons are strengthened by an increase in chemical bonding among the polymers.
- Development of the exposed resist in isopropanol-water (7:3, IPA) developer

for 10 minutes at room temperature without agitation. This procedure results in the dissolution of any unexposed HSQ material.

Since HSQ is a positive photo-resist material, the stamp carries a positive nano-structure consisting of standing walls with a height of 300 nm and widths of 150, 200, 300, and 500 nm (see Fig. 2).

On top of the HSQ nanostructure, we will now superpose a microstructure manufactured in SU-8. SU-8 is a negative tone, photoresist material based on epoxy resin. Under UV exposure and in the presence of a photo-initiator, the SU-8 molecules form a highly cross-linked network. This cross-linked network cannot be removed by the developer. Due to its low optical adsorption, SU-8 can be patterned using optical lithography to a thickness of hundred micrometers with very high aspect ratios. For the substrate, it is possible to use the above described stamp carrying the HSQ nanostructure. Accordingly, by the combination of the two different lithography processes, i.e., one in HSQ with PBW and another one in SU-8 with UV, it is possible to produce a stamp with a (positive) microstructure superposed on an underlying nanostructure.

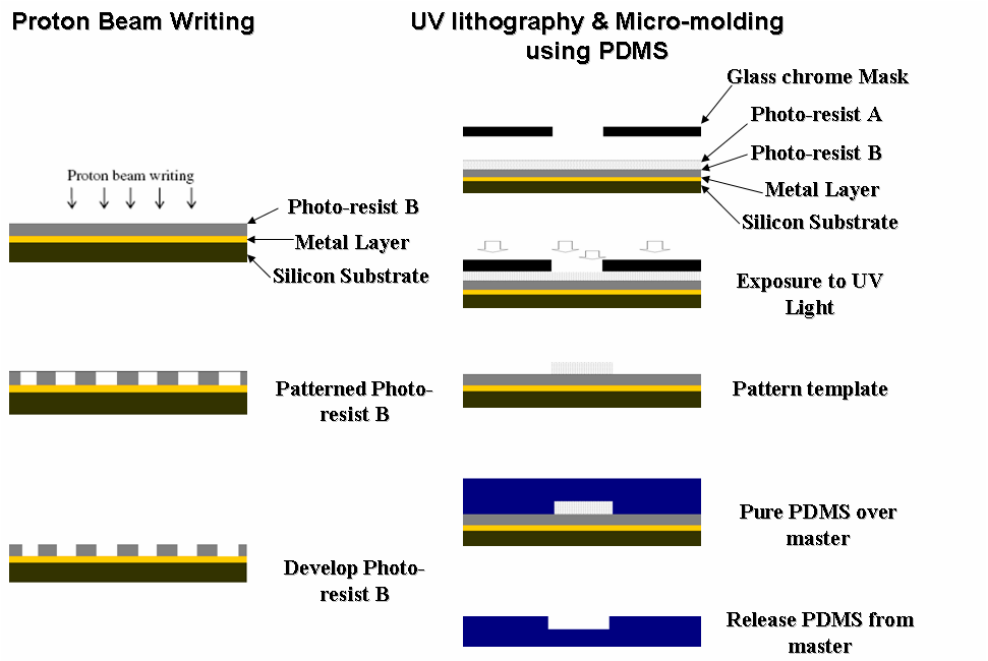

Figure 1. Schematic illustration of the fabrication process of the micro- and nano-fluidic device. (a) Nanostructure patterning in HSQ photoresist by PBW. (b) Superpositioning of the SU8 microstructure on the HSQ nanostructure by UV lithography.

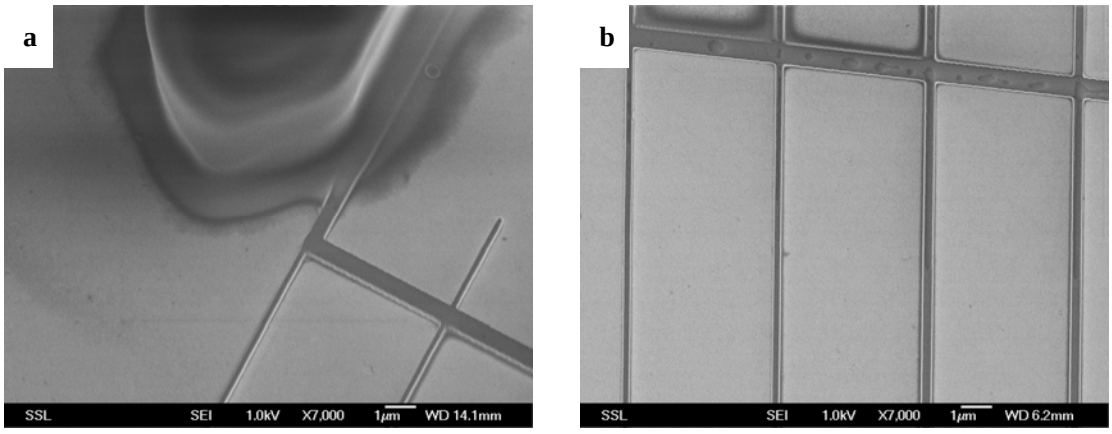

Figure 2. Scanning electron micrographs of a wall array on a gold coated silica wafer. (a) Top view showing the standing microstructure with a cross section and height of about 5 micrometer and an array of standing nanostructures with a width of 300 and 500 nm and a height of 300 nm. (b) Close view of an array of parellel nano-walls with a width of 150 and 200 nm connected by a wall with a width of 500 nm. The height of the nanostructures is 300 nm.

The spin-coating and lithography procedures to produce 5 μm thick SU-8 microstructures superposed on a stamp which bears a HSQ nanostructure include:

- The substrate needs to be preheated on a hot plate at 200 ℃ for 120 s.
- The SU-8 is subsequently spin-coated on the substrate at 2000 rpm for 30 s.
- The SU-8 coated substrate is then baked on a hot plate at 95 ℃ for 120 s in order to evaporate the solvent.
- The nanostructure on the substrate is aligned with the microstructure on the UV mask with an UV mask aligner system. The substrate is exposed to UV light (365 nm) for 30 s.
- The exposed substrate is post-baked at 95 ℃ for 120 s.
- The SU-8 is developed by immersion in SU-9 developer (MicroChem^{TM}) for 120 s, followed by a brief rinse with IPA, then a rinse with deionized water, and eventually drying with a gentle stream of dry nitrogen gas.

Scanning electron micrographs of the resulting stamp are shown in Fig. 2. The images show an array of parallel, nanoscale standing walls fabricated in HSQ and a superposed micronscale 'feeder' wall in SU-8.

4.2.2. Replication

In order to prepare the micro/nanofluidic chip, the stamp is replicated in PDMS. The used elastomer is Sylgard^{TM} 184 from Dow Coring Corporation. It is supplied in a two-parts kit: a liquid silicon rubber base (a vinyl-terminated PDMS) and a catalyst or curing agent (a mixture of a platinum complex and copolymers of methyl

hydrosiloxane). The chemical formula for PDMS is $(H_3C)_3[Si(CH_3)_2O]_nSi(CH_3)_3$, where n is the number of repeating monomer [SiO(CH3)2] units, as shown below:

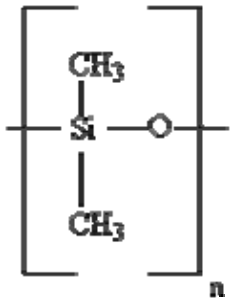

Figure 3. Chemical Structure of poly(dimethylsiloxane) monomer.

The curing agent was added to the PDMS base in a weight ratio of 10:1 and mildly blended to facilitate the dissolution of the catalyst into the base polymer. The mixture was then degassed in a glass desiccator connected to a vacuum pump. The PDMS-catalyst mixture was poured onto the stamp and again degassed to draw out any air bubbles possibly trapped inside the deep and narrow trenches. The PDMS was then cured by placing it in an oven for 12 hours at 65 ℃. The cured PDMS slab was carefully peeled off from the master stamp from the outer edge inwards. The separated PDMS structure was inspected with an optical microscope. Access holes (1 mm in diameter) were punched through each end of the micro-channels using a needle punch (Harris Uni-Core, Jed Pella Inc.).

4.2.3. Air Plasma Treatment

The bonding quality of the PDMS capping layer to a cover glass slide is critical in micro/nano fluidic applications. In general, these devices are designed to process very small quantities of fluids. The pressures exerted on the fluidic channels are inversely proportional to their cross-sectional diameters and can be become become very high. Without a good seal, leakage of fluids will inevitably occur due to a breakdown of the bonding between the PDMS and glass cover slide.

A treatment with oxygen plasma can be used to create an effective bonding of PDMS to glass. The oxygen plasma improves adhesion by removing surface contaminants, by roughening the bonding surfaces, and by chemical modification of surface groups. In particular, the $–O\text{-}Si(CH_3)_2\text{-}$ unit in PDMS can be converted into a silanol group (Si–OH) (see Figure 4). As a result, the PDMS surface changes from hydrophobic to hydrophilic. The oxidized PDMS surface resists adsorption of hydrophobic and negatively charged molecules. Furthermore, they are stable for approximately 30 minutes in air. After this period, the hydrophobicity of the surface is recovered, irrespective whether the medium is vacuum, air, or water. Figure 5 shows the difference in wetting properties of PDMS induced by the plasma treatment.

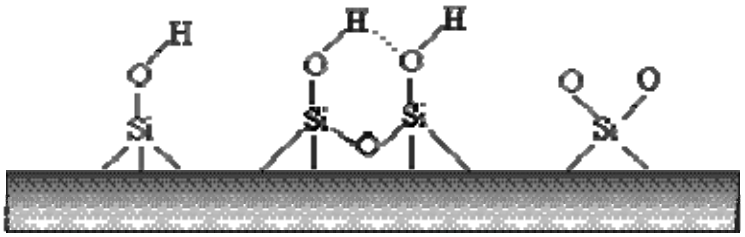

Figure 4. Schematic of the different types of hydroxyl groups on a silica surface

After being peeled off from the master, the PDMS samples were cut into strips of length 10 mm, width 5 mm, and height 2 mm. The strips were then pretreated with air plasma in a cylindrical type glow discharge cell with medium plasma energy (10.5 W) and a radio frequency of 40 kHz. The PDMS strip and glass cover slide were placed between the two electrodes and subjected to the glow discharge for a period of 30 s at an air pressure of 0.3 Torr. After the treatment, the PDMS sample was immediately brought into contact with the glass slide for bonding. The bonding strength was further improved by post-baking the assembly on a hot plate at 85 °C for 120 s.

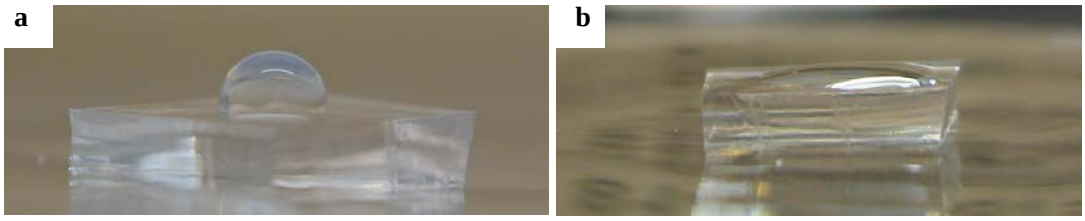

Figure 5. Wetting of PDMS by deionized water. (a) Water droplet on PDMS without air-plasma processing, (b) Water droplet on PDMS following plasma treatment.

4.2.4. Filling the Channels

λ-phage (48,502 bp; BioLabs) and T4 DNA (165,600 bp; Nippon Gene) were suspended in 10 ml of 5 times TBE buffer, which is made of 45 mM Tris base, 1 mM EDTA and 45 mM boric acid. The DNA solution was incubated for 1 hour at room temperature. DNA was visualized with an inverted fluorescence microscope (Olympus IX71) equiped with an intensified CCD camera (Olympus DP 70). The DNA was stained with the bisintercalating dye YOYO-1 (Invitrogen, Carlsbad, CA)

(488 nm excitation). Various dye-to-basepair ratios were employed to investigate the effect of intercalation on the extension of DNA (these results will be presented in Chapter 6). To obtain a good view of DNA molecules during transport in channels, a maximum dye-to-base pair ratio of 4 to 1 was used. The DNA molecules were loaded into the microchannels through capillary action and driven through the nanochannels with the help of an electric field. For this purpose, platinum electrodes were immersed into the two reservoirs and connected to a high-voltage power supply (PowerPAC 300, BioRAD) ranging from 10 to 200 V (Fig. 6).

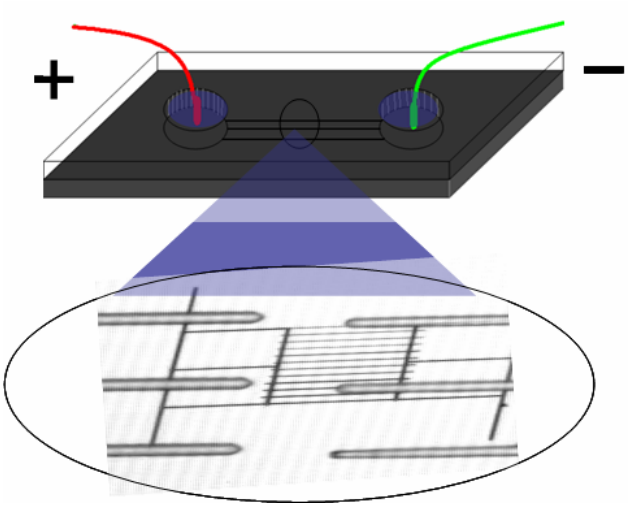

Figure 6. Schematic diagram of the nanofluidic system. Two platinum electrodes were immersed into the two reservoirs, so that the DNA molecules can be driven into the nanochannels with the application of an electric field.

4.3. Applications

4.3.1. DNA Extension

We have investigated the extension of single DNA molecules confined in the nanochannels. In Figure 7, we show the typical distribution in the extension as obtained from over 1000 individual measurements. Due to the photo-bleaching effect of the fluorescence dye, about 120 DNA molecules can be visualized by using a single biochip. Accordingly, in order to measure the extension of over 1000 individual molecules, we have used eight replicated biochips. As can be seen in Figure 7, the distribution is approximately Gaussian and is a bit skewed in the direction of the smaller extensions. Note that the distribution does not refer to statistical error in the measurement, but rather to the distribution in extension resulting from a large number of measurements of individual molecules. The average values and the widths of the distribution, as a function of the ionic strength of the supporting medium, will be discussed in Chapter 6. Here, we will further discuss the effect of the DNA contour length on the extension of DNA molecules confined in a nanochannel.

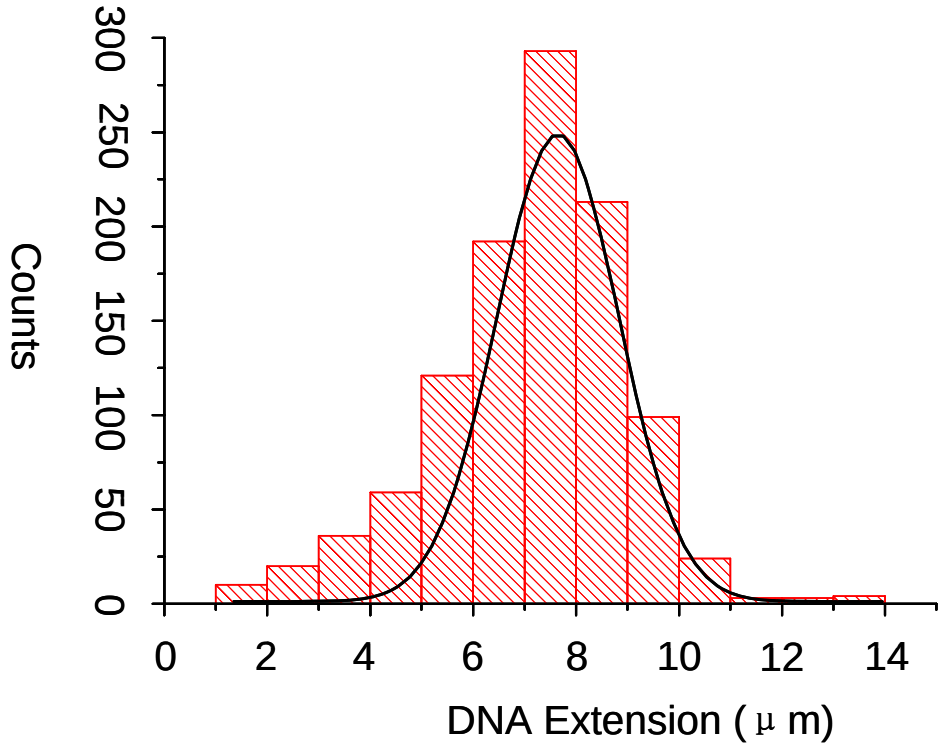

Fig. 7 Distribution of the extension of individual DNA molecules confined in 300 by 300 nm^2 nanochannels resulting from the measurement of over 1000 molecules. The images were analyzed using Image-J software (http://rsb.info.nih.gov/ij/). The solid line represents a fit of a Gaussian distribution with average extension 7.6 micrometer and width 2.8 micrometer. The DNA molecules are immersed in 5 times TBE buffer.

To estimate the relationship between DNA extension and contour length, we have measured the extension of λ-phage (48,502 base-pairs) and T4 (165,600 base-pairs) DNA in 5 times TBE. The elongation of DNA is greatly enhanced when the scale of the confinement geometry is smaller than the radius of gyration of the free molecule (around 1.5 micrometer for T4 DNA). Brochard and de Gennes developed a scaling argument, which explains the stretching under confinement within a channel with a diameter less than the radius of gyration of the free DNA coil, but larger than the DNA persistence length [218,199]. In this model, a self-avoiding chain is

considered as a series of blobs packed in a linear array. As a key result, the relative extension scales as

$$R_{\parallel}/L \simeq \left(D/L_p\right)^{-2/3} \quad (1.1)$$

with L being the contour length, L_p the persistence length, and D the cross-sectional diameter of the nanochannel. For asymmetric channel cross-sections, we have taken the square root of the depth times the width as the effective channel cross-sectional diameter.

Figure 8a shows some fluorescence images of T4 DNA confined in nanochannels of various cross-sections. It is clear that the DNA molecule becomes more extended with decreasing value of the cross-sectional diameter. Figure 8b shows a log-log plot of the extension of λ-phage and T4 DNA extensions divided by their respective contour lengths ($R_{\parallel}/L$) versus the geometric average of the diameter divided by the persistence length (D/L_p). In this calculation, the persistence length L_p was taken to be 50 nm, i.e. the commonly accepted value for DNA in the B-form in a medium of high ionic strength. It should be noted that at the saturating intercalation level (4 basepairs per YoYo-1 molecule) the contour length of the T4-DNA molecule has increased from 56.6 to 73.2 micrometer and the contour length of λ-phage DNA (nominally 16.2 um) been reported as 21 micrometer [169,170]

. Divided by L_{T4} = 73.2 micrometer and L_λ = 21 micrometer, the relative extensions of λ-phage and T4 DNA extensions are in reasonable agreement, which is in accordance with the fundamental assumption of the scaling theory that the polymer can be seen as a sequence of blobs packed in a linear array. The blobs are repulsive

due to the effects of self avoidance. Furthermore, in the double logarithmic representation, a linear scaling of the relative extension versus the channel diameter is observed. The fitted value of the slope is -0.703 $\pm$ 0.09, which is close to the value predicted by the scaling theory -2/3.

. Each blob fluctuates with a second moment of its distribution of mass $\left\langle \delta R_b^{\,2} \right\rangle = D^2$. For a string of independently fluctuating blobs, each with a second moment in size D^2, the second moment of the extension is given by $\left\langle \delta R_{\parallel}^{\,2} \right\rangle \simeq L L_p^{2/3} D^{1/3}$ and the standard deviation in the distribution of the relative extension takes the form

$$\left\langle \delta R_{\parallel}^{\,2} \right\rangle^{1/2} \Big/ L \simeq L^{-1/2} L_p^{1/3} D^{1/6} \qquad (1.2)$$

The values of the widths in the distribution as derived from the experiments and displayed in Figure 8 are in fair agreement with this scaling result. With increasing contour length, the distribution is expected to become sharper. This seems not to be born out by the experiments. On the other hand, we observe that the width in the distribution does not depend on the channel diameter to a significant degree, which agrees with the weak $D^{1/6}$ scaling. We will present a better estimate of the relative extensions and widths of the distribution in Chapter 6 and show that the blob model gives a description of the data.

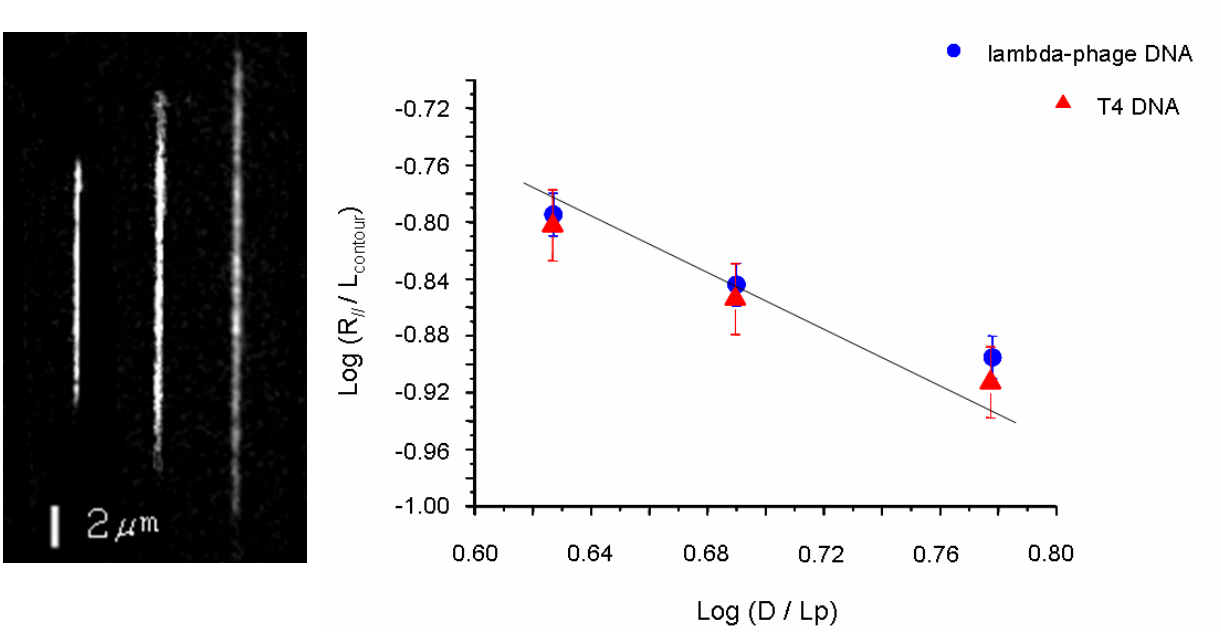

Figure 8. (a) Fluorescence images of T4 DNA molecules in nanochannels with 300 × 150 nm^2, 300 × 200 nm^2 and 300 × 300 nm^2 cross-section (right to left). (b) Relative DNA extension $R_{\parallel}/L$ in 300 × 150 nm^2, 300 × 200 nm^2 and 300 × 300 nm^2 channels against the scaled channel cross-sectional diameter D/L_p . The circles refer to λ -phage DNA, whereas the triangles pertain to the T4 DNA. The bars denote the width of the distribution following from the measurement of at least 200 different DNA molecules for each data point. The solid line refers to the prediction of the scaling theory -2/3.

4.3.2.Transport of DNA Molecules in Nano-channels

λ-phage DNA molecules were loaded into the reservoirs through capillary action. As imaged by fluorescence microscope (FM), the negatively charged DNA was driven into the microchannels by the electric field. This means that the flow properties are determined by the properties of both the biopolymer chains (contour length and charge densities etc.) and buffer conditions (ionic strength etc.). Without the application of an electric field, the DNA molecules diffuse into the micro-channels from the connected reservoirs. When a dc (direct current) voltage (~10 V) is applied, DNA molecules are driven from the wider microchannels into the narrower nanochannels. As illustrated in Fig. 10, a λ -phage DNA molecule is driven 'around the corner' from a 500 into a 200 nm wide channel in the direction of the electric field. The molecule clearly stretches under the electric force and relaxes to its equilibrium extension once the field is switched off.

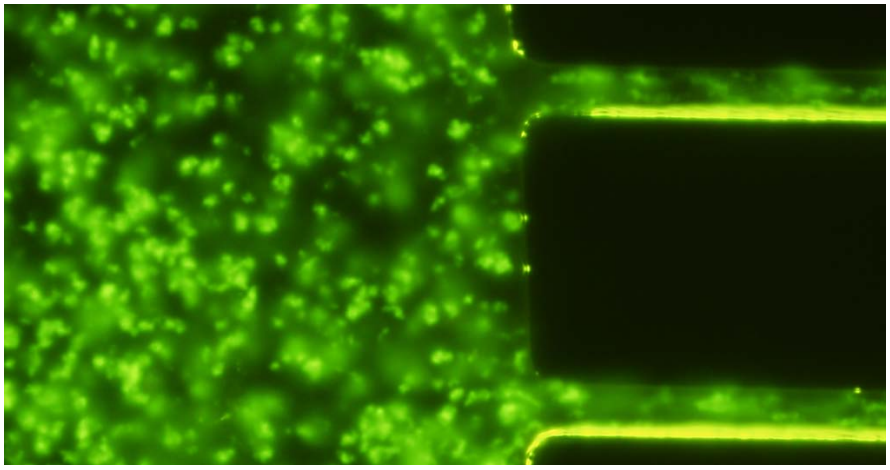

Figure 9. Fluorescence images of λ-phage DNA molecules at the interface of the microchannels and the reservoir. The molecules enter the microchannels by diffusion and/or coherent transport by the application of an electric field.

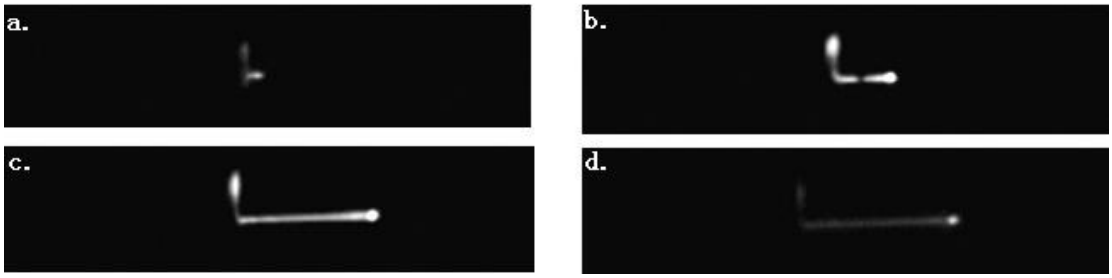

Figure 10. A T4 DNA molecule electrophoretically driven from a 500 into a 200 nm wide nanochannel. The molecule stretches as the electric force pulls in the direction of the electric field.

4.4. Conclusion

In summary, we have presented the fabrication of biochips by replica molding in PDMS and plasma-assisted bonding to glass using a two-step lithography process. As some examples of possible biophysically inspired experiments, we have shown the extension and kinetics of single DNA molecules confined in homogenous micro- and nanochannels. The transparency of PDMS allows direct observation of fluorescence stained DNA molecules in the nanofluidic device with optical microscopy. Potential applications of this biochip were tested by inserting phage DNA molecules in a complicated network of micro- and nanochannels. The need for an electric driving force at the early stage of the injection is due to the presence of some air bubbles inside the channels. These bubbles are driven out once rhe DNA molecules are transported through the channels with a low applied dc voltage (less than 10 V). The unique features of the cheap PDMS-based biochip make it possible to study the beahviour of single biomolecules, including DNA and DNA-protein interactions. In the next Chapter, we will further elaborate on this by the systematic investigation of the effect of ionic strength on the conformation of DNA.

Chapter 5

Effects of electrostatic screening on the conformation of single DNA molecules confined in a nanochannel

Abstract

Single T4-DNA molecules were confined in rectangular-shaped channels with a depth of 300 nm and a width in the range 150-300 nm casted in a poly(dimethylsiloxane) nanofluidic chip. The extensions of the DNA molecules were measured with fluorescence microscopy as a function of the ionic strength and composition of the buffer as well as the DNA intercalation level by the YOYO-1 dye. The data were interpreted with scaling theory for a wormlike polymer, including the effects of confinement, charge, and self-avoidance. It was found that the elongation of the DNA molecules with decreasing ionic strength can be interpreted in terms of an increase of the persistence length. Self-avoidance effects are moderate due to the small correlation length imposed by the channel cross-sectional diameter. Intercalation of the dye results in an increase of the DNA contour length and a partial neutralization of the DNA charge, but besides effects of electrostatic origin it has no significant effect on the bare bending rigidity. In the presence of divalent cations, the DNA molecules were observed to contract, but they do not collapse into a condensed structure. It is proposed that this contraction results from a divalent counterion mediated attractive force between the segments of the DNA molecule.

5.1.Introduction

In recent years, micro- and nanofluidic devices have been developed and utilized for the analysis of the properties of long biopolymers including DNA. Different architectures have been designed, including entropic trap arrays, micro and nanopillar arrays, nanopores and nanochannels.[208,209,210,211] The nanofluidic devices are complementary to other single molecule manipulation techniques such as those based on optical tweezers.[212,213,214] In the case of confinement in a long and straight nanochannel, a long biomolecule elongates because of the restriction in configurational degrees of freedom imposed by the channel walls. This effect is similar to the situation in a single molecule stretching experiment, in which the biomolecule is subjected to a tensional force. The role of the strength of the stretching force is the same as the value of the cross-sectional diameter of the nanochannel, in the sense that both a stronger force and a decrease in diameter result in a more extended conformation. Besides the similarities of these single-molecule manipulation techniques, there are also some important differences. For instance, in the confinement experiment there is no need for chemical modification to attach the biomolecule to molecular pincers. Furthermore, the stretching data are usually interpreted with the wormlike Gaussian chain model.[215] The Gaussian chain model does not include the effects of self-avoidance or, in other words, excluded volume effects. In the analysis of the confinement experiment, the latter effects are included in a straightforward way, just as in the case of the description of the swelling of a single polymer coil in a good solvent.

The statistics of a DNA molecule confined in a nanochannel depends on the ratio of the cross-sectional channel diameter and the DNA persistence length.[216] In a narrow channel, with a width less than the persistence length, the molecule will undulate inside the channel and will only bend when it bounces off the wall.[217] In the present contribution, the channel diameters exceed the persistence length, but they are smaller than the radius of gyration of the unconstrained, free DNA coil. In the latter situation, the elongated DNA molecule inside the channel remains coiled at all length scales.[218] The advantage of such configuration is that the data can be interpreted using well established polymer theory, including the effects of the local bending rigidity (persistence length) and interaction of spatially close segments which are separated over a long distance along the contour (excluded volume). The scaling relations for the extension of DNA molecules confined in nanochannels of various diameters have been verified by Reisner et al.[219] The effects of electrostatic screening on the conformation of DNA molecules inside nanoslits and nanochannels of various dimensions also have been reported before.[220,221] In general, the DNA molecule has been observed to stretch out with decreased screening of Coulomb interaction. The variation in extension with the ionic strength of the supporting medium was interpreted in terms of a variation in the persistence length. Contradictive results were reported however for the relative importance of excluded volume effects. Accordingly, we thought it of interest to reinvestigate the effects of electrostatic screening and, in particular, to gauge the relative importance of self-avoidance with respect to the bending rigidity for the understanding of the

conformational response to changes in ionic environment.

Most, if not all of the previously reported experiments on DNA were done using nanofluidic devices made out of fused silica. We have used a lithography process with proton beam writing to fabricate a nanopatterned stamp.[222,223] The stamp was subsequently replicated in poly(dimethyl siloxane) (PDMS) polymer, followed by curing and sealing with a glass slide.[224,225] In order to visualize the DNA molecules with fluorescence microscopy it is necessary to stain them with a dye. We have used YOYO-1, which bis-intercalates between three adjacent base-pairs with a concomitant increase in DNA contour length. The maximum level of intercalation is four base-pairs per dye molecule. Furthermore, YOYO-1 carries four positive charges, so that it also partially neutralizes the DNA phosphate charge (for maximum loading the DNA charge is thus reduced by a factor of two). We have systematically investigated the effect of the YOYO-1 intercalation level on the DNA conformation. In particular, we have explored the minimum level of staining in order to obtain the structural DNA properties as close to the native state as possible and, yet, to achieve a sufficiently intense fluorescence signal for accurate imaging. At higher staining levels, we will show that the effect of intercalation can be accounted for by the partially compensating effects of the increase in contour length and the decrease in persistence length due to the reduced net DNA charge.

Most of our experiments were done using conventional buffers, which primarily contain monovalent ions. In order to investigate a possible dependence of the DNA conformation on the ionic composition of the buffer, we have done experiments using

both a high (Tris-HCl) and a low (Tris-boric acid) ionic strength solvent medium. Furthermore, we have investigated the effects of divalent magnesium, calcium, and the polyamine putrescine on the extension of the DNA molecules inside the nanochannels. The changes in DNA conformation in response to changes in ionic environment were evaluated using screened electrostatics, based on an effective DNA charge density following from the solution of the non-linear Poisson–Boltzmann equation for a rod-like polyelectrolyte immersed in an excess of mono- or divalent salt. As we will see shortly, for the (primarily) monovalent buffer systems this procedure gave quite satisfactorily results. In the case of the divalent ions significant discrepancies were observed, which cannot be reconciled with the theory for a wormlike polymer in a good solvent. We tentatively explain these discrepancies in terms of a divalent counter-ion mediated attraction between DNA segments, which is not predicted by the conventional mean-field theory.

5.1.1. THEORY

5.1.1.1. Confinement in a nanochannel

The conformation of a DNA molecule confined in a channel depends on, among others, the channel diameter D and the DNA persistence length L_p.[216,218,226] In a narrow channel with $D < L_p$ the molecule will be aligned and takes a highly extended conformation. In the present contribution, the channel diameters are in the range 150 to 300 nm, whereas the persistence lengths are between, say 50 and 150 nm. Furthermore, the size of the free DNA coil, as characterized by its radius of gyration

R_g, is larger than the channel diameter so that $L_p < D < R_g$ (R_g = 1.4 μm for T4-DNA in 10 mM salt). In this situation, the DNA molecule coils inside the channel, but it will be anisotropic with a certain elongation in the longitudinal direction. As we will see shortly, the elongation depends on the channel diameter and screening conditions in the supporting buffer medium. For now, we will ignore specific interaction between the DNA molecule and the wall of the channel. All derived properties of the confinement are thus related to the restriction in configurational degrees of freedom and screening of excluded volume interactions.

In de Gennes' scaling approach, the DNA molecule inside the channel is considered as a linear sequence of sub-coils of uniform size.[216,218] These sub-coils are commonly referred to as blobs. Within the blobs the DNA molecule is thought to be unaffected by the presence of the channel walls. Furthermore, excluded volume effects are screened beyond the blob size, because segments pertaining to different blobs can not form contact pairs. Successive blobs have a second virial coefficient of repulsive interaction of the order of their volume and, hence, they are packed into a linear array (for a discussion of the free energy of confinement see below). The size of the blobs is characterized by their radius of gyration R_b, which should be on the order of the cross-sectional diameter of the channel (do not confuse R_b with the radius of gyration of the free DNA coil R_g). In the scaling treatment, the exact relationship between R_b and D is unknown. We simply assume a linear dependence $D = CR_b$ with C being an adjustable parameter on the order of unity. The parameter C is universal, in the sense that its value should not depend on the chain statistics inside the blobs. It

might include however certain wall-induced effects such as depletion at the wall interface.[227] If the contour length stored in a single blob is given by L_b, the total number of blobs in the aligned sequence of blobs is L / L_b with L being the total contour length of the DNA molecule. The average relative extension in the longitudinal direction of the channel then takes the form $R_{\|} / L = D / L_b = CR_b / L_b$. Each blob fluctuates with a second moment of its distribution of mass $\left\langle \delta R_{\|}^{\,2} \right\rangle = R_b^{\,2}$. For a string of L / L_b independently fluctuating blobs, each with a second moment in size $C^2R_b^2$, the second moment of the extension is given by $\left\langle \delta R_{\|}^2 \right\rangle = C^2 R_b^2 L / L_b$.

The relationship between the blob size R_b and the contour length L_b depends on the chain statistics. Inside the blobs the DNA chain is swollen due to excluded volume interactions. Self-avoidance can be taken into account by defining a swelling factor α_s, which relates the radius of gyration of the swollen blob to the one pertaining to the hypothetical unperturbed Gaussian blob $R_b = \alpha_s R_b^0$. The swelling factor α_s is related to the excluded volume expressed in terms of the parameter [21]

$$z = \frac{3}{16}\left(\frac{3}{\pi}\right)^{1/2}\left(\frac{L_b}{L_p}\right)^{1/2} D_{eff} / L_p \qquad (1)$$

The parameter z is proportional to the scaled effective diameter of the DNA molecule D_{eff} / L_p and the square root of the number of persistence length segments inside the blob $\left(L_b / L_p\right)^{1/2}$. For DNA confined in nanochannels, the values of z are typically less than 0.45. For such small values of z , the swelling factor α_s is given by the series expansion up to and including second order in z:

$$\alpha_s^2 = 1 + 1.276z - 2.082z^2 \qquad (2)$$

For a long Gaussian chain, the unperturbed radius of gyration of the coil is given by $\left(R_b^0\right)^2 = L_b L_p / 3$. However, due to the relatively small number of persistence length segments, inside the blob the limiting long chain expression does not suffice. It is our contention that for quantitative calculations it is essential to use the full Benoit-Doty equation for the unperturbed radius of gyration of the relatively short section of the DNA molecule within the blob [230]

$$\left(R_b^0\right)^2 = \frac{L_p}{3L_b^2}\left[L_b^3 - 3L_b^2 L_p + 6L_b L_p^2 - 6L_p^3\left(1 - \exp\left(-\frac{L_b}{L_p}\right)\right)\right] \tag{3}$$

For a given channel diameter D, persistence length L_p , and effective diameter D_{eff}, the contour length stored in the blob L_b can be obtained by numerically solving $D = \alpha_s C R_b^0$. The average of the relative extension then follows from

$$R_{\|} / L = D / L_b = \alpha_s C R_b^0 / L_b \tag{4}$$

with the values for α_s and R_b^0 given by Eq. (2) and (3), respectively. The width of the distribution in relative extension following from a large number of measurements of individual molecules takes the form

$$\left\langle \delta R_{\|}^2 \right\rangle^{1/2} / L = D / (L L_b)^{1/2} = \alpha_s C R_b^0 / L_b \tag{5}$$

It is interesting to compare the extension of a DNA molecule confined inside a nanochannel with the one of a molecule subjected to a tensional force f in a tweezers set-up. In the single molecule stretching experiment, the blob size is determined by the balance of the elastic stretching energy and the thermal energy $fR_b = kT$. With $D=CR_b$ we obtain $f = CkT / D$. With C of the order of unity, it follows that confinement inside a channel with a cross-sectional diameter of about 200 nm corresponds with a stretching force of about 0.02 pN.

For a polymer chain in a relatively wide channel, the free energy of confinement is related to the channel diameter D and the radius of gyration of g R of the free coil through the scaling relation [216,218]

$$F_{conf} = kT(R_g / D)^{5/3} \tag{6}$$

Note that the free, unconstrained DNA coil exerts a full excluded volume effect and its radius of gyration is given by the Flory expression $R_g \simeq \left(L_p D_{eff}\right)^{1/5} L^{3/5}$ (the proportionality factor is around 0.75). The repulsive energy per blob follows from conf $DF_{conf} / R_{\|}$ and should be constant and on the order of the thermal energy kT .

5.1.1.2. DNA as a polyelectrolyte

DNA is a polyelectrolyte and both the persistence length and the effective diameter depend on the electrostatic screening conditions of the supporting buffer medium.[216] In the Debye-Hückel approximation, the effective diameter of a rodlike persistence length segment takes the form

$$D_{eff} = D_0 + k^{-1}\left(\ln \omega' + \gamma - 1/2 + \ln 2\right) \tag{7}$$

with $\omega' = \omega \exp\left(-kD_0\right)$ and $\omega = 2\pi v_{eff}^2 l_B k^{-1}$.[216,228] Here, D_0 is the bare diameter (2 nm for DNA in the B-form), γ denotes Euler's constant, and ν_{eff} is the effective number of charges per unit contour length of the DNA molecule. The electrostatic screening length κ^{-1} is given by $k^2 = 8\pi l_B \mu$ with μ being the ionic strength of the solvent medium and the Bjerrum length $l_B = e^2 / 4\pi\varepsilon kT$. Electrostatic interaction also modifies the bending rigidity of the DNA molecule, i.e. its persistence length. In the Odijk-Skolnick-Fixman theory, the total persistence length

$$L_p = L_p^0 + L_p^e \tag{8}$$

is given by the sum of the bare and the electrostatic part.[231,232] For DNA in the B-form, the value of the bare persistence length is around 50 nm.[212,213,214] The electrostatic part also has been derived in the Debye-Hückel approximation by considering the electrostatic energy cost of bending a wormlike chain

$$L_p^e = \nu_{eff}^2 l_B / \left(4k^2\right) \tag{9}$$

The electrostatic persistence length depends on the screening conditions of the supporting medium through the electrostatic screening length κ^{-1} as well as the effective number of charges per unit contour length of the DNA molecule ν_{eff}.

The key parameter in the calculation of the effective diameter and the electrostatic contribution to the persistence length is ν_{eff}. The latter parameter was obtained from the numerical solution of the non-linear Poisson-Boltzmann equation for a cylindrical polyelectrolyte in excess monovalent and/or divalent salt using a fourth order Runge-Kutta method.[216] Note that the value of ν_{eff} depends on the screening conditions of the supporting medium due to the high non-linearity in the inner double layer region. In our fluorescence imaging experiments we have stained the DNA molecules with the YOYO-1 dye. Each YOYO-1 molecule carries four positive charges, so that the net DNA charge is substantially reduced for higher degrees of intercalation (our highest employed intercalation level was four base-pairs per YOYO-1 molecule). Furthermore, YOYO-1 increases the contour length of the DNA molecule by 0.4 nm per dye molecule.[233,234,235] Both the charge neutralization effect and the increase of the contour length by the staining dye were included in our

calculations of the effective diameter and electrostatic persistence length.

Fig. 1 displays the calculated D_{eff} and L_p as a function of the ionic strength of the supporting medium. In accordance with our experimental conditions, these calculations were done for an intercalation level of 23 base-pairs per YOYO-1 molecule and for a buffer composed of monovalent ions only. In the case of a buffer with added divalent salt, we have obtained similar results by solving the non-linear Poisson-Boltzmann equation for the relevant mixture of mono- and divalent ions. With decreasing ionic strength and hence decreased screening of electrostatic interaction both the persistence length and the effective diameter increases. Eventually, for very low ionic strength less than, say, 0.3 mM the values of these structural parameters become on the order of the width of our narrowest channel (150 nm). For a fixed ionic strength of the supporting buffer (μ = 0.61 mM), the effect of the level of intercalation is displayed in Fig. 2. With increased staining levels (less base-pairs per YOYO-1 molecule) both D_{eff} and L_p decreases due to concomitant charge neutralization and the increase of the DNA contour length (decrease in linear DNA charge density). Note that in the theoretical calculations the value of the bare persistence length was kept fixed at 44 nm in accordance with the experimental observations to be discussed below. All variations in the structural parameters come from variation in the buffer screening conditions and the DNA charge density through intercalation of the YOYO-1 dye.

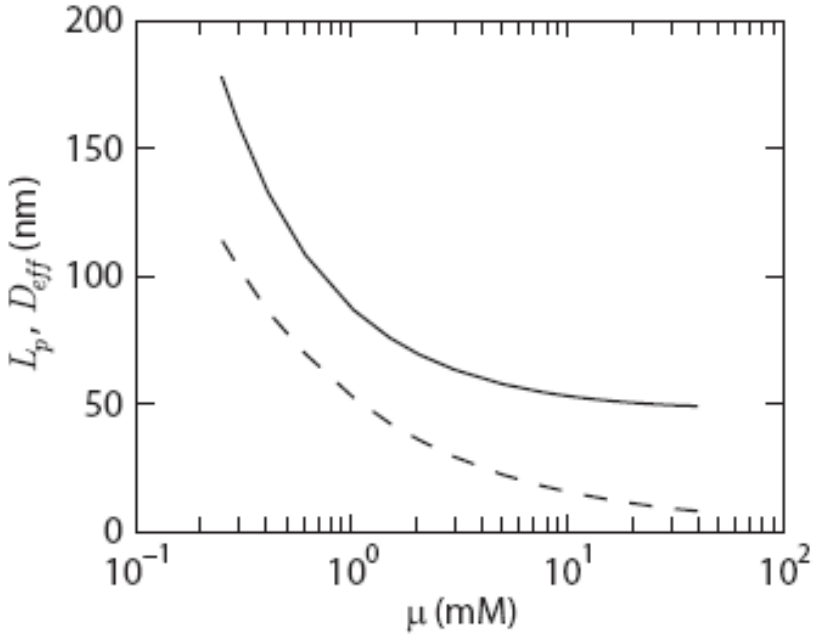

Fig. 1 Persistence length L_p (solid curve) and effective diameter D_{eff} (dashed curve) versus the ionic strength μ of the buffer medium calculated with the effective number of charges per unit DNA length from the numerical solution to the non-linear Poisson-Boltzmann equation for DNA in the B-form and 23 base-pairs per YOYO-1 molecule (bare diameter eter D_0 = 2 nm and bare persistence length 0 44 L_p = nm).

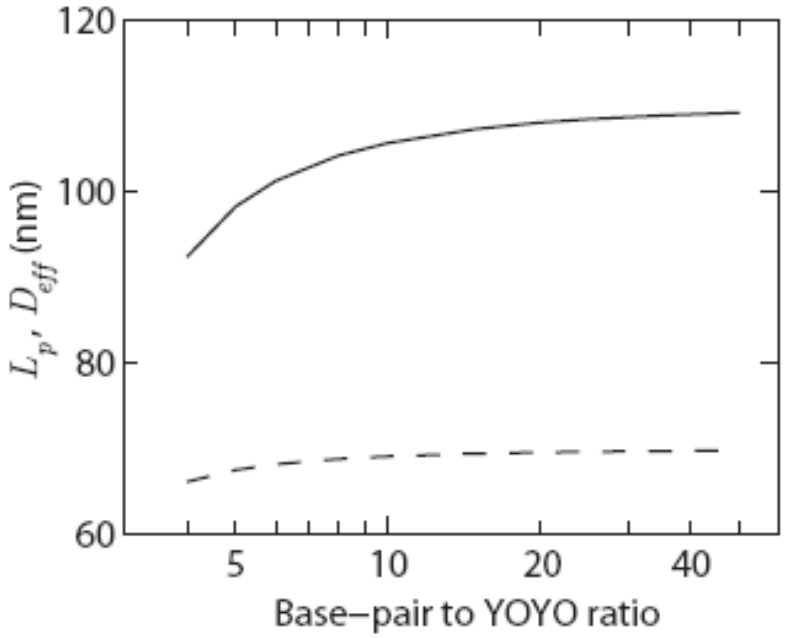

Fig. 2 Persistence length L_p (solid curve) and effective diameter D_{eff} (dashed curve) versus the number of base-pairs per YOYO-1 molecule calculated with the effective number of charges per unit DNA length from the numerical solution to the non-linear Poisson-Boltzmann equation for DNA in the B-form in 1/50×TBE buffer (ionic strength μ = 0.61 mM).

5.2. Experimental Section

5.2.1.Fabrication of the nanofluidic chip

The nanofluidic device was made by replication in PDMS of a patterned master stamp. The stamp was fabricated in HSQ resist (Dow Corning, Midland, MI) using a lithography process with proton beam writing.[222,223] A scanning electron microscopy image of the HSQ stamp bearing the positive nanostructures is displayed in Fig. 3a. The image shows two channel wall pairs with 150 and 200 nm width, respectively (a third channel structure with 300 nm width is outside the field of view). The 300 nm height of the positive channel structures on the stamp was measured with atomic force microscopy (Dimension 3000, Veeco, Woodbury, NY). The stamp was replicated in PDMS followed by curing with a curing agent (Sylgard, Dow Corning).[224,225] An atomic force microscopy image of a section of the negative PDMS replica showing 200 nm wide channels is displayed in Fig. 3b. Finally, the PDMS replica was sealed with a glass slide after both substrates have been plasma oxidized (Harrick, Ossining, NY). The widths of the channels in the PDMS replica were measured with atomic force microscopy and the values agreed with those obtained from the scanning electron microscopy images of the HSQ master stamp. The nanochannels were rectangular-shaped and have a depth of 300 ± 5 nm and a width of 150 ± 5, 200 ± 5, and 300 ± 5 nm, respectively. More details about the chip design and fabrication will be published elsewhere.

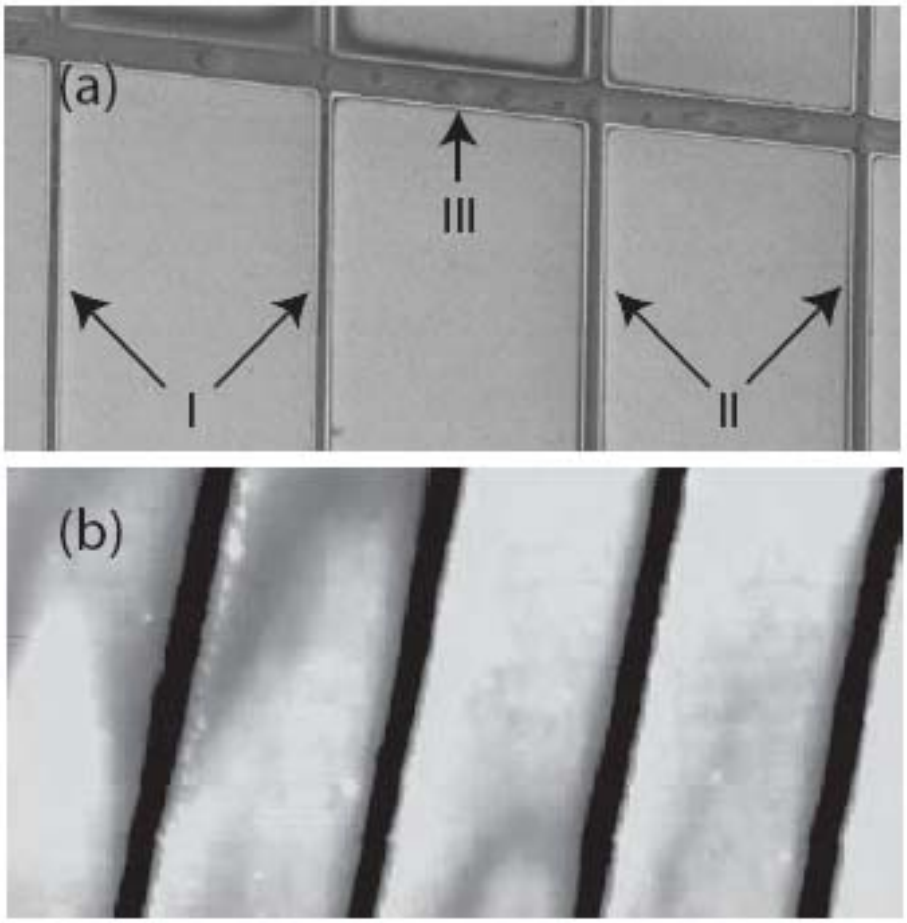

Fig. 3 (a): Scanning electron microscopy image of the HSQ master showing a positive standing channel structure with a width of 150 (I) and 200 (II) and a uniform height of 300 nm (the height was determined by atomic force microscopy). Feature III is a 500 nm wide 'feeder' channel. (b): Atomic force microscopy image of the PDMS replica showing a set of parallel channels with a width and depth of 200 and 300 nm, respectively.

5.2.2.DNA sample preparation

T4 GT7 DNA (T4-DNA, 165.65 kbp) and λ-phage DNA (λ-DNA, 48.502 kbp) were purchased from Nippon Gene, Tokyo and New England Biolabs, Ipswich, MA, respectively, and used without further purification. YOYO-1 fluorescence staining dye was purchased from Invitrogen, Carlsbad, CA. Water was deionized and purified by a Millipore system and had a conductivity less than 1×10^{-6} $\Omega^{-1}cm^{-1}$. Samples were prepared by dialyzing solutions of T4-DNA against the relevant buffer solutions in micro-dialyzers. The buffer systems were Tris-borate/EDTA (TBE), Tris/HCl (T), or TBE with added $MgCl_2$, $CaCl_2$ or putrescine-Cl_2 (TBE/Mg, TBE/Ca, or TBE/Pu, respectively). After dialysis, the T4-DNA was stained with YOYO-1 and diluted with the relevant buffer to a final DNA concentration of 0.008 g/L. The dye intercalation ratio was 4.0, 5.7, 12, 15, 23, or 46 base-pairs per YOYO-1 molecule. In TBE, the final buffer concentrations were 1/100, 1/75, 1/50, 1/30, 1/15, 1/3, and 1×TBE (1×TBE is 90 mM Tris, 90 mM boric acid, and 2 mM EDTA, pH 8.5). For the relatively high ionic strength T buffer system, the concentrations were 1/10, 1, and 10×T (1×T is 10 mM Tris adjusted with HCl to pH 8.5). The TBE/Mg, TBE/Ca, and TBE/Pu buffer systems were composed of 1/100×TBE with 0.09, 0.56, and 3.33 mM added $MgCl_2$, $CaCl_2$, or putrescine-Cl_2. We also prepared a matching sample pair of T4-DNA and λ-DNA with an intercalation ratio of 4.0 base-pairs per YOYO-1 molecule immersed in 5×TBE buffer. The ionic strengths and buffer compositions were calculated with the Davies equation for estimating the activity coefficients of the ions. The utilized pKa's are 10.17, 6.11, 2.68, 2.00 for EDTA, 13.80, 12.74, and 9.24

for boric acid, and 8.08 for Tris.

5.2.3.Fluorescence imaging

The YOYO-1-stained DNA molecules dispersed in the relevant buffer were loaded into two reservoirs connected by the nanochannels. The DNA molecules were subsequently driven into the channels by an electric field. For this purpose, two platinum electrodes were immersed in the reservoirs and connected to an electrophoresis power supply with a voltage in the range 10-30 V (Bio-Rad, Hercules, CA). Once the DNA molecules were localized inside the channels, the electric field was switched off and the molecules were allowed to relax to their equilibrium state for at least 60 seconds. The fluorescence of the stained DNA molecules were visualized with an Olympus IX71 inverted fluorescence microscope equipped with a 100 W mercury lamp, a UV filter set and a 100 times oil immersion objective. The exposure time of the YOYO-1 fluorescence was controlled by a UV light shutter. Images were collected with a charge coupled device (CCD) camera (Olympus DP 70) and the extension of the elongated DNA molecules inside the channels was measured with the public domain software ImageJ (http://rsb.info.nih.gov/ij/). Reported relative extensions, i.e. extensions divided by the contour length of the DNA molecule, represent an average of at least 200 individual measurements. A montage of fluorescence images of T4-DNA in 300×300 nm^2 channels under various TBE buffer conditions is shown in Fig. 4.

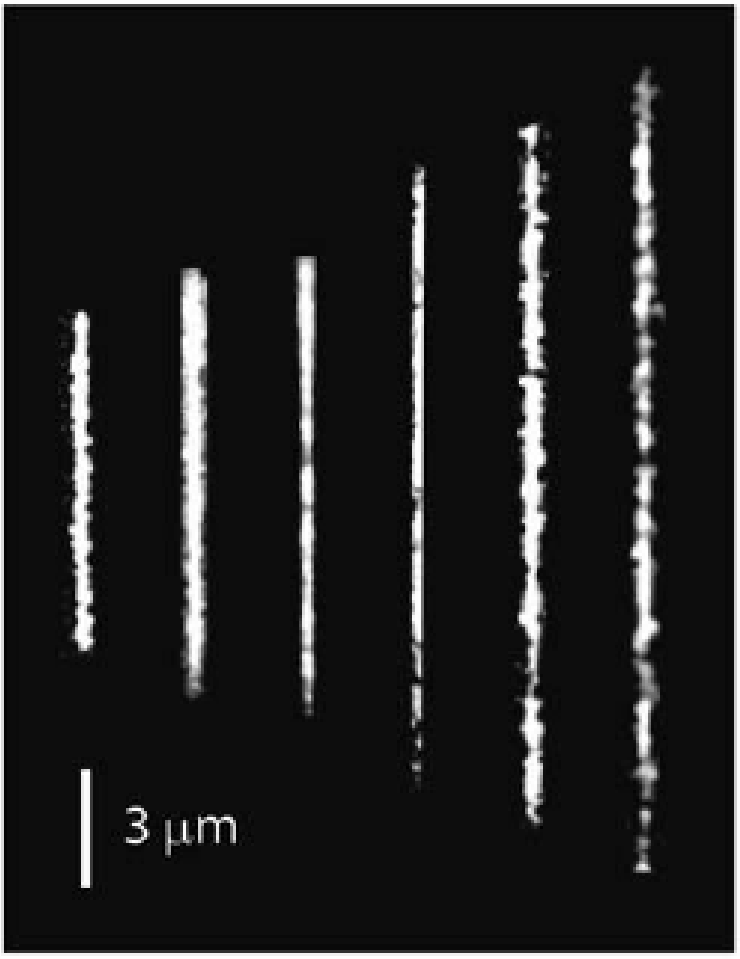

Fig. 4 Montage of fluorescence images of T4-DNA molecules confined in 300×300 nm^2 channels. The buffer concentration decreases from left to right according to 1, 1/15, 1/30, 1/50, 1/75, and 1/100×TBE. The molecules were stained with an intercalation level of 23 base-pairs per YOYO-1 molecule.

5.3.Results and Discussion

5.3.1.Effect of contour length

An implication of the scaling approach is that the extension should be proportional to the contour length of the DNA molecule [see Eq. (4)]. A linear scaling of the extension with the contour length has been reported before.[236] In order to check our experimental procedures and to reconfirm the linear scaling we have measured the extensions of T4 and λ-DNA with an equal intercalation ratio of 4.0 base-pairs per YOYO-1 molecule and immersed in 5×TBE buffer. In the 200×300 nm^2 channel, the extensions have the values 8.1 ± 2.4 and 2.5 ± 0.5 μm for T4 and λ-DNA, respectively (in the 300×300 nm^2 channel slightly smaller values were obtained). Note that the standard deviations refer to the width of the distribution following from the measurement of at least 200 different DNA molecules for each data point. Based on the linearity of the extension in the contour length, the ratio of the extensions in the nanochannels should match the ratio of the DNA contour lengths. The contour length of T4–DNA exceeds the one of λ–DNA by a factor 3.41, which is close to the experimental ratio 3.2 ± 1.2 of the corresponding extensions. Accordingly, the extension is indeed proportional to the contour length, which supports the use of the linearly packed blob model for a polymer chain in a good solvent.[218]

5.3.2.Effects of ionic strength

The DNA molecules were stained with the YOYO-1 dye in order to image them with fluorescence microscopy. We did a series of experiments with a relatively low

level of intercalation of 23 base-pairs per YOYO-1 molecule. This level of intercalation results in a sufficiently intense fluorescence for imaging (see Fig. 4). Yet, the distortion of the secondary DNA structure is minimal; the contour length has increased from 56.6 to 59.5 micrometer and the DNA charge is reduced by a factor 42/46 only.[234,235] Furthermore, we have employed two different solvents: the Tris-borate/EDTA (TBE) and Tris/HCl (T) buffer systems. TBE buffer contains some multivalent ions (divalent boric acid and di-, tri-, and tetravalent EDTA), but at pH 8.5 their concentrations are vanishingly small. The T buffer system contains monovalent ions only. We measured the extensions of individual T4-DNA molecules confined in the channels with three different cross-sections: 300×300, 200×300, and 150×300 nm^2. The relative extensions are set out in Fig. 5 as a function of the ionic strength of the buffer medium. For both buffer systems, the experimental results match, irrespective the channel cross-section and ionic strength. Notice that the molecules significantly elongate below an ionic strength of around 5 mM, but they remain coiled with maximum extensions of about 35% of their contour length. Our results are qualitatively similar to those reported before for λ-phage DNA in fused silica channels and slits of comparable dimensions.[219,220]

The theoretical extension Eq. (4) was fitted to the data in Fig. 5 by optimizing the values for the constant C and the bare persistence length L_p^0. The effective DNA diameters and electrostatic persistence lengths were calculated as described in the theoretical section. For the relevant buffer and YOYO-1 staining conditions the effective diameter and the total persistence lengths are displayed in Fig. 1. In order to

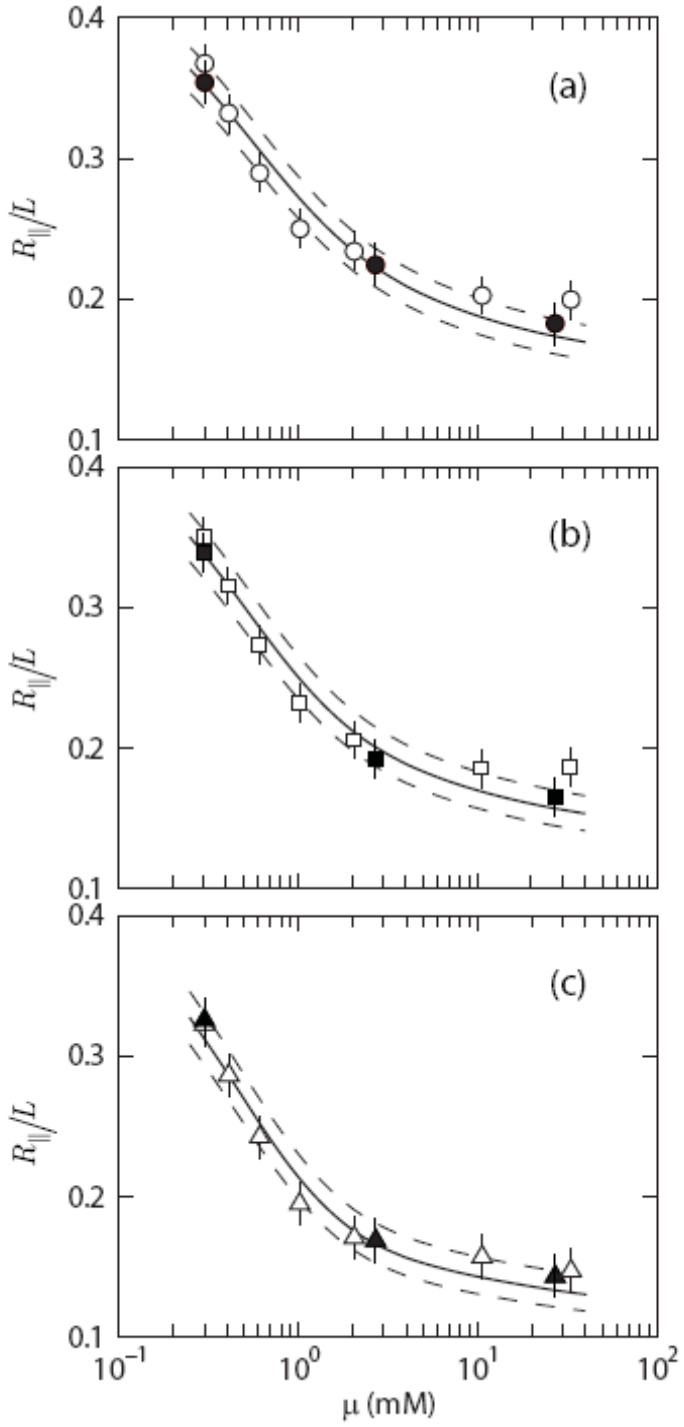

Fig. 5 Relative extension $R_{//}/L$ of T4-DNA in 150×300 (a), 200×300 (b), and 300×300 (c) nm^2 channels versus the ionic strength μ of the solvent medium. The open symbols refer to TBE buffer conditions, whereas the closed symbols pertain to the T buffer system. The error bars denote the width of the distribution following from the measurement of at least 200 different DNA molecules for each data point. The solid curves represent a fit of the theoretically predicted extensions to the data with the persistence lengths and effective diameters displayed in Fig. 1 and optimized scaling constant C = 1.45 and bare persistence length 0 44 p L = nm. The dashed curves represent the fluctuation bandwidth. The molecules were stained with an intercalation level of 23 base-pairs per YOYO-1 molecule.

take into account the effect of the electrostatic interaction of the DNA molecule with the negatively charged channel wall, we have used a reduced channel diameter by subtracting two times the electrostatic screening length from the bare cross-sectional diameter. Furthermore, for asymmetric channel cross-sections we have taken the square root of the depth times the width as the effective channel cross-sectional diameter. All data are well reproduced with the optimized values for the constant nt C = 1.45 and bare persistence length $L_p^0 = 44nm$. The fitted value of L_p^0 agrees with the commonly accepted value for DNA in the B-form of around 50 nm.[212] The value of the constant C is indeed of the order unity and there is no significant dependence on the channel cross-section and solvent ionic strength. Furthermore, the experimental widths of the distribution in relative extension agree with the theoretically predicted bandwidth Eq. (5).

In the theoretical procedure, the elongation of the DNA molecule with decreased screening of Coulomb interaction is interpreted in terms of changes in local bending rigidity of the DNA duplex (persistence length) and self-avoidance effects of interacting rod-like DNA segments inside the blobs (excluded volume effects). The strong increase in persistence length with decreasing solvent ionic strength is illustrated in Fig. 1. As a result of the increase in persistence length, the number of persistence length segments per blob L_b / L_p decreases with decreasing ionic strength (see Fig. 6). At very low ionic strength, less than 0.3 mM, the number of persistence length segments per blob becomes very small of the order of three. Due to the relatively small number of persistence length segments per blob and, in particular, in

the case of low ionic strengths, it is essential to use the full Benoit-Doty Eq. (3) rather than the long Gaussian chain result for the unperturbed radius of gyration. Note that excluded volume effects are accounted for through the swelling parameter α_s (see below). The blob model becomes inapplicable when the value of the persistence length surpasses the channel cross-sectional diameter, but this situation does not occur under the present experimental conditions. The repulsive energy per blob $DF_{conf} / R_{||}$ has been calculated with the help of Eq. (6) and is also set out in Fig. 6. In the 300×300 nm^2 channel the repulsive energy is almost constant in the range of ionic strength below 5 mM where the DNA molecule significantly elongates. The small residual ionic strength dependence of $DF_{conf} / R_{||}$ for higher ionic stengths and/or smaller channel cross-sectional diameters is probably related to deficiencies of the blob model such as an imperfect estimation of the swelling parameter or wall-induced effects on the excluded volume.

It is interesting to gauge the relative importance of the swelling of the blobs by excluded volume effects in the interpretation of the ionic strength dependence of the extension data. Excluded volume effects were accounted for by using the series expansion of the swelling factor Eq. (2), which is only valid for small values of the parameter z . With decreasing ionic strength, the effective diameter increases, but so does the persistence length (see Fig. 1). Furthermore, the number of persistence length segments per blob decreases with decreased screening of Coulomb interaction. As a result of these partially compensating effects, the value of the excluded volume parameter z remains small and exhibits a maximum at an intermediate ionic strength

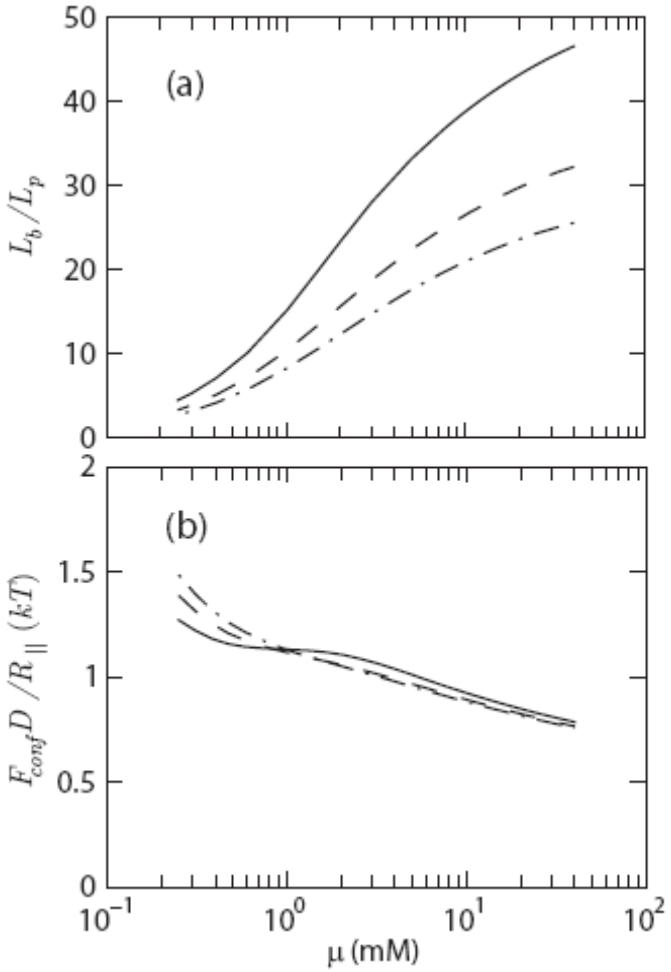

Fig. 6 (a) Number of persistence length segments per blob L_b / L_p in 150×300 (dashed-dotted curve), 200×300 (dashed curve), and 300×300 (solid curve) nm2 channels versus the ionic strength μ of the solvent pertaining to the fit of the theoretical extension to the data in Fig. 5. (b) As in panel (a), but for the repulsive energy per blob $DF_{conf} / R_{||}$ in units kT .

around 2 mM. The values of z and the resulting swelling parameter α_s are displayed in Fig. 7. The swelling parameter shows a very small variation about the mean value 1.087 within a bandwidth of $\pm$ 0.008 . Since according to Eq. (4) the extension is proportional to $\alpha_s C$, the data could almost equally well be fitted without the consideration of excluded volume effects, i.e., by setting α_s=1 and with a 9 % larger value of the parameter C. Note that this does not imply that the DNA molecule behaves as a random Gaussian chain. Irrespective the channel cross-sectional diameter, the repulsive energy per blob remains on the order of kT and the blobs are packed in a linear array (see Fig. 6). The ionic strength dependence of our extension data can hence be explained by a variation of the persistence length alone. This finding is at odds with the earlier reported conclusion by Reisner et al., who explicitly stated that it is necessary to include self-avoidance effects in order to apprehend the conformational response of single and confined DNA molecules to changes in the ionic environment.[221] The latter authors also interpreted their results with the scaling model of de Gennes, but they used the Flory radius for the blob size which is exclusively valid for long chain segments. We have used the relevant combination of the unperturbed radius of gyration and swelling parameter for shorter chains, in accordance with the relatively small correlation lengths imposed by the channel cross-sectional diameters. This difference in the description of the chain statistics within the blob explains the discrepancy between our and the previously reported conclusion about the significance of self-avoidance effects in the interpretation of the ionic strength dependence of the extension of single DNA

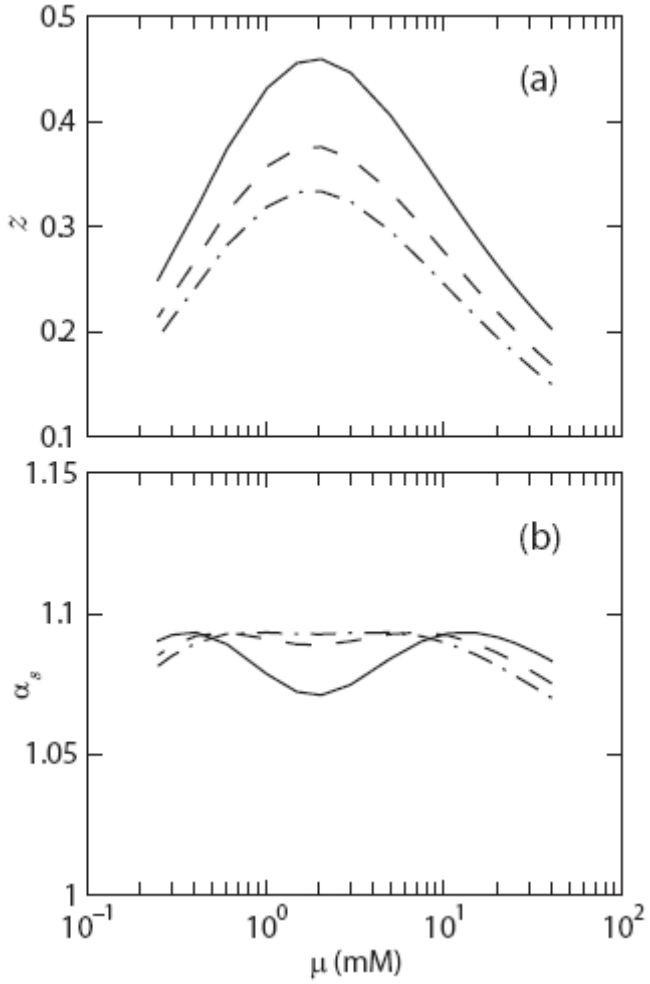

Fig. 7 (a) Excluded volume parameter z in 150×300 (dashed-dotted curve), 200×300 (dashed curve), and 300×300 (solid curve) nm^2 channels versus the ionic strength μ of the solvent pertaining to the fit of the theoretical extension to the data in Fig. 5. (b) As in panel (a), but for the swelling parameter α_s.

molecules confined in a nanochannel.

5.3.3.Effects of intercalation

The above discussed experiments were done employing a relatively low level of intercalation of 23 base-pairs per YOYO-1 molecule. This low level of intercalation ensures a minimal distortion of the DNA secondary structure and net charge. In order to gauge the effect of intercalation on the conformation, we have measured the relative extension of T4-DNA with the saturating intercalation level of four base-pairs per YOYO-1 molecule as a function of the ionic strength of the supporting TBE medium. It should be noted that at the saturating intercalation level the contour length of the T4-DNA molecule has increased from 56.6 to 73.2 micrometer and the net DNA charge is reduced by a factor of two (the spine axis projected distance between charges of the labeled T4-DNA is thus increased from 0.171 to 0.442 nm).[234,235] The results obtained in channels of a cross-section of 200×300 nm^2 are displayed in Fig. 8. For the other channel cross-sections similar results are obtained (data not shown). With the saturating level of intercalation, the relative extensions are somewhat smaller than the values obtained with an intercalation level of 23 base-pairs per YOYO-1 molecule.

The theoretical extension Eq. (4) was fitted to the data in Fig. 8 by optimizing the values for the constant C and the bare persistence length L_p^0. The effective diameters and persistence lengths were also obtained by solving the non-linear Poisson Boltzmann equation, but with the relevant linear charge density pertaining to

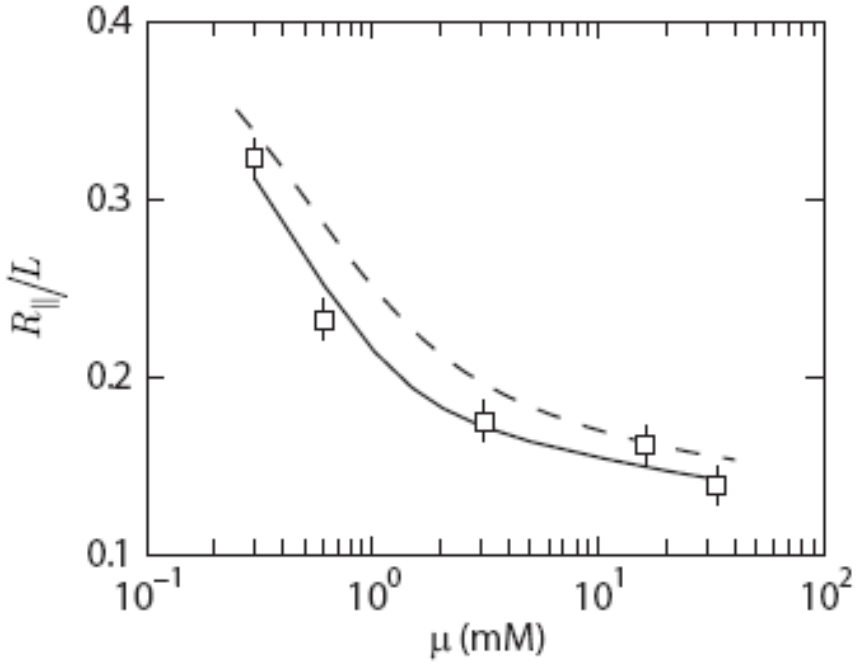

Fig. 8 Relative extension $R_{\|} / L$ of T4-DNA stained with the saturating intercalation ratio of 4 base-pairs per YOYO-1 molecule in the 200×300 nm^2 channel versus the ionic strength μ of the TBE medium. The solid curve represents a fit of the theoretically predicted extension calculated with the relevant linear DNA charge density and optimized scaling constant C = 1.43 and bare persistence length L_p^0 = 44 nm. The dashed curve is included for comparison and represents the corresponding theoretical result for T4-DNA with 23 base-pairs per YOYO-1 molecule (see Fig. 5).

the highly intercalated DNA molecule. The optimized values for the fit parameters rs are C = 1.43 and L_p^0 = 44 nm, which are in excellent agreement with the results presented above obtained for T4-DNA with an intercalation level of 23 base-pairs per YOYO-1 molecule. As a surprising result, we find that the bare persistence length is insensitive to the level of intercalation. This insensitivity is at odds with the reported DNA persistence length of as short as 12 nm obtained by single molecule optical tweezers experiments on λ-phage DNA stained with the YOYO-1 dye with a much higher intercalation level of 0.73 base-pair to YOYO-1 ratio.[237] An explanation for this discrepancy is that at such low base-pair to dye ratio not all dye molecules can be accommodated in the regular way of one YOYO-1 molecule bis-intercalated between three adjacent base-pairs. A fraction of the YOYO-1 molecules might be intercalated in an irregular way (such as multiple intercalated dye molecules per stretch of four base-pairs) or bound sideways to the duplex. These irregular forms of intercalating and binding of the 'surplus' of YOYO-1 molecules are expected to have a profound effect on the persistence length, since they disrupt the base-pair stacking interaction to which DNA largely owes its bending rigidity.

The effect of intercalation on the DNA conformation at a constant buffer concentration of 1/50×TBE is demonstrated in Fig. 9. Here, the theoretical extension Eq. (4) was fitted to the data by only optimizing C = 1.39 and by using the effective diameters and persistence lengths as displayed in Fig. 2. The optimized values of the constant C obtained from the various data sets are all very close with an average value C = 1.42±0.03. This shows that C is indeed a universal constant and does not

depend on the screening conditions or net DNA charge. The variation of the extension with the degree of intercalation is reasonably well reproduced by the theoretical prediction using a constant value of the bare persistence length of L_p^0 = 44 nm. With decreasing level of intercalation (higher base-pair to YOYO-1 ratio), the contour length decreases by 0.4 nm per dye molecule.[234,235] Concurrently, the linear charge density increases, which results in an increase of the total persistence length and effective diameter (see Fig. 2). As a result of these two partially compensating effects, the relative extension of the DNA molecule confined in the channel first shows a modest increase after it levels off at an ionic strength dependent, but constant value for intercalation levels exceeding 10 base-pairs per YOYO-1 molecule.

5.3.4. Effects of divalent salt

It is well known that cations of valence three or greater can induce a condensed structure, i.e. a highly packaged state of single or multiple DNA molecules with an ordered morphology.[238,239,240] Divalent cations can also induce condensation provided the dielectric constant of the medium is reduced by the addition of alcohol.[241] Here, we have investigated the conformation of the T4-DNA molecules confined in the nanochannels in the presence of divalent magnesium, calcium, or putrescine. In order to drive the DNA molecules inside the channels, we found that the solvent needs to be buffered. Accordingly, we have measured the relative extension in 1/100×TBE with various amounts of added $MgCl_2$, $CaCl_2$, or putrescine-Cl_2. The intercalation ratio was 23 base-pairs per YOYO-1 molecule, so

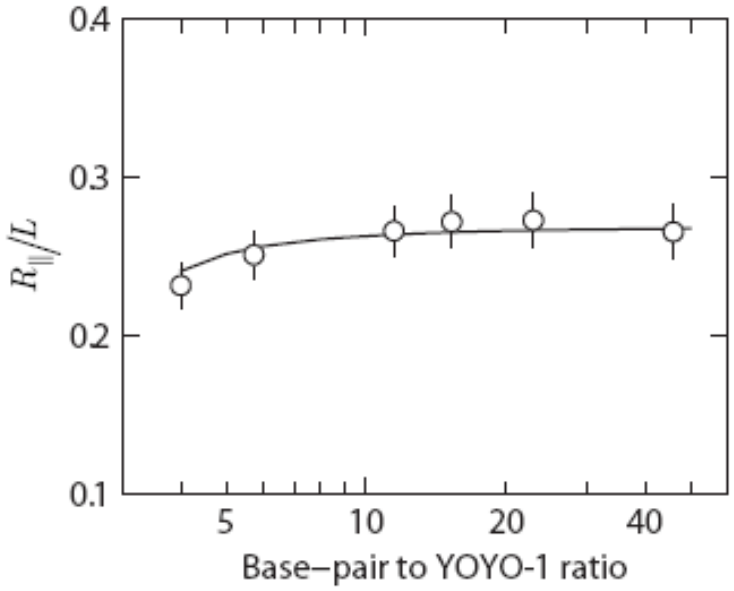

Fig. 9 Relative extension $R_{\|} / L$ of T4-DNA versus the base-pair to YOYO-1 ratio in 1/50×TBE buffer. The solid curve represents a fit of the theoretically predicted extension to the data with the persistence lengths and effective diameters shown in Fig. 2 (optimized with a fixed value C = 1.39).

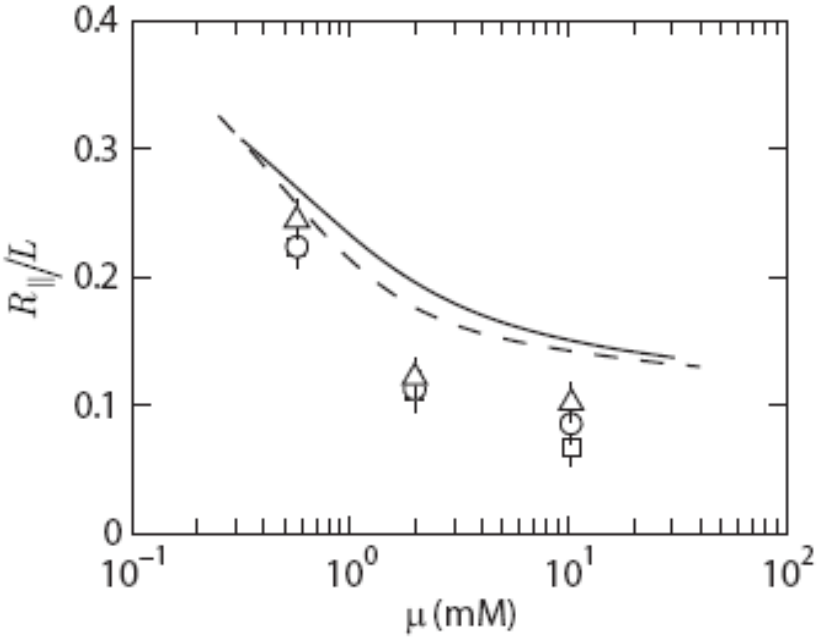

Fig. 10 Relative extension $R_{\|} / L$ of T4-DNA versus the ionic strength of the TBE/Mg (triangular), TBE/Ca (circle), and TBE/Pu (rectangular) buffers in 300×300 nm^2 channels. The intercalation ratio is 23 base-pairs per YOYO-1 molecule. The solid curve represents the theoretically predicted extension based on the solution of the non-linear Poisson-Boltzmann equation including the effect of the divalent salt. The dashed curve is included for comparison and represents the corresponding result for the relative extension in a monovalent salt buffer (see Fig. 5).

the distortion of the secondary DNA structure was minimal. The experimental results obtained with a channel cross-section of 300×300 nm^2 are displayed in Fig. 10. With increasing ionic strength generated by the addition of the divalent salt, the relative extension reduces. The molecules are however not condensed into a compact structure. Furthermore, the results for the various divalent cations are quite similar, but in the presence of the linear polyamine putrescine the chain takes a somewhat more extended conformation.

The theoretically predicted extension based on the solution of the non-linear Poisson-Boltzmann equation for the relevant mixture of mono- and divalent ions is shown in Fig. 10 (calculated with C = 1.45 and L_p^0 = 44 nm). For comparison we also have included the optimized theoretical prediction pertaining to the extension of T4-DNA under TBE buffer conditions without added divalent salt. The experimental values fall clearly below the mark set by the theoretical prediction, in particular for the higher ionic strengths. We verified that in the presence of divalent cations Eq. (4) is unable to reproduce the extension data with a swelling parameter larger than unity. With increasing divalent salt concentration the DNA molecule contracts with a more compact statistics than the swollen chain. Note that for a polymer chain in a theta or poor solvent the scaling model is no longer applicable. Nevertheless, the results show that divalent cations give rise to an attractive force among the segments of a long DNA molecule in a single coil, but apparently the force is not strong enough to induce condensation. An attractive force mediated by divalent counterions between very short DNA fragments (8-25 base pairs) was recently observed in a small angle X-ray

scattering (SAXS) study of the second virial coefficient.[242] Full atomic scale Molecular Dynamics simulations have revealed attractive ion bridges, i.e., multivalent ions which are simultaneously and temporarily bound to opposing DNA duplexes with a lifetime on the order of a few nanoseconds.[243] Furthermore, a small angle neutron scattering (SANS) study of the synthetic poly(styrenesulfonic acid) (PSS) has shown that the chain contracts below the Gaussian chain limit in the presence of calcium counterions.[244] The similarity in behavior of PSS and DNA suggests that the multivalent ion mediated attraction is a general phenomenon pertaining to highly charged linear polyelectrolytes.

5.4. Conclusion

Single DNA molecules can be confined and extended in long and straight nanochannels casted in a PDMS nanofluidic chip. The cross-sectional diameters of the channels were in the range 150-300 nm, which are larger than the persistence length, but smaller than the radius of gyration of the free, unconstrained T4-DNA coil. Inside the channel the DNA molecule hence remains coiled at all length scales, but it is extended in the longitudinal direction due to the restriction imposed by the channel walls. With the help of fluorescence microscopy, the DNA molecules were visualized and their extensions were measured. It was checked that the extension is proportional to the contour length of the DNA molecule. The relative extensions were interpreted with a modification of de Gennes' scaling theory for a polymer chain in a good solvent including the effects of charge. Because of the fact that the correlation length is relatively small, it is essential to use the full Benoit-Doty equation for the unperturbed radius of gyration of the relatively short chain segment within the blob rather than the commonly used expression for the long Gaussian chain. Self-avoidance effects were included by using the perturbation series expansion of the coil swelling parameter in terms of the excluded volume parameter. Due the relatively small number of statistical segments within the blob, the values of the excluded volume parameter are small and the chain statistics is only mildly perturbed. Furthermore, the value of the swelling parameter was found to be rather robust against a variation in ionic strength. The variation of the extension of the confined DNA molecule with a change in ionic strength of the supporting buffer medium can

be described by a variation of the DNA persistence length induced by screening of the Coulomb interaction. Note that successive blobs remain packed in a linear array with a repulsive energy per blob on the order of the thermal energy kT.

In order to visualize the DNA molecules with the help of fluorescence microscopy, it is necessary to stain them with an intercalating dye. Intercalation of the YOYO-1 dye molecule results in an increase of the contour length as well as a partial compensation of the DNA charge. We observed a moderate decrease in the relative extension with increasing level of intercalation. The extensions could be interpreted using the polymer scaling theory, including the effects of the intercalating dye on the secondary DNA structure as well as the partial DNA charge neutralization. All extension data agree with a single value of the bare persistence length L_p^0 = 44 nm, irrespective the intercalation level and the screening conditions of the supporting medium. Although YOYO-1 increases the contour length of the DNA molecule, our experiments show that it has no significant effect on the bending rigidity (at least in the intercalation level range of 46 to four base-pairs per dye molecule). Furthermore, we found that the radius of gyration of the blob is related to the channel diameter through a constant. This constant $C = D / R_b$ was found to be universal with an average value C =1.42$\pm$0.03, in the sense that it is independent on the DNA charge (degree of intercalation), screening conditions, and channel cross-sectional diameter. The effect of the electrostatic interaction of the DNA molecule with the plasma oxidized negatively charged channel wall was accounted for by using a reduced channel diameter through the subtraction of two times the electrostatic screening

length from the bare cross-sectional diameter.

In the presence of divalent counterions, the relative extension also reduces with increased screening of Coulomb interaction. Here, the experimental values of the relative extensions fall however clearly below the mark set by the theoretical prediction including the effects of divalent ions on the screened electrostatics. The extension results imply that the DNA molecule inside the channel contracts with a more compact statistics than the swollen chain. This change in conformation is proposed to result from divalent counterion mediated attractive bridging interactions between the DNA segments. These interactions are counterion specific, because in the case of the linear putrescine the DNA molecule was observed to take a slightly more extended conformation than in the presence of the small and spherical calcium and magnesium counterions. The divalent ions do however not induce condensation and, in this respect, their behavior is similar to that in the bulk phase.

Chapter 6

Elongation/Compaction of single DNA molecules confined in a nanochannel caused by depletion interaction with dextran particle

Abstract

Structural changes in T4 DNA induced by the addition of a neutral dextran nanoparticles were examined by the method of single-molecule observation in nanochannels. We present a new experimental strategy for the study of the depletion effect on large DNA chains exerted by nanoparticles. A clear phase diagram is observed as a function of the nanoparticle concentration. In nanochannels DNA molecules exhibit a more extended conformation with the addition of nanoparticles at relatively low concentration, irrespective of the ionic strength of the medium. Under concentrated nanoparticle conditions, individual DNA molecules assume a highly compacted state. Surprisingly, the nanoparticle molecular weight has no obvious effect on the phase diagram.

6.1. Introduction

Condensation of DNA may be achieved either by adding multivalent counterions or other oppositely charged species, or by adding sufficiently high concentrations of "crowding agents" such as nanoparticles (small globular proteins, dextran). This phenomenon mimics some important aspects of the behavior of DNA in vivo. For instance, the segregation of DNA in bacterial cells has been described in terms of crowding-induced condensation [244]. Condensation induced by multivalent counterions is promoted by low ionic strength, whereas crowding-induced condensation by neutral nanoparticles is promoted by high ionic strength [245,246]. At higher ionic strength, DNA chains are more flexible and electrostatic repulsion is progressively screened, so that it is easier to form a highly compacted structure.

In this research, micro- and nanofluidic devices have been developed and utilized for the analysis of the condensation of DNA by dextran. As observed by fluorescence microscopy (FM), the effect of the ionic strength on the crowding induced condensation is greatly compromised for DNA confined in a nanochannel. Surprisingly, a single DNA molecule was observed to be more extended in the presence of smaller amounts of dextran particles. At a critical high nanoparticle concentration, a sudden collapse of an extended DNA chain to a highly compacted form was observed. On the basis of these results we propose a simple interpolation for the free energy of inserting nanoparticles in the DNA coil in their free state. To determine whether DNA will condense or extend in a nanochannel, the free energy of inserting a nanoparticle into the DNA coil has to be taken into account. More

specifically, the insertion of a nanoparticle into the DNA coil in free solution is related to several factors including nanoparticle concentration, ionic strength and equilibration time.

6.2. Experimental Section

6.2.1.Fabrication of the nanofluidic chip

The stamp for the nano/micro fluidic device was made in a two-step lithography process. In the first step, a nano-patterned structure was fabricated on Hydrogen Silsequioxane (HSQ) (Dow Coming Co.) photo-resist using proton beam writing (PBW). In the second step, a microstructure was superposed on this nanostructure utilizing SU-8 (MicroChem) photo-resist and UV lithography. The widths of the channels in the PDMS replica were measured with atomic force microscopy and the values agreed with those obtained from the scanning electron microscopy images of the HSQ master stamp. The nanochannels were rectangular-shaped and have a depth of 300 ± 5 nm and a width of 150 ± 5, 200 ± 5, and 300 ± 5 nm, respectively. More details about the chip design and fabrication are presented in Chapter 4.

6.2.2.DNA & dextran sample preparation

T4 GT7 DNA (T4-DNA, 165.65 kbp) was purchased from Nippon Gene, Tokyo and used without further purification. YOYO-1 fluorescence staining dye was purchased from Invitrogen, Carlsbad, CA. Water was deionized and purified by a Millipore system and had a conductivity less than 1×10^{-6} $\Omega^{-1}cm^{-1}$. Samples were

prepared by dialyzing solutions of T4-DNA against the relevant buffer solutions in micro-dialyzers. The buffer systems were Tris/HCl with various concentrations. The concentrations were 1/10, 1, and 10×T (1×T is 10 mM Tris adjusted with HCl to pH 8.5). Dextran with molecular weights (MW) of 5,000, 50,000 and 410,000 Da (Sigma-Aldrich) were used as depletant and dissolved in the same buffer solutions. Dextran and T4 DNA were mixed with equal volume fractions and incubated for 24 hours at room temperature. Before fluorescence microscopy (FM), T4-DNA was stained with YOYO-1 and diluted with the relevant buffer to a final DNA concentration of 0.008 g/L. The dye intercalation ratio was 23 base-pairs per YOYO-1 molecule. The ionic strengths and buffer compositions were calculated with the Davies equation for the estimation of the activity coefficients of the ions. The relationship between the radius of gyration Rg of Dextran and its molecular weight (MW) in units of g/mol is $R_g\left[\overset{o}{A}\right] = 0.66\left(MW\right)^{0.43}$ [249].

6.2.3.Fluorescence imaging

The YOYO-1-stained DNA molecules dispersed in the relevant buffer soluttion were loaded into two reservoirs connected by the nanochannels. The DNA molecules were subsequently driven into the channels by an electric field. For this purpose, two platinum electrodes were immersed in the reservoirs and connected to an electrophoresis power supply with a voltage in the range 10-30 V (Bio-Rad, Hercules, CA). Once the DNA molecules were localized inside the channels, the electric field was switched off and the molecules were allowed to relax to their equilibrium state

for at least 60 seconds. The fluorescence of the stained DNA molecules were visualized with an Olympus IX71 inverted fluorescence microscope equipped with a 100 W mercury lamp, a UV filter set and a 100 times oil immersion objective. The exposure time of the YOYO-1 fluorescence was controlled by a UV light shutter. Images were collected with a charge coupled device (CCD) camera (Olympus DP 70) and the extension of the elongated DNA molecules inside the channels was measured with the public domain software ImageJ (http://rsb.info.nih.gov/ij/). Reported extensions represent an average of at least 200 individual measurements.

6.3.Results and Discussion

Depletion interactions are perhaps best understood in the context of suspensions of small-diameter hard-spheres in large biopolymer chains. Neutral nanoparticles such as dextran lack attractive and long-range interactions with the negatively charged DNA chains. It typically competes with entropic effects to produce ordered phases. Nonetheless, in mixtures of biopolymer chains and nanoparticles, a condensed form of large polymers can increase the total entropy of the system by increasing the entropy of the small particles. The entropy of nanoparticles depends on the number of positions it can occupy in the total volume, i.e. its free volume. More free volume means more entropy for the particles.

6.3.1. Time-related dextran & DNA equilibrium state

Depletion effects are perhaps best understood in the context of suspensions of large

and small diameter hard-spheres. Since the center of mass of the small spheres cannot penetrate within the radius of the large sphere surface, a region of "excluded volume" surrounds each large sphere. The smaller spheres can be non-obsorbed polymer chains or nanoparticles. Free non-adsorbing polymer chains avoid the space between two big spheres, leading to an unbalanced pressure, which pushes them towards each other. Such depletion forces for an isolated pair of immersed particles or for a single immersed particle near a wall have been measured in recent experiments [250]. In the mixture of DNA and dextran, the situation is different. Here, excluded volume interactions are related to the diameter of the DNA duplex and the radius of gyration of dextran. In the same manner as in the above delineated scenario for a mixture of spheres, the DNA segments can be 'pushed' towards each other due to the unbalanced pressure exerted by the dextran nanoparticles.

The relationship between the radius of gyration R_g of dextran and its molecular weight (MW) in units of g/mol is $R_g = 0.66(MW)^{0.43}$ [262]. The reason for the small exponent 0.43 is due to the fact that dextran is a branched polymer. In the calculation of the volume fraction of dextran, we used a particle radius R_g = 2.6, 6.9, and 17. 1 for 5, 50. and 410 kDA dextran, respectively. Nanoparticles smaller than 10 nm in size may easily enter a large DNA coil, the associated increase in free energy being less than the thermal energy [251,252]. Considering a T4 DNA coil as a porous membrane, the difference in dextran concentration inside and outside the coil domain induces an osmotic pressure. To reach an equilibrium state, an individual DNA coil could either decrease its volume, or dextran particles diffuse into the DNA coil to compensate the

concentration difference. Competing with the DNA elastic energy, diffusion of dextran particles inside DNA coil is energetically preferred. The penetration of the DNA coil by dextran particles may take certain time. To ensure that the system is in thermodynamic equilbrium we have incubated the DNA solution with the nanoparticles for 48 hours before the samples were loaded into the nanofluidic device.

6.3.2.Effects of the dextran concentration

We measured the extensions of individual T4-DNA molecules confined in the 300×300, 300x200 and 300x150 nm^2 channels with three different buffer conditions: 1 mM, 10 mM and 100 mM Tris-HCl. A montage of some fluorescence images is shown in Fig. 2. The extensions are set out in Fig. 3 as a function of the dextran concentration. For all buffer systems, the experimental results show the same behavior. Notice that the molecules significantly elongate with dextran volume fractions up to 0.02, after which the extension levels off at constant value depending on buffer conditions and channel cross-section. As we will observe shortly, for even higher dextran volume fractions, the DNA coils will collapse in a condensed structure. To study the effect of dextran molecular weight, we employed three different dextran molecular weights (5, 50 and 410 kDa). As is shown in Fig. 3 A, the extensions of T4 DNA induced by dextran of different moleculr weighrts collapse to single master curve if they are set out against the volume fraction.

Fig. 2 B shows typical fluorescence images of individual, condensed DNA molecules at a dextran volume fraction exceeding 0.1. Note that the long axis of an

elongated DNA chain (Fig. 2 A) is only about 10 times larger than the one in the compacted state. To understand this relatively small length ratio, we have to take into account the resolution of the fluorescence microscopy. For commonly used dyes and high numerical aperture oil immersion objectives, the resolution limit is on the order of 250–300 nm. Fig. 4 shows the extension in 300x300 nm channels including data at higher dextran volume fraction. The DNA molecule is collapsed for a dextran volume fraction exceeding, say 0.1. Note that DNA molecules enter all nanochannels in a compact form, which is probably due to the friction force of the channel wall during movement.

6.4. Discussion

A collapse of individual DNA molecules in free solution induced by neutral polymer PEO has been reported before by Yoshikawa et al. This collapse occurs at relatively high volume fraction and can be rationalized in terms of a depletion induced attractive force between segments of the DNA molecule which eventually leads to a compacted state. Our results for the collapse inside the nanochannels at high dextran volume fraction exceeding 0.01 are in qualitative and quantitative agreement with this earlier results. A new observation is that the DNA molecules swell with respect to the situation without nanoparticles for lower dextran volume fractions up to 0.01. The swelling is related to the nanoparticle volume fraction. It should be noted that nanoparticle induced depletion interaction between DNA segments, which eventually leads to condensation, can also not be responsible for the swelling. The latter

interaction is attractive and should result in a decrease rather than an increase in the extension of the DNA coil inside the channel. The swelling can not be explained on pure entropic reasons, because the reduced free volume accessible for the nanoparticles within the domain of the coil results in a decrease in translational entropy. The nanoparticle concentration within the domain of the coil would accordingly be depleted and, hence, the chain should shrink due to osmotic pressure exerted by the surrounding medium.

We can offer two plausible explanation for the swelling of the DNA molecules induced by the dextran nanoparticles. The first explanation is based on a decrease in dielectric permittivity of the medium by the presence of the nanoparticles. Since there is no obvious relation with the buffer concentration, the latter effect seems to be relatively unimporrtant. The other explanation is that there exist an attractive interaction between the DNA duplex and the neutral dextran nanoparticle. This attractive interaction might be due to van der Waals and/or hydrophobic interaction between dextran and the DNA backbone. Due to this interaction, there might be a (small) excess of nanoparticles inside the DNA coil, which results in swelling of the chain in much the same way as a gas inside an elastic balloon. In order to check these explanations, some further experiments are called for. In order to check the effect of the dielectric permittivity of the medium, experiments can be done using mixtures of water and glycerol. To verify the effect of a possible attractive interaction beween DNA and dextran, experiments with another depletant such as PEO can be done.

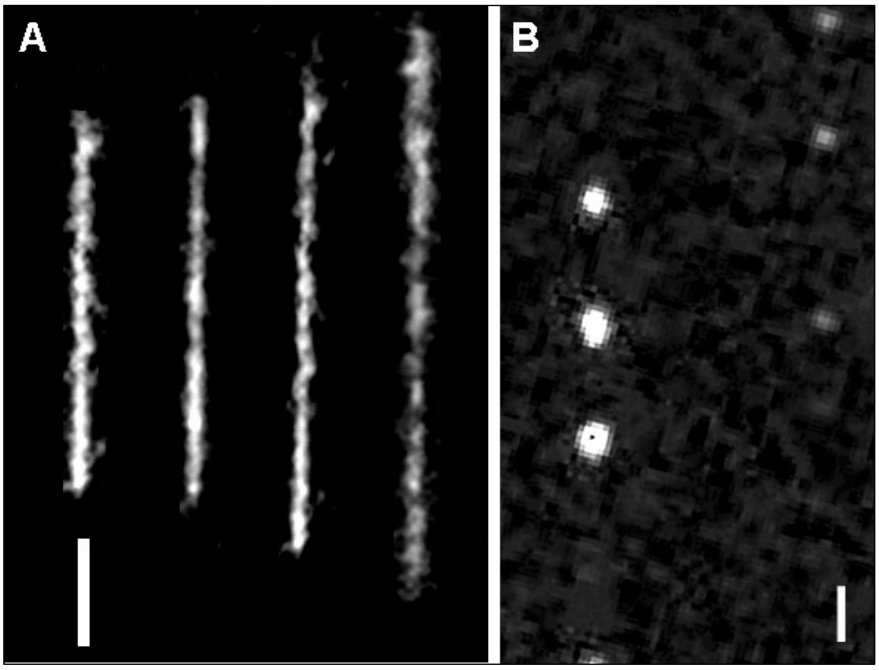

Fig. 2 Montage of fluorescence images of T4-DNA molecules confined in 300×300 nm^2 channels and immersed in 10 mM Tris-HCl. (a) Extended molecules with 0, 0.025, 0.25, and 2.5 g of dextran/L. (b) Condensed T4-DNA at dextran concentration 7.5 g/L. The scale bar in image A denotes 3 micrometer. The scale bar in image B denotes 2 micrometer. The molecules were stained with an intercalation level of 23 base-pairs per YOYO-1 molecule.

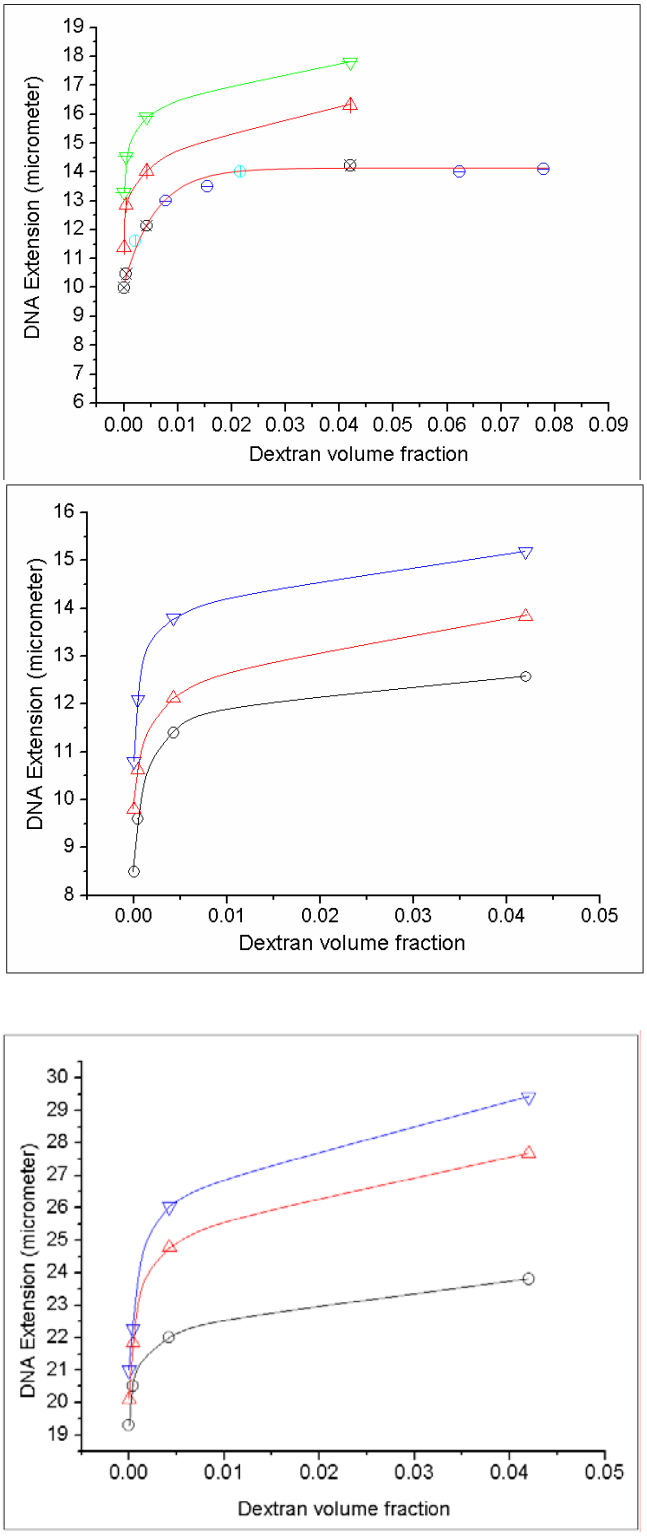

Fig. 3 Extension of T4-DNA in 10 mM Tris-HCl (a), 1 mM Tris-HCl (b), and 100 mM Tris-HCl (c) buffers versus the dextran volume fraction in the solvent medium. The open circles refer to DNA extension in 300×300 nm^2 channels. The triangles (pointing up) refer to DNA extension in 200×300 nm^2 channels. The triangles (pointing down) refer to DNA extension in 150×300 nm^2 channels. The molecules were stained with an intercalation level of 23 base-pairs per YOYO-1 molecule.

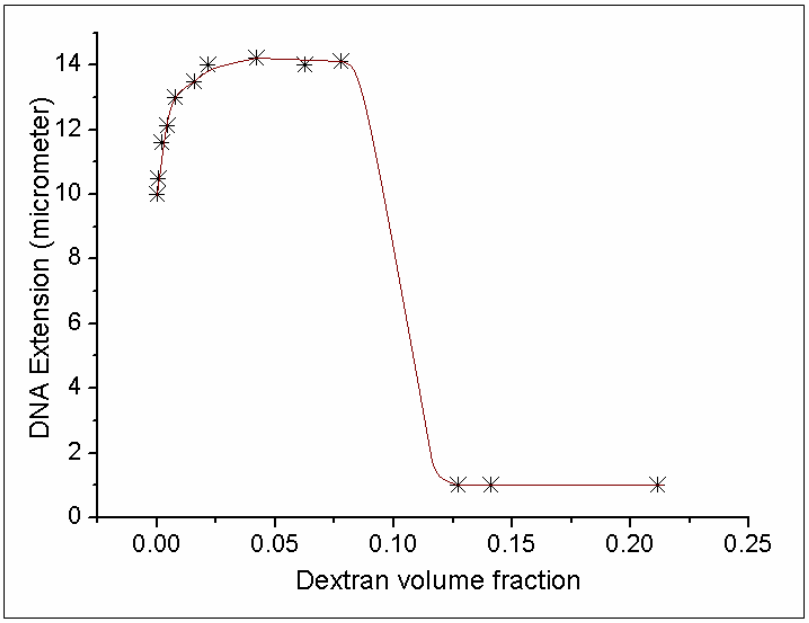

Fig. 4 Extension of T4-DNA in 10 mM Tris-HCl buffers versus the dextran volume fraction in the solvent medium. The stars refer to DNA extension in 300×300 nm^2 channels with the presence of 5, 50 and 410 kDa dextran. The molecules were stained with an intercalation level of 23 base-pairs per YOYO-1 molecule. STRANGE CURVE

6.4. Conclusion

To summarize, inside the nanochannels extended DNA molecules were observed at dextran concentrations in the range 0.076 – 7.6 g/L. A compact form of DNA was observed when the dextran volume fraction increased over 0.127. In the lower dextran concentration range, the coils swell with respect to the nanoparticle free state. A plausible explanation for the swelling is the existence of a net attractive force beween DNA and dextran. Due to an excess of nanoparticles inside the domain of the DNA coil, the concommittant osmotic pressure results in a swelling of the chain. At high dextran concentration, the DNA molecule collapse. The latter effect is similar to the one observed in the bulk phase and cn be interpreted with a depletion induced attraction between DNA segments.

Chapter 7
Conclusion

The main focus of this thesis is the investigation of conformational responses of DNA to various experimental conditions. These conditions include the presence of divalent and nanoparticles. Future expectations of two independent research areas (surface-directed and nano-channel-directed) are reviewed in the following sections.

There are several interesting directions for future work in the areas of biopolymer conformation including DNA condensation. The two main subjects of this research are AFM investigation of surface-directed biopolymer topology and FM investigation of nano-channel enhanced biopolymer behavior. One possible avenue of future work is the extension from surface-directed DNA conformations to in-solution AFM investigation of real-time biopolymer topological response to various DNA condensation agents. It is of great importance to conduct a real-time biopolymer investigation on mica surface from both theoretical and technological point of view. One promising factor, which might contribute to the future work, is the bonding properties of biopolymer chains to mica surface. The loosely bonded biopolymer chains are allowed to move laterally on mica surface. Considering the time scale of biopolymer condensation process, the experimental strategy mentioned in Chapter 3 shows great potential in controlling biopolymer diffusion speed, which could effectively lower biopolymer mobility on mica surface and allows a real-time scanning during DNA condensation.

The lateral movement of biopolymer chains on mica surface offers the possibility to study dsDNA in nano-confinements. The conformation of highly packed biopolymer chains has been a hot topic for many years. Nevertheless, experimental work on the

phenomena is still limited, possibly due to the several technological limitations:

1. Topological responses of DNA molecules to nano-confinements are too small to be visually observed (such as Fluorescence Microscopy etc.).
2. To investigate DNA conformations by AFM, biopolymer molecules are usually tightly bonded to a solid surface, which could eliminate DNA topological responses to the presence of a range of experimental conditions (such as biopolymer condensation agents).

Our experimental strategy, in combination with the utilization of nano-fabricated mica surface may for the first time allow the possibility of investigation of DNA highly packed structure in biological cells.

As described in Chapter 4, micro- and nano-fluidics can be employed to investigate biopolymer responses to several important issues, associated with packing of large DNA chains into a highly compact form. This system had been proven to be a platform for single molecule study of DNA extension in nano-confinements, which could be the representative of various biological effects. For example, in presence of histone-like proteins (such as HU and HNS) the DNA conformation could be greatly modified to a highly compact form. The phenomena could be observed as spots with high light intensity in FM experiments.

Another interesting area for FM investigation is DNA topological responses to the presence of polysaccharide, which is composed of many glucose molecules joined into chains of varying lengths. Suppose dextran is mixed with T4 DNA molecules in nano-confinements and dextran can diffuse into the coil of the large biopolymer chain

in nano-channel. As a neutral particle, dextran can act as small particles surrounding a big particle. To gain the lowest overall energy, the distance between DNA segments may increase to allow an ordered arrangement of the small particles known as depletion effect. This effect can be represented by an increase in DNA extension in nano-confinements.

Chapter 8

Reference

1. Bloomfield V. A. (1997) Biopolymers 44, 269–282.
2. Hud N. V., Allen M. J., Downing K. H., Lee J. and Balhorn R. (1993) Biochem. Biophys. Res. Commun. 193, 1347–1354.
3. Ward W. S. and Coffey D. S. (1991) Biol. Reprod. 44, 569.
4. Thomas T. and Thomas T. J. (2001) Cell. Mol. Life Sci. 58, 244–258.
5. Hougaard D. (1992) Int. Rev. Cytol. 138, 51–88.
6. Gelbart W. M., Bruinsma R. F., Pincus P. A. and Parsegian V. A. (2000) Phys. Today 53, 38–44.
7. Rouzina I. and Bloomfield V. A. (1996) J. Phys. Chem. 100, 9977–9989.
8. Oosawa F. (1968) Biopolymers 6, 1633.
9. Kornyshev A. A. and Leikin S. (1999) Phys. Rev. Lett. 82, 4138–4141.
10. Shklovskii B. I. (1999) Phys. Rev. Lett. 82, 3268–3271.
11. Shklovskii B. I. (19999) Phys. Rev. E 60, 5802–5811.
12. Nguyen T. T., Rouzina I. and Shklovskii B. I. (2000) J. Chem. Phys. 112, 2562–2568.
13. Dame R. T. (2005) Mol. Microbiol. 56, 858–870.
14. Johnson R. C., Johnson L. M., Schmidt J. W. and Gardner J. F. Major Nucleoid Proteins in the Structure and Function of the Escherichia coli Chromosome (ed. Higgins, N. P.) (ASM, Washington DC, 2005).
15. Huisman O., Faelen M., Girard D., Jaffe A., Toussaint A. and Rouviere-Yaniv J. (1989) J. Bacteriol. 171, 3704 - 3712.
16. Hillyard D. R., Edlund M., Hughes K. T., Marsh M. and Higgins N. P. (1990) J.

Bacteriol., 172, 5402 – 5407.

17. Dri A. M., Rouviere-Yaniv J. and Moreau P. L. (1991) J. Bacteriol. 173, 2852 – 2863.
18. Paull T. T. and Johnson R. C. (1995) J. Biol. Chem., 270, 8744 – 8754.
19. Wills P. R., Y. Georgalis, J. Dijk and D. J. Winzor. (1995) Biophys. Chem. 57, 37–46.
20. Minton A. P. (1998) Methods Enzymol. 295, 127–149.
21. Rouzina I. and Bloomfield V. A. (1998) Biophys. J. 74, 3152–3164.
22. Kerppola T. K. (1998) Structure 6, 549–554.
23. D. H. Atha and K. C. Ingham, (1981) J. Biol. Chem. 256, 12108.
24. D. A. Knoll and J. Hermans, (1981) Biopolymers 20, 1747.
25. Walter Reisner, Keith J. Morton, Robert Riehn, Yan Mei Wang, Zhaoning Yu, Michael Rosen, James C. Sturm, Stephen Y. Chou, Erwin Frey and Robert H. Austin1, (2005) PRL 94, 196101.
26. Walter Reisner, Jason P. Beech, Niels B. Larsen, Henrik Flyvbjerg, Anders Kristensen and Jonas O. Tegenfeldt, (2007) PRL 99, 058302.
27. Murphy L. D. and Zimmerman S. B. (1995) Biophys. Chem., 57, 71 – 92.
28. 28. Murphy L. D. and Zimmerman S. B. (1994) BBA-Gene Struct. Expr., 1219, 277 – 284.
29. Emil P. Kartalov, Christopher Walker, Clive R. Taylor, W. French Anderson and Axel Scherer, PNAS, 2006, 103, 12280.
30. Ulrich F. Keyser, Bernard N. Koeleman, Stijn Van Dorp, Diego Krapf, Ralph M.

M. Smeets, Serge G. Lemay, Nynke H. Dekker and Cees Dekker, Nature Physics, 2006, 2.

31. Keith A. Williams, Peter T. M. Veenhuizen, Beatriz G. de la Torre, Ramon Eritja and Cees Dekker, Nature, 2002, 420, 761.
32. A. Podesta, L. Imperadori, W. Colnaghi, L. Finzi, P. Milani and D. Dunlap, Journal of Microscopy, 2004, 215, 236.
33. Shou-Shing Hsieh, Hung-Chun Lin and Chih-Yi Lin, Colloid Polym. Sci., 2006, 284, 1275.
34. Yuichi Hahimoto and Takeshi Sakakibara, Jpn. J. Appl. Phys., 2000, 39, 231.
35. McDonald J. C., Duffy D. C., Anderson J. R., Chiu, D. T., Wu H., Schueller O. J. A. and Whitesides G. M., Electrophoresis, 2000, 21, (1), 27.
36. H. Hillborg, J.F. Ankner, U.W. Gedde, G.D. Smith, H.K. Yasuda and K. Wikstrom, Polymer, 2000, 41, (18), 6851.
37. Lee J. N., Park C. and Whitesides G. M., Anal. Chem. 2003, 75, (23), 6544.
38. Duffy D. C., McDonald J. C., Schueller O. J. A. and Whitesides G. M., Anal. Chem., 1998, 70, 4974.
39. 11 Unger M. A., Chou H. P., Thorsen T., Scherer A. and Quake S. R., Science, 2000, 288, 113.
40. Studer V., Hang G., Pandolfi A., Ortiz M., Anderson W. F. and Quake S. R., J. Appl. Phys. 2004, 95, 393.
41. Thorsen T., Maerkl S. J. and Quake S. R., Science, 2002, 298, 580.
42. Feynman R. F., J. MEMS, 1992, 1, 60.

43. Feynman R. F., J. MEMS, 1993, 2, 4.

44. Kartalov E. P., Anderson W. F. and Scherer A., J. Nanosci. Nanotechnol., 2006, 6, 1.

45. Hansen C. L., Skordalakes E., Berger J. M. and Quake S. R., Proc. Natl. Acad. Sci., 2002, USA, 99, 16531.

46. Kartalov E. P. and Quake S. R., Nucleic Acids Res., 2004, 32, 2873.

47. Liu J., Hansen C. and Quake S. R., Anal. Chem., 2003, 75, 4718.

48. Sohn L. L., Saleh O. A., Facer G. R., Beavis A. J., Allan R. S. and Notterman D. A., Proc. Natl. Acad. Sci., 2000, USA, 97, 10687.

49. Hong J. H., Studer V., Hang G., Anderson W. F. and Quake S. R., Nat. Biotechnol., 2004, 22, 435.

50. Emil P. Kartalov, Christopher Walker, Clive R. Taylor, W. French Anderson and Axel Scherer, Proc. Natl. Acad. Sci., U S A., 2006, 103, (33), 12280.

51. Anderson J. R., Chiu D. T., Jackson R. J., Cherniavskaya O., McDonald J. C., Wu H., Whitesides S. H. and Whitesides G. M., Anal. Chem., 2000, 72, 3158.

52. Chiu D. T., Jeon N. L., Huang S., Kane R. S., Wargo C. J., Choi I. S., Ingber D. E. and Whitesides G. M., Proc. Natl. Acad. Sci., 2000, USA, 97, 2409.

53. Jo B. H., Van Lerberghe L. M., Motsegood K. M. and Beebe, D. J., J. Microelectromech. Syst., 2000, 9, 76.

54. Wu H. K., Odom T. W., Chiu D. T. and Whitesides G. M., J. Am. Chem. Soc., 2003, 125, 554.

55. Bustamante C., Marko J. F., Siggia E. D. and Smith S., Science, 1994, 265, 1599.

56. Leger J. F., Robert J., Bourdieu L., Chatenay D. and Marko J. F., Proc. Natl. Acad. Sci., 1998, USA, 95, 12295.

57. Smith S. B., Cui Y. J. and Bustamante C., Science, 1996, 271, 795.

58. Tinland B., Pluen A., Sturm J. and Weill G., Macromolecules, 1997, 30, 5763.

59. Mills J. B., Vacano E. and Hagerman P. J., J. Mol. Biol., 1999, 285, 245.

60. Ulrich Rant, Kenji Arinaga, Marc Tornow, Yong Woon Kim, Roland R. Netz, Shozo Fujita, Naoki Yokoyama, and Gerhard Abstreiter, Biophysical Journal, 2006, 90, 3666.

61. Sassanfar M. and Roberts J.W., J. Mol. Biol., 1990, 212, 79.

62. Bishop D.K., Park D., Xu L. and Kleckner N., Cell, 1992, 69, 439.

63. Lydall D., Nikolsky Y., Bishop D. K. and Weinert T., Nature, 1996, 383:, 840.

64. Huang L.C., Clarkin K. C. and Wahl G. M., Proc. Natl Acad. Sci. USA, 1996, 93:, 4827.

65. Okazaki R., Okazaki T., Sakabe K., Sugimoto K. and Sugino A., Proc. Natl Acad. Sci. USA, 1968, 59:, 598.

66. Henson P., J. Mol. Biol., 1978, 119, 487.

67. Wanka F., Brouns R. M., Aelen J. M., Eygensteyn A. and Eygensteyn J., Nucleic Acids Res., 1977, 4, 2083.

68. Tapiero H., Leibowitch S. A., Shaool D., Monier M. N. and Harel J. Nucleic Acids Res., 1976, 3, 953.

69. Cordeiro-Stone M., Makhov A. M., Zaritskaya L. S. and Griffith J. D., J. Mol. Biol., 1999, 289, 1207.

70. Watanabe I., Toyoda M., Okuda J., Tenjo T., Tanaka K., Yamamoto T., Kawasaki H., Sugiyama T., Kawarada Y. and Tanigawa N., Jpn. J. Cancer Res., 1999, 90, 188.

71. Frankfurt O. S., Robb J. A., Sugarbaker E. V. and Villa L., Exp. Cell Res., 1996, 226, 387.

72. Raderschall E., Golub E. I. and Haaf T., Proc. Natl Acad. Sci. USA, 1999, 96, 1921.

73. Sugawara N. and Haber J. E., Mol. Cell. Biol., 1992, 12, 563.

74. Sun H., Treco D. and Szostak J. W. Cell, 1991, 64, 1155.

75. Dionne I. and Wellinger R. J., Proc. Natl Acad. Sci., 1996, USA, 93, 13902.

76. Makarov V. L., Hirose Y. and Langmore J. P., Cell, 1997, 88, 657.

77. Garvik B., Carson M. and Hartwell L., Mol. Cell. Biol., 1995, 15, 6128.

78. Polotnianka R. M., Li J. and Lustig A. J., Curr. Biol., 1998, 8, 831.

79. Bloomfield V. A., Curr. Opin. Struct. Biol., 1996, 6, 334.

80. Sali A., Shakhnovich E. and Karplus M., Nature, 1994, 369, 248.

81. Wolynes P. G. and Eaton W. A., Phys. World, 1999, 12, 39.

82. de Gennes, P. G. Scaling Concepts in Polymer Physics (Cornell University Press, Ithaca, 1979).

83. Gosule L. C. and Schellman J. A., Nature, 1976, 259, 333.

84. Takahashi M., Yoshikawa K., Vasilevskaya V. V. and Khokhlov A. R. J. Phys.

85. Chem. B, 1997, 101, 9396.

86. Widom J. and Baldwin R. L., J. Mol. Biol., 1980, 144, 431.

87. Melnikov S. M., Sergeyev V. G. and Yoshikawa K., J. Am. Chem. Soc., 1995, 117, 2401.

88. Melnikov S. M., Sergeyev V. G., Melnikova, Y. S. and Yoshikawa K., J. Chem. Soc. Faraday Trans., 1997, 93, 283.

89. Gelbart W. M., Bruinsma R. F., Pincus P. A. and Parsegian V. A., Phys. Today, 2000, 53, (9), 38.

90. Huang L. C., Clarkin K. C. and Wahl G. M., Proc. Natl Acad. Sci., USA, 1996, 93, 4827.

91. Okazaki R., Okazaki T., Sakabe K., Sugimoto K. and Sugino A., Proc. Natl Acad. Sci. USA, 1968, 59, 598.

92. David Pastré, Olivier Piétrement, Stéphane Fusil, Fabrice Landousy, Josette Jeusset, Marie-Odile David, Loïc Hamon, Eric Le Cam and Alain Zozime, Biophys J., 2003, 85(4), 2507.

93. Mao Sun, Marjatta Son and Philip Serwer, Biochemistry, 1997, 36, 13018.

94. Barrat J. L. and Joanny J. F., AdV. Chem. Phys., 1996, XCIV, 1-66.

95. Polyelectrolyte models in theory and simulation. In Handbook of polyelectrolytes and their applications; Tripathy, S. K., Kumar, J., Nalwa, H. S., Eds.; American Scientific Publishers: Stevenson Ranch, CA, 2002; Vol. 3.

96. de Gennes P. G., Pincus P., Velasco R. M. and Brochard F., J. Phys. (Paris), 1976, 37, 1461.

97. Everaers R., Milchev A. and Yamakov V., Eur. Phys. J. E, 2002, 8, 3.

98. Dobrynin A. V. and Rubinstein M., Prog. Polym. Sci., 2005, 30, 1049.

99. De Gennes P. G., Scaling Concepts in Polymer Physics; Cornell University Press: Ithaca, NY, 1979.

100. S. K. Pattanayek and J. Ravi Prakash, Macromolecules, 2008, 41, 2260.

101. T. Odijk, Macromolecules, 1983, 16, 1340.

102. M. D. Dijkstra, D. Frenkel, and H. N.W. Lekkerkerker, Physica A (Amsterdam), 1993, 193, 374.

103. C. Bouchiat, M. D. Wang, J. F. Allemand, T. Strick S. M. Block and V. Croquette, Biophys. J., 1999, 76, 409.

104. E. H. Yamakawa, Modern Theory of Polymer Solutions, Kyoto University, Japan.

105. U. Bockelmann, Ph. Thomen, B. Essevaz-Roulet, V. Viasnoff, and F. Heslot, Biophys. J., 2002, 82 (3), 1537.

106. Markus Hammermann, Nathalie Brun, Konstantin V. Klenin, Roland May, Katalin and J. Langowski, Biophys. J., 1998, 75, 3057.

107. Guthold M., M. Bezanilla, D. A. Erie, B. Jenkins, H. G. Hansma and C. Bustamante. Proc. Natl. Acad. Sci. USA., 1994, 91, 12927.

108. Han W., S. M. Lindsay, M. Dlakic and R. E. Harrington., Natur, 1997, 386, 563.

109. Hansma H. G. and D. E. Laney, Biophys. J., 1996, 70, 1933.

110. Israelachvili J. N., 1992, Intermolecular and Surface Forces. Academic Press Inc., San Diego.

111. Jiao Y., D. I. Cherny, G. Heim, T. M. Jovin and T. E. Schaffer., J. Mol. Biol., 2001, 314, 233.

112. Kjellander R. and S. Marrelja., J. Phys. Chem., 1986, 90, 1230.

113.Koppelman M. H., and J. D. Dillard, Clays Clay Miner, 1977, 73, 457.

114.Kornyshev A. A. and S. Leikin, Phys. Rev. Lett., 1996, 82, 4138.

115.Lau A. W. C., 2000, Fluctuation and Correlation Effect in Electrostatics on Highly Charged Surface. University of California, Santa Barbara, CA.

116.Lau A. W. C. and P. Pincus, Eur. Phys. J. B., 1999, 10, 175.

117.Levin Y., Physica A., 1999, 265, 432.

118.Manning G. S., Q. Rev. Biophys., 1978, 11, 179.

119.Foquet M., J. Korlach, W. Zipfel, W. W. Webb and H. G. Craighead., Anal. Chem., 2002, 74, 1415.

120.Chou H. P., C. Spence, A. Scherer and S. Quake., Proc. Natl. Acad. Sci. USA, 1999, 96, 11.

121.Foquet M., J. Korlach, W. R. Zipfel, W. W. Webb and H. G. Craighead, Anal. Chem., 2004, 76, 1618.

122.Stavis S. M., J. B. Edel, K. T. Samiee and H. G. Craighead, Lab Chip, 2005, 5, 337.

123.Stavis S. M., J. B. Edel, Y. G. Li, K. T. Samiee, D. Luo and H. G. Craighead, Nanotechnology, 2005, 16, S314.

124.Stavis S. M., J. B. Edel, Y. G. Li, K. T. Samiee, D. Luo and H. G. Craighead, J. Appl. Phys., 2005, 98, 044903.

125.Stavis S. M., S. C. Corgié, B. R. Cipriany, H. G. Craighead and L. P. Walker, Biomicrofluidics, 2007, 1, 034105.

126.Mannion J. T. and H. G. Craighead, Biopolymers, 2007, 85, 131.

127.Craighead H., Nature, 2006, 442, 387.

128.Perkins T. T., D. E. Smith and S. Chu, Science, 1997, 276, 2016.

129.Phillips K. M., J. W. Larson, G. R. Yantz, C. M. D'Antoni, M. V. Gallo, K. A. Gillis, N. M. Goncalves, L. A. Neely, S. R. Gullans and R. Gilmanshin, Nucleic Acids Res., 2005, 33, 5829.

130.Chan E. Y., N. M. Goncalves, R. A. Haeusler, A. J. Hatch, J. W. Larson, A. M. Maletta, G. R. Yantz, E. D. Carstea, M. Fuchs, G. G. Wong, S. R. Gullans and R. Gilmanshin, Genome Res., 2004, 14, 1137.

131.Bakajin O. B., T. A. J. Duke, C. F. Chou, S. S. Chan, R. H. Austin and E. C. Cox, Phys. Rev. Lett., 1998, 80, 2737.

132.Larson J. W., G. R. Yantz, Q. Zhong, R. Charnas, C. M. D'Antoni, M. V. Gallo, K. A. Gillis, L. A. Neely, K. M. Phillips, G. G. Wong, S. R. Gullans and R. Gilmanshin, Lab Chip, 2006, 6, 1187.

133.Tegenfeldt J. O., C. Prinz, H. Cao, S. Chou, W. W. Reisner, R. Riehn, Y. M. Wang, E. C. Cox, J. C. Sturm, P. Silberzan and R. H. Austin, Proc. Natl. Acad. Sci. U. S. A., 2004, 101, 10979.

134.X. Yang, L. A. Wenzler, J. Qi, X. Li and N. C. Seeman (1998) J. Am. Chem. Soc. 120, 9779.

135.E. Winfree, F. Lui, L. A. Wenzler and N. C. Seeman, (1998) Nature 394, 539.

136.C. Mao, W. Sun, Z. Shen and N. C. Seeman, (1999) Nature 397, 144.

137.F. Lui, F. Sha, N. C. Seeman, (1999) J. Am. Chem. Soc. 121, 917.

138.Yonghai Song, Zhuang Li, Zhiguo Liu, Gang Wei, Li Wang, Lanlan Sun, Cunlan

Guo, Yujing Sun and Tao Yang (2006) J. Phys. Chem. B 110, 10792-10798.

139. Pastre, D., Pietrement O., Fusil S., Landousy F., Jeusset J., David M. O., Hamon, L., Cam E. L. and Zozime A. (2003) Biophys. J. 85, 2507-2518.

140. Israelachvili J. N., Intermolecular and Surface Force; Academic Press: San Diego, CA, 1992.

141. Saenger W. Principles of Nucleic Acid Structure; Cantor, Ch. R., Ed., Springer Advanced Texts in Chemistry; Springer-Verlag: New York, 1984.

142. Lyubchenko Y. L., Shlyakhtenko L. S. (1997) Proc. Natl. Acad. Sci.U.S.A. 94, 496-501.

143. Thundat T., Allison D. P., Warmack R. J. (1994) Nucleic Acids Res. 22, 4224-4228.

144. Hansma H. G. and Laney D. E. (1996) Biophys. J. 70, 1933-1939.

145. Jozef Adamcik, Francesco Valle, GuillaumeWitz, Kristian Rechendorff1 and Giovanni Dietler1 (2008) Nanotechnology 19, 384016.

146. Marion B. Hochrein, Judith A. Leierseder, Leonardo Golubovic and Joachim O. Radler, Phys. Rev. Lett. 96, 038103.

147. Zhanwen Xiao, Mingxiang Xu, Keisuke Sagisaka and Daisuke Fujita (2003) Thin Solid Films, 438 –439.

148. Zhiguo Liu, Zhuang Li, Hualan Zhou, Gang Wei, Yonghai Song and Li Wang (2005) Microscopy Research and Technique (66) 179 – 185.

149. Yonghai Song, Zhuang Li, Zhiguo Liu, Gang Wei, Li Wang, Lanlan Sun, Cunlan Guo, Yujing Sun and Tao Yang (2006) J. Phys. Chem. B (110) 10792-10798.

150.C. Zhang and J.R.C. van der Maarel (2008) The Journal of Physical Chemistry B 112, 3552-3557.

151.Bloomfield, V.A. Curr. Opin. Struc. Biol. 1996, 6, 334-341.

152.Hud, N.V.; Vilfan, I.D. Annu. Rev. Biophys. Biomol. Struc. 2005, 34, 295-318.

153.Pelta, J.; Durand, D.; Doucet, J.; Livolant, F. Biophys. J. 1996, 71, 48-63.

154.Raspaud, E.; Durand, D.; Livolant, F. Biophys. J. 2005, 88, 392-403.

155.Allen, M.J.; Bradbury, E.M.; Balhorn, R. Nucleic Acids Res., 1997, 25, 2221–2226.

156.Fang, Y.; Hoh, J.H. Nucleic Acids Res., 1998, 26, 588–593.

157.Xiao, Z.; Xu, M.; Sagisaka, K.; Fujita, D. Thin Solid Films 2003, 438-439, 114-117.

158.Song, Y.; Li, Z.; Liu, Z.; Wei, G.; Wang, L.; Sun, L.; Guo, C.; Sun, Y.; Yang, T. J. Phys. Chem. B. 2006, 110, 10792-10798.

159.Arscott, P.G.; Ma, C.; Wenner, J.R.; Bloomfield, V.A. Biopolymers 1995, 36, 345-364.

160.Fang, Y.; Spisz, T.S.; Hoh, J.H. Nucleic Acids Res. 1999, 27, 1943–1949.

161.Adamcika, J.; Klinovc, D.V.; Witza, G.; Sekatskiia, S.K.; Dietlera, G. FEBS Letters 2006, 580, 5671–5675.

162.Bustamante, C.; Vesenka, J.; Tang, C.L.; Rees, W.; Guthold, M.; Keller, R. Biochemistry 1992, 31, 22–26.

163.Schaper, A.; Pietrasanta, L.I.; Jovin, T.M. Nucleic Acids Res. 1993, 21, 6004–6009.

164.Thundat, T.; Allison, D.P.; Warmack, R.J. Nucleic Acids Res. 1994, 22, 4224–4228.

165.Wilson, R.W.; Bloomfield, V.A. Biochemistry 1979, 18, 2192-2196.

166.Schellman, J.A.; Parthasarathy, N. J. Mol. Biol., 1984, 175, 313-329.

167.Duffy, D. C., McDonald, J. C., Schueller, O. J. A. and Whitesides, G. M. (1998) Anal. Chem. 70, 4974–4984.

168.Unger, M. A., Chou, H.-P., Thorsen, T., Scherer, A. and Quake, S. R. (2000) Science 288, 113–116.

169.Perkins, T. T.; Smith, D. E.; Larson, R. G.; Chu, S. (1995) Science, 268, 83-87.

170.Bensimon, A.; Simon, A.; Chiffaudel, A.; Croquette, V.; Heslot, F.; Bensimon, D. (1994) Science, 265 (5181, Genome Issue), 2096-2098.

171.Studer, V., Hang, G., Pandolfi, A., Ortiz, M., Anderson, W. F. and Quake, S. R. (2004) J. Appl. Phys. 95, 393–398.

172.Thorsen, T., Maerkl, S. J. and Quake, S. R. (2002) Science 298, 580–584.

173.Kartalov, E. P., Anderson, W. F. and Scherer, A. (2006) J. Nanosci. Nanotechnol. 6, 1–13.

174.Hansen, C. L., Skordalakes, E., Berger, J. M. and Quake, S. R. (2002) Proc. Natl. Acad. Sci. USA 99, 16531–16536.

175.Kartalov, E. P. and Quake, S. R. (2004) Nucleic Acids Res. 32, 2873–2879.

176.Liu, J., Hansen, C. and Quake, S. R. (2003) Anal. Chem. 75, 4718–4723.

177.Sohn, L. L., Saleh, O. A., Facer, G. R., Beavis, A. J., Allan, R. S. and Notterman, D. A. (2000) Proc. Natl. Acad. Sci. USA 97, 10687–10690.

178.Hong, J. H., Studer, V., Hang, G., Anderson, W. F. and Quake, S. R. (2004) Nat. Biotechnol. 22, 435–439.

179.Jiang, X., Ng, J. M. K., Stroock, A. D., Dertinger, S. K. W. and Whitesides, G. M. (2003) J. Am. Chem. Soc. 125, 5294–5295.

180.Kartalov, E. P., Zhong, J. F., Scherer, A., Quake, S. R., Taylor, C. R. and Anderson, W. F. (2006) BioTechniques 40, 85–90.

181.Wu, H., Wheeler, A. and Zare, R. (2004) Proc. Natl. Acad. Sci. USA 101, 12809–12813.

182.Taylor, A. M., Blurton-Jones, M., Rhee, S. W., Cribbs, D. H., Cotman, C. W. and Jeon, N. L. (2005) Nat. Methods 2, 599–605.

183.Ionescu-Zanetti, C., Shaw, R. M., Seo, J., Jan, Y.-N., Jan, L. Y. and Lee, L. P. (2005) Proc. Natl. Acad. Sci. USA 102, 9112–9117.

184.Balagadde, F. K., You, L., Hansen, C. L., Arnold, F. H. and Quake, S. R. (2005) Science 309, 137–140.

185.Lee, C.-C., Sui, G., Elizarov, A., Shu, C. J., Shin, Y. S., Dooley, A. N., Huang, J., Daridon, A., Wyatt, P., Stout, D., et al. (2005) Science 310, 1793–1796.

186.Shaikh, K. A., Ryu, K. S., Goluch, E. D., Nam, J.-M., Liu, J., Thaxton, C. S., Chiesl, T. N., Barron, A. E., Lu, Y., Mirkin, C. A. and Liu, C. (2005) Proc. Natl. Acad. Sci. USA 102, 9745–9750.

187.Dutta P, Kim MJ, Kihm KD, Beskok A (2001) “Electroosmotic flow in a grooved micro-channel configuration: a comparative study of μPIV measurements and numerical simulations,” Proceedings of 2001 ASME international mechanical

engineering congress and exposition, New York, NY, USA, 11–16 November 2001

188.Kim MJ, Kim HJ, Kihm KD (2001) “Micro-scale PIV for electroosmotic flow measurement.” In: Proceedings of PSFVIP-3, Maui, Hawaii, USA, 18–21 March 2001

189.Kim, J.; Chaudhury, M. K.; Owen, M. J. J. (2000) Colloid Interface Sci. 226, 231-236.

190.Kim, J.; Chaudhury, M. K.; Owen, M. J.; Orbeck, T. J. (2001) Colloid Interface Sci., 244, 200-207.

191.Duffy, D. C.; McDonald, J. C.; Schueller, O. J. A.; Whitesides, G. M. (1998) Anal. Chem., 70, 4974-4984.

192.Xiao, D.; Le, T. V.; Wirth, M. J. (2004) Anal. Chem., 76, 2055-2061.

193.Hu, S. W.; Ren, X. Q.; Bachman, M.; Sims, C. E.; Li, G. P.; Allbritton, N. L. (2004) Anal. Chem., 76, 1865-1870.

194.Hu, S. W.; Ren, X. Q.; Bachman, M.; Sims, C. E.; Li, G. P.; Allbritton, N. L. (2004) Langmuir, 20, 5569-5574.

195.J.A. van Kan, A.A. Bettiol, F. Watt, (2003) Appl. Phys. Lett. 83, 1629.

196.Reisner, W.; Morton, K. J.; Riehn, R.; Wang, Y. M.; Yu, Z.; Rosen, M.; Sturm, J. C.; Chou, S. Y.; Frey, E.; Austin, R. H. (2005) Phys. ReV. Lett. 94, 196101.

197.Schaefer, D. W.; Joanny, J. F.; Pincus, P. (1980) Macromolecules, 13, 1280-1289.

198.J.A. van Kan, A.A. Bettiol, F. Watt, (2003) Mat. Res. Soc. Symp. Proc., 777, T2.1.1.

199.R. M. Jendrejack, D. C. Schwartz, M. D. Graham, and J. J. Pablo, (2003) J. Chem. Phys., 119, 1165.

200.D.W. Schaefer, J. F. Joanny, and P. Pincus, (1980) Macromolecules 13, 1280.

201.Perkins, T. T.; Smith, D. E.; Larson, R. G.; Chu, S. (1995) Science, 268, 83-87.

202.Bensimon, A.; Simon, A.; Chiffaudel, A.; Croquette, V.; Heslot, F.; Bensimon, D. (1994) Science, 265 (5181, Genome Issue), 2096-2098.

203.Johansen, F.; Jacobsen, J. P. J. Biomol. (1998) Struct. Dyn., 16, 205-222.

204.Bakajin, O. B., T. A. J. Duke, C. F. Chou, S. S. Chan, R. H. Austin, and E. C. Cox. (1998) Phys. Rev. Lett. 80, 2737–2740.

205.Perkins, T. T., D. E. Smith, R. G. Larson, and S. Chu. (1995) Science. 268:83–87.

206.Sischka, A., K. Toensing, R. Eckel, S. D. Wilking, N. Sewald, R. Ros, and D. Anselmetti. (2005) Biophys. J. 88, 404–411.

207.Smith, D. E.; Chu, S. (1998) Science, 281, 1335-1340.

208.G. W. Slater, Y. Gratton, M. Kenward, L. McCormick, and F. Tessier, Soft Matter 1, 365 (2003).

209.J. Han and H. G. Craighead, Science, 288, 1026 (2000).

210.N. Kaji, Y. Tezuka, Y. Takamura, M. Ueda, T. Nishimoto, H. Nakanishi, Y. Horiike, and Y. Baba, Anal. Chem. 76, 15 (2004).

211.J. L. Li, M. Gershow, D. Stein, E. Brandin, and J. A. Golovchenko, Nat. Mat. 2, 611 (2003).

212.C. Bustamante, J. F. Marko, E. Siggia, and S. Smith, Science, 265, 1599 (1994).

213.M. D. Wang, H. Yin, R. Landick, J. Gelles, and S. M. Block, Biophys. J. 72, 1335

(1997).

214.C. G. Baumann, S. B. Smith, V. A. Bloomfield, and C. Bustamante, Proc. Natl. Acad. Sci. USA 94, 6185 (1997).

215.M. Fixman and J. Kovac, J. Chem. Phys 58, 1564 (1973).

216.J. R. C. van der Maarel, Introduction to biopolymer physics, World Scientific, Singapore, 2008.

217.T. Odijk, Macromolecules 16, 1340 (1983).

218.P.-G. de Gennes, Scaling concepts in polymer physics, Cornell University Press, Ithaca, New York, 1979.

219.W. Reisner, K. J. Morton, R. Riehn, Y. M. Wang, Z. Yu, M. Rosen, J. C. Sturm, S. Y. Chou, E. Frey, and R. H. Austin, Phys. Rev. Lett. 94, 196101 (2005).

220.K. Jo, D. Dhingra, T. Odijk, J. de Pablo, M. Graham, R. Runnheim, D. Forrest, and D. Schwartz, Proc. Natl. Acad. Sci. U.S.A. 104, 2673 (2007).

221.W. Reisner, J. P. Beech, N. B. Larsen, H. Flyvbjerg, A. Kristensen, and J. O. Tegenfeldt, Phys. Rev. Lett. 99, 058302 (2007).

222.J. A. van Kan, A. A. Bettiol, and F. Watt, Appl. Phys. Lett. 83, 1629 (2003).

223.J. A. van Kan, A. A. Bettiol, and F. Watt, Nano Lett. 6, 579 (2006).

224.M. L. Chabinyc, D. T. Chiu, J. Cooper McDonald, A. D. Strook, J. F. Christian, A. M. Karger, and G. M. Whitesides, Anal. Chem. 73, 4491 (2001).

225.P. G. Shao, J. A. van Kan, K. Ansari, A. A. Bettiol, and F. Watt, Nucl. Instr. & Methods Phys. Res. B 260, 479 (2007).

226.A. Y. Grosberg and A. R. Khokhlov, Statistical physics of macromolecules, AIP

Series in Polymers and Complex Materials, AIP Press, New York, 1994.

227.T. Odijk, J. Chem. Phys. 125, 204904 (2006).

228.M. Fixman and J. Skolnick, Macromolecules 11, 863 (1978).

229.H. Yamakawa, Modern theory of polymer solutions, Harper & Row, New York, 1971.

230.H. Benoit and P. Doty, J. Phys. Chem. 57, 958 (1953).

231.T. Odijk, J. Polym. Sci. Polym. Phys. 15, 477 (1977).

232.J. Skolnick and M. Fixman, Macromolecules 10, 944 (1977).

233.H. P. Spielmann, D. E. Wemmer, and J. P. Jacobsen, Biochemistry 34, 8542 (1995).

234.F. Johansen and J. P. Jacobsen, J. Biomol. Struct. Dyn. 16, 205 (1998).

235.O. B. Bakajin, T. A. J. Duke, C. F. Chou, S. S. Chan, R. H. Austin, and E. C. Cox.. Phys. Rev. Lett. 80, 2737 (1998).

236.J. O. Tegenfeldt, C. Prinz, H. Cao, S. Chou, W. W. Reisner, R. Riehn, Y. M. Wang, E. C. Cox, J. C. Sturm, P. Silberzan, and R. H. Austin, Proc. Natl. Acad. Sci. USA 101, 10979 (2004).

237.A. Sischka, K. Toensing, R. Eckel, S. D. Wilking, N. Sewald, R. Ros, and D. Anselmetti, Biophys. J. 88, 404 (2005).

238.J. A. Schellman and N. Parthasarathy, J. Mol. Biol. 175, 313 (1984).

239.V. A. Bloomfield, Curr. Opin. Struc. Biol. 6, 334 (1996).

240.N. V. Hud and I. D. Vilfan, Annu. Rev. Biophys. Biomol. Struc. 34, 295 (2005).

241.R. W. Wilson and V. A. Bloomfield, Biochemistry 18, 2192 (1979).

242.X. Qiu, K. Andresen, L. W. Kwok, J. S. Lamb, H. Y. Park, and L. Pollack, Phys. Rev. Lett. 99, 038104 (2007).

243.L. Dai, Y. Mu, L. Nordenskiöld, and J. R. C. van der Maarel, Phys. Rev. Lett. 100, 118301 (2008).

244.E. Dubois and F. Boue, Macromolecules 34, 3684 (2001).

245.Odijk, T. 1998. Osmotic compaction of supercoiled DNA into a bacterial nucleoid. Biophys. Chem. 73:23–29.

246.Tang, J. X., T. Ito, T. Tao, P. Traub, and P. A. Janmey. 1997. Opposite effects of electrostatics and steric exclusion on bundle formation by F-actin and other filamentous polyelectrolytes. Biochemistry. 36: 12600–12607.

247.Tang, J. X., and P. A. Janmey. 1998. Two distinct mechanisms of actin bundle formation. Biol. Bull. 194:406–408.

248.Thundat, T.; Allison, D.P.; Warmack, R.J. Nucleic Acids Res. 1994, 22, 4224–4228.

249.F. R. Senti, N. N. Hellman, N. H. Ludwig, G. E. Babcock, R. Tobin, C. A. Glass, and B. L. Lamberts, J. Poly. Sci. 17, 527 (1955).

250.Rudhardt D, Bechinger C and Leiderer P 1998 Phys. Rev. Lett. 81 1330

251.P.G. de Gennes, C.R. Acad. Sci. B 288 (1979) 359.

252.T. Odijk, Macromolecules 29 (1996) 1842.

253.V.B. Tolstoguzov, Food Hydrocolloids 4 (1991) 429.

254.P.R. Wills, Y. Georgalis, J. Dijk, D.J. Winzor, Biophys. Chem. 57 (1995) 37.

255.M.P. Pileni, Langmuir 13 (1997) 3266.

256.T. Hyeon, M. Fang, K.S. Suslick, J. Am. Chem. Soc. 118 (1996) 5492.

257.K.S. Suslick, M. Fang, T. Hyeon, J. Am. Chem. Soc. 118 (1996) 11 960.

258.J.P.A. Buining, B.M. Humbel, A.P. Philipse, A.J. Verkleij, Langmuir 13 (1997) 3921.

259.N. Feltin, M.P. Pileni, Langmuir 13 (1997) 3927.

260.P.C. Zamora, C.F. Zukoski, Langmuir 12 (1996) 3541.

261.R. Pelster, U. Simon, Coll. Polym. Sci. 277 (1999) 2.

262.F. R. Senti, N. N. Hellman, N. H. Ludwig, G. E. Babcock, R. Tobin, C. A. Glass, and B. L. Lamberts, J. Poly. Sci. 17, 527 (1955).

263.C. Zhang, F. Zhang, J.A. van Kan, and J.R.C. van der Maarel, 'Effects of electrostatic screening on the conformation of single DNA molecules confined in a nanochannel', The Journal of Chemical Physics 128, 225109 (2008), DOI: 10.1063/1.2937441

264.M. Kojima, K. Kubo, and K. YoshikawaJ. Chem. Phys. 124, 024902 (2006); DOI:10.1063/1.2145752

265.C. F. Jordan, L. S. Lerman, and J. Venable, Nature New Biology 236, 67 (1971).

266.F. Livolant and A. Leforestier, Prog. Polym. Sci. 21, 1115 (1996).

267.H. H. Strey, V. A. Parsegian, and R. Podgornik, Phys. Rev. Lett 78, 895 (1997).

268.M. Leonard, H. Hong, and H. H. S. N.Easwar, Polymer 42, 5823 (2001).

269.H. M. H. et al., Phys. Rev. Lett. 89, 018303 (2002).

270.L. S. Lerman, Proc. Nat. Acad. Sci. USA 68, 1886 (1971).

271.U. K. Laemnli, Proc. Nat. Acad. Sci. USA 72, 4288 (1978).

272.K. Minagawa, Y. Matsuzawa, K. Yoshikawa, A. R. Khokhlov, and M. Doi, Biopolymers 34, 555 (1994).

273.K. Yoshikawa and Y. Matsuzawa, Physica D 84, 220 (1995).